Kobe University Repository : Kernel

PDF issue: 2026-11-23

Functional mechanisms of membrane-active peptides

Yamamoto, Naoki

(Degree)
博士（理学）

(Date of Degree)
2010-03-25

(Date of Publication)
2015-07-31

(Resource Type)
doctoral thesis

(Report Number)
甲4909

(URL)
https://hdl.handle.net/20.500.14094/D1004909

※ 当コンテンツは神戸大学の学術成果です。無断複製・不正使用等を禁じます。著作権法で認められている範囲内で、適切にご利用ください。

Doctoral Dissertation

Functional mechanisms of membrane-active peptides

January 2010

Graduate School of Science, Kobe University

Naoki Yamamoto

Table of contents

Abbreviations -iii

Chapter I: General Introduction -1
References -3

Chapter II: NMR based structure–activity relationship analysis of an antimicrobial peptide, thanatin, engineered by site-specific chemical modification
Abstract -5
Introduction -6
Materials and methods -7
Results -9
Discussion -10
References -13
Tables -16
Figures -18

Chapter III: Designed low amphipathic peptides with α-helical propensity exhibiting antimicrobial activity via a lipid domain formation mechanism
Abstract -23
Introduction -24
Materials and methods -25
Results -33
Discussion -38
References -44
Tables -51
Figures -56

Chapter IV: Designing α-helical peptides that can agglutinate *Escherichia coli*, *Bacillus subtilis* and sheep erythrocytes

Abstract -63
Introduction -64

Materials and methods -65
Results -66
Discussion -75
Table -77
Figures -78

Chapter V: General Conclusion -87

Acknowledgement -89

Publication list -90

Abbreviations

ACN, acetonitrile
C6-NBD-PC,1-Palmitoyl-2-[6-[(7-nitro-2-1,3-benzoxadiazol-4-yl)amino]hexanoyl]-s
-Glycero-3-Phosphocholine
CD, circular dichroism
COSY, correlated spectroscopy
dansyl-DHPE,N-(5-dimethylaminonaphthalene-1-sulfonyl)-1,2-dihexadecanoyl-
sn-glycero-3-phosphoethanolamine, triethylammonium salt
DIPEA, diisopropylethylamine
DLS, dynamic light scattering
DMF, N,N-dimethylformamide
DMPC, 1,2-dimyristoyl-sn-glycero-3-phosphocholine
DMPG, 1,2-dimyristoyl-sn-glycero-3-phospho-(1'-rac-glycerol)
DQF-COSY, double quantum filtered-corretated spectroscopy
DSC, differential scanning calorimetry
EDTA, ethylenediaminetetraacetic acid
Fmoc, 9-fluorenylmethoxycarbonyl
HATU,N-[(dimethylamino)-1H-1,2,3-triazolo-[4,5-b]pyridin-1-yl-methylene]-
-mehylmethanaminium hexafluorophosphate N-oxide
HOBt, N-hydroxybenzotriazole
HPLC, high performance liquid chromatography
MALDI, matrix-assisted laser desorption/ionization
MIC, minimal inhibitory concentration
NMR, nuclear agnetic resonance
NOE, nuclear Overhauser effect
NOESY, nuclear Overhauser enhancement pectroscopy
OD, optical density
PEG, polyethylene glycol
POPC, 1-Palmitoyl-2-Oleoyl-sn-Glycero-3-Phosphocholine
POPG, 1-Palmitoyl-2-Oleoyl-sn-Glycero-3-[Phospho-rac-(1-glycerol)]
RMSD, root mean square deviation
sRBC, sheep red blood cells
tBu, tertbutyl roup
TFA, trifluoroacetic acid
TOCSY, total orrelated spectroscopy

TOF, time of flight
WATERGATE, water suppression by gradient-tailored excitation
WWscale, Wimley-White scale

Chapter I

General Introduction

Proteins are essential molecules for all of the organisms to live, move and maintain the bodies. Their complex and sophisticated structures express a wide variety of functions such as enzyme reaction, body movements or deposits of organic or inorganic compounds. Therefore, the functional mechanisms are needed to be solved not only to answer the question “What is life?” but also to design architectural biological systems that enrich the life of human being. Based on places where proteins exist, they can be divided into three kinds of groups. The first is soluble in water and functions in aqueous environments, the second stably exists in membranes but easily aggregates in water, and the last is soluble in water and can also interact with the membranes.

Proteins belonging to the third group are usually small, composed of several dozen amino-acids, and thus usually called membrane-active peptides [1; 2]. While they easily dissolve in water, they retain strong tendency to partition into membrane surfaces, resulting in exhibiting a number of important functions on or in membranes *in vivo*; membrane permeation [3], membrane fusion [4], membrane inserting [5], membrane disruption [6], or membrane aggregation [7]. Though studies on their functions have been energetically done, the mechanisms of action are not well understood. This is mainly because (i) they exhibit functions not by themselves but rather with membranes, which are assemblies of a number of amphipathic molecules such as phospholipids, and (ii) it is usually difficult to precisely determine their *in situ* structures. Therefore, various *in vitro* studies need to be performed to elucidate their mechanisms of action. The *in vitro* studies include determining structures in solution or on artificially constructed membranes, or monitoring how they behave when they interact with the artificial membranes. Then their mechanisms of action are discussed by comparing structural or physicochemical parameters obtained from these experiments with *in vivo* activities. In the thesis, I tried to reveal mechanisms of action of two kinds of membrane-active peptides. One is antimicrobial peptides, and the other is

cell-agglutinating peptides.

Antimicrobial peptides are one of the typical membrane-active proteins [2]. They have been found in a wide variety of living things and secretion of them is an important innate immune system, especially for invertebrates that do not have an acquired immune system [8]. To understand their mechanisms, much effort has been done and mechanisms of several amphipathic peptides have been partially revealed [9]. However, because of the difficulties described above, a large part of their mechanism remains to be solved. In the thesis, I present two cases of antimicrobial peptides whose mode of action have been scarcely solved. In Chapter II, I studied mechanisms of an antimicrobial peptide, thanatin, based on solution structures. In Chapter III, mode of action of nonamphipathic antimicrobial peptides with helical propensity was studied by focusing on how they act on or in membrane surfaces.

Membrane-aggregation by membrane-active peptides is different from other membrane activities in that the peptides must retain capabilities to attract two or more membrane structures. Artificial anionic membranes such as liposomes are known to be agglutinated by cationic organic polymers including peptides such as poly-lysine [7; 10]. In these cases, electrostatic interactions seem to be enough to attract membranes. On the other hand, electrostatic interactions are not enough to agglutinate membranes of living cells such as gram-positive bacteria, gram-negative bacteria and erythrocytes, because poly-lysine never agglutinates these cells [11]. Examples of some organic bacterial-agglutinating compounds suggest that it is essential for the compounds not only to interact with the bacterial surface but also to self-associate [12; 13]. Especially, the capability to self-associate seems to play the key role to induce aggregation. Then, in Chapter IV, I tried to design peptide that effectively agglutinate typical living cells such as *Escherichia coli*, *Bacillus subtilis* and sheep erythrocytes based on the philosophy that peptides retaining tendencies to self-associate could be cause cell aggregation.

The aim of the thesis is to obtain general design principles of membrane-active peptides by dealing with a variety of cases in which membrane-active peptides perform their activities in biological systems. Since the principles inevitably contain various kinds of interaction patterns, i.e. peptide-peptide, peptide-membrane and membrane-membrane interactions, the factors that govern the function and structure of membrane-related phenomena in living organisms is expected to be shed light on.

References

[1] R. Rathinakumar, W.F. Walkenhorst, and W.C. Wimley, Broad-spectrum antimicrobial peptides by rational combinatorial design and high-throughput screening: the importance of interfacial activity. J Am Chem Soc 131 (2009) 7609-17.

[2] R. Rathinakumar, and W.C. Wimley, Biomolecular engineering by combinatorial design and high-throughput screening: small, soluble peptides that permeabilize membranes. J Am Chem Soc 130 (2008) 9849-58.

[3] S. Kobayashi, K. Takeshima, C.B. Park, S.C. Kim, and K. Matsuzaki, Interactions of the novel antimicrobial peptide buforin 2 with lipid bilayers: proline as a translocation promoting factor. Biochemistry 39 (2000) 8648-54.

[4] L.K. Tamm, J. Crane, and V. Kiessling, Membrane fusion: a structural perspective on the interplay of lipids and proteins. Curr Opin Struct Biol 13 (2003) 453-66.

[5] A.S. Ladokhin, and S.H. White, Interfacial folding and membrane insertion of a designed helical peptide. Biochemistry 43 (2004) 5782-91.

[6] S.E. Blondelle, and R.A. Houghten, Hemolytic and antimicrobial activities of the twenty-four individual omission analogues of melittin. Biochemistry 30 (1991) 4671-8.

[7] D. Volodkin, V. Ball, P. Schaaf, J.C. Voegel, and H. Mohwald, Complexation of phosphocholine liposomes with polylysine. Stabilization by surface coverage versus aggregation. Biochim Biophys Acta 1768 (2007) 280-90.

[8] M. Zasloff, Antimicrobial peptides of multicellular organisms. Nature 415 (2002) 389-95.

[9] Y. Shai, and Z. Oren, From "carpet" mechanism to de-novo designed diastereomeric cell-selective antimicrobial peptides. Peptides 22 (2001) 1629-41.

[10] A.A. Yaroslavov, E.A. Kiseliova, O.Y. Udalykh, and V.A. Kabanov, Integrity of mixed liposomes contacting a polycation depends on the negatively charged lipid content. Langmuir 14 (1998) 5160-3.

[11] K. Colville, N. Tompkins, A.D. Rutenberg, and M.H. Jericho, Effects of Poly(l-lysine) Substrates on Attached Escherichia coli Bacteria. Langmuir (2009).

[12] M.D. Disney, J. Zheng, T.M. Swager, and P.H. Seeberger, Detection of bacteria with carbohydrate-functionalized fluorescent polymers. J Am Chem Soc 126 (2004) 13343-6.

[13] M.K. Muller, and L. Brunsveld, A supramolecular polymer as a self-assembling polyvalent scaffold. Angew Chem Int Ed Engl 48 (2009) 2921-4.

Chapter II

Structure–activity relationship analysis of an antimicrobial peptide, thanatin, engineered by site-specific chemical modification

Abstract

Activity improvement of an antimicrobial peptide, thanatin, has been achieved up to 4-fold higher than natural original one by site-specific chemical modifications with *tert*-butyl group at two cysteine residues which form an intramoleular disulfide bridge. The chemically modified thanatin (C11tBu/C18tBu) exhibited improved antimicrobial activity toward Gram-positive bacteria, *Micrococcus luteus,* whereas lowered activity toward Gram-negative bacteria, *Escherichia coli*. This finding suggests that disulfide-bridge formation is not only indispensable for exhibition of antimicrobial activity of thanatin but also closely related to the activity specificity towards bacteria. NMR analysis indicates that thanatin acts against *E.coli* stereospecifically by taking advantage of its C-terminal β-hairpin structure, while the activity against *M. luteus* does not relate to structures and correlates very well to side-chain hydrophobicity.

Introduction

Antimicrobial peptides (AMPs) are humoral effector molecules of innate immune systems found in different groups of various organisms, including microorganisms, higher plants, insects, amphibians and mammals. In particular, AMPs derived from insects have extensively developed as an efficient defense system that is rapidly induced in response to a microbial challenge or body injury [1]. To date, more than 150 AMPs have been identified . Some of AMPs exhibit bactericidal activity likely as antibiotics derived from actinomycetes, but this class of peptides appears to be refractory to the development of resistance [3]. This property makes them attractive candidates as next-generation of the therapeutic agents against the multidrug-resistant microbial infections. Structure–function studies on AMPs have also added significance in this direction, as there is a rapid increase in the emergence of microbes resistant to conventionally used antibiotics in recent years [4; 5].

It is expected that the key features for the efficient bactericidal or hemolytic activities are given by the understanding of the secondary and tertiary structures of AMPs, and that the knowledge of key structure to its function may assist the rational design toward the improved analogs for clinical use. Many of such studies have been limited to linear peptides with a tendency for amphiphilic α-helical structure or amphiphilic β-sheet peptides stabilized by multiple disulfide bridges [6; 7]. In contrast to this, a few non-helical AMPs with a single disulfide bridge, like thanatin [8] and bactenecin [9], have been used in structure–function studies [10; 11]. Thanatin is the 21-residue inducible defense peptide found in the hemipteran insect *Podisus maculiventris* [8]. The range of antimicrobial activity toward the target (termed here “activity spectrum”) of thanatin is broadest so far characterized [8]. Thanatin is important in the sense that it displays sequence similarity to the brevinin family of AMPs that was isolated from frog skin [12; 13]. These homologous peptides share the common structural feature that contains a disulfide loop with a strong cation at its C-terminal region. The NMR solution structure analysis demonstrated that thanatin adopts a well-defined anti-parallel β-sheet structure from 8 to the C-terminus [10]. Relationship between primary structure and function of thanatin has been analyzed by systematically synthesizing the analogs with N- and C-terminal truncations [8] or deletion and insertion within the disulfide loop (11). Additionally, based on the in vivo functional mapping strategy, we previously demonstrated the importance of a hydrogen bonding network formed within the C-terminal loop joining the β-strands arranged anti-parallel to one another that are supposed to be crucial for exhibiting anti-*Escherichia coli* activity [14].

In this study, we prepared a homolog of thanatin by introducing a *tert*-butyl group into the cysteine residues by which the disulfide bridge between them is disarmed (at positions of 11 and 18), in order to examine the effects of chemical modification with non-biological moiety on antimicrobial activity and activity spectrum. Fortunately, an improved antimicrobial activity was observed against a Gram-positive bacterium, *Micrococcus luteus*, by the artificial peptide modification (C11tBu/C18tBu). This observation suggests that the disulfide-formed covalent linkage is dispensable for exhibition of the bactericidal activity. We also found that other three analogs, with substitution of one or two cysteine residues to serine residues (C11S and C18S, C11S/S18S), retains antibacterial activity against *M. luteus*. By contrast, it is of interest that remarkable activity decrease took place in the case of Gram-negative bacterium, *E. coli*, by both artificial and natural modifications. The activity-spectrum alteration of wild-type, chemically modified, and double mutant thanatins is also discussed based on their NMR tertiary structures and functional data.

Materials and Methods

General procedure for solid-phase peptide synthesis

Peptide synthesis was carried out using automated multiple peptide synthesizer (PSSM-8, Shimadzu) according to the standard Fmoc solid-phase peptide synthesis protocol. The peptide sequence was extended on methionine-preloaded PEG resin (25 μmol scale), which provided C-terminal peptide carboxylic acid on cleavage. Protected amino acids were coupled using 3 equiv of Fmoc amino acids, 3 equiv of HATU, 3 equiv of HOBt and 6 equiv of DIPEA in DMF. Amino acid side-chains were protected as follows: *tert*-butyl (Ser, Thr, Tyr, Cys), trityl (Asn, Gln, Cys), *tert*-butyloxycarbonyl (Lys), pmc (Arg). Cleavage of the peptide from the resin and deprotection of all side-chain protecting groups were accomplished by treating the resin with reagent K for 2 h. The solution was filtered and the resin was rinsed with the cocktail. To the filterate was added diethyl ether to precipitate the peptide. HPLC purification of the crude peptide was performed on a C_{18} reverse-phase column (5 μm, 4.6 × 250 mm) with solvent A (0.1% TFA in H_2O) and solvent B (0.1% TFA in ACN) as mobile phase. The gradient system used for peptides with *tert*-butyl group was as follows: 0–50% B (50 min), then 50–100% B (10 min). The gradient system used for peptides without *tert*-butyl group was as follows: 0–20% B (5 min), then 20–30% B (50 min) and 30–100% B (5 min). The flow rate was 0.5 mL/min and the elution was monitored at 225 nm. Desired product was recovered from the appropriate fractions by

lyophilization to give colorless foam. The molecular masses of the peptides were analyzed by MALDI-TOF mass spectrometry using a Voyager-DE STR-H (Applied Biosystems) with alpha-cyano-4-hydroxy cinnamic acid as a matrix. The observed mass value agreed well with the theoretical value.

Bioassay based on minimal inhibitory concentration (MIC)

Prior to the assay, the peptide concentration was determined based on the tyrosine absorbance at 280 nm (ε = 1280 $dm^3\ mol^{-1}\ cm^{-1}$). The antimicrobial activity assay was performed at 25 °C by adding 20 µl of prefiltered peptide samples, at various concentrations (serially 2-fold diluted), to 80 µl of PB medium (1% bacto tryptone and 0.9% NaCl) including *Escherichia coli* (300 cells) and YEB medium (1% bacto tryptone, 0.2% bacto yeast extract, 0.5% NaCl, 0.5% glucose and 1% meat extract) including *Micrococcus luteus* (300 cells), respectively, in each well of the 96-well micro-titer plate. The minimal inhibitory concentration (MIC) was defined as the lowest concentration of the peptide at which there was no growth of bacteria. Experimental reproducibility was confirmed by three trials.

Two-dimensional NMR spectroscopy and structure calculation

Each peptide powder or pellet was dissolved in 90%H_2O/10%D_2O at final concentration of 1–2 mM. pH of each solution was adjusted to 3.2–3.5 by adding 1 M HCl or 1 M NaOH. To determine structures of each peptide, we took a series of 2D-NMR measurements; COSY [15], TOCSY [16], NOESY [17] and DQF-COSY [18] using DMX750 spectrometer (Bruker Co., Ltd) equipped with the Z-field magnetic gradient pulse emitter operating at proton frequency of 750.03 MHz. The mixing time of TOCSY and NOESY was 80 ms and 250 ms, respectively. To eliminate ^1H signals originated from water, its magnetization was saturated by irradiating weak magnetic field on its frequency in COSY and DQF-COSY experiments, or WATERGATE pulse sequence [19] was used in TOCSY and NOESY experiments. All measurements were taken at 5 °C. Data processing was performed by NMRDraw ver. 2.4 packaged in NMRPipe [20]. To display all spectra and assign cross peaks in NOESY spectra, we used Sparky ver. 3.111 (T.D. Goddard and D.G. Kneller, University of California). Peak assignments in NOESY spectra were done using the sequential assignment method [21]. φ angle constraints were determined from $^3J_{HN\text{-}H\alpha}$ obtained from DQF-COSY spectra [22]. They were classified into three categories: −90° to −40°, −160° to −80° and −140° to −100° corresponding to $^3J_{HN\text{-}H\alpha} < 5.5$ Hz, >8.0 Hz and >10.0 Hz, respectively. Solution structures were calculated using DYANA ver.1.5 [23] using a modified library

to include tBu-Cys residues. First, volumes of cross peaks of NOESY spectra were converted to upper distance restraints using the macro CALIBA, then structure calculations were performed by running the simulated annealing macro, ANNEAL. Structure calculations of 11tBu/18tBu and C11S/C18S were done using 417 upper distance restraints and 2φ angle restraints, and 227 upper distance restraints and 1φ angle restraints, respectively. Finally 10 structures having no distance violation exceeding 0.3 Å and no φ angle violation beyond 3° were obtained out of 100 initial structures generated in random conformations. Credibility of structures was confirmed by using the PROCHECK_NMR program [24]. Structures were displayed and analyzed on MOLMOL [25].

Results

Design of thanatin mutants

Thanatin has the amino acid sequence: GSKKPVPIIYCNRRTGKCQRM (underlines indicate pairing cysteines capable of forming a disulfide bridge). As an attempt to improve the antimicrobial activity of wild-type thanatin (WT), several thanatin mutants were designed by engineering cysteine residues involved in disulfide bridge. We have designed a chemically modified mutant (C11tBu/C18tBu) in which two cysteine residues are modified with *tert*-butyl group. This peptide lacks the ability to form intramolecular disulfide bridge, because side-chains of both residues are protected. However this peptide might adopt a loop structure stabilized by hydrophobic interaction between modified cysteine residues with high hydrophobicity. We have also designed double mutant (C11S/C18S) in which both cysteine residues are substituted with serine structurally similar to cysteine. Though the hydroxyl group of serine residue is unable to form covalent bond, it could contribute to the stabilization of loop conformation through hydrogen bond formation. For comparison of antimicrobial activity of serine double mutant, single mutants (C11S and C18S) in which either of cysteine residues is substituted with serine were also designed. We have synthesized both wild-type and mutant thanatins reported herein. The structure of the synthetic peptides was confirmed by MALDI-TOF mass analysis.

Activity improvement and activity-spectrum alteration of antimicrobial activity

As shown in Table 1, chemically modified mutant, C11tBu/C18tBu, exhibited approximately 4-fold higher activity specifically toward *M. luteus*. On the other hand, remarkable decrease in antimicrobial activity of this chemical mutant took place for *E.*

coli. Activity-spectrum alteration caused by chemical modification suggests different mode of action of thanatin towards *M. luteus* and *E. coli*. Also, almost same tendency was observed for all of the cysteine residue altered mutants (C11S, C18S, C11S/C18S). Disulfide-bridge formation was not essential for activity exhibition of thanatin in particular towards *M. luteus*.

Secondary structure

11tBu/18tBu: In the NOESY spectrum of 11tBu/18tBu, there are many long-range NOEs between the side-chains of Ile8-Met21, Tyr10-Gln19, Tyr10-Met21, Asn12-Lys17, Asn12-Gln19, Ile9-tBu-Cys18, Ile9-Arg20 and tBu-Cys11–tBu-Cys18 as shown in Figure 1A. $C_\alpha H_i/C_\alpha H_j$ strong NOEs between residues C11tBu–C18tBu, and between Ile9-Arg20 are also observed. These results indicate that 11tBu/18tBu forms a β-hairpin structure.

C11S/C18S: In contrast to 11tBu/18tBu, there is no long-range NOE in the NOESY spectra of C11S/C18S as shown in Figure 1B, indicating that C11S/C18S forms no β-hairpin structure. On the other hand, medium intensity HN_i–HN_{i+1} NOEs exist from Asn12 to Lys17 (data not shown), suggesting that C11S/C18S forms a turn structure in this region, while other NOEs which support a formation of a turn structure in this region are poor (Figure 1B). Thus, we deduce that a turn structure, if formed, must be unstable.

Calculated structure

11tBu/18tBu: Structure statistics and overall structures of 11tBu/18tBu are shown in Table 2 and Figure 2A, respectively. As shown in Figure 2A, 11tBu/18tBu forms a β-hairpin structure from Ile8 to Met21, while the rest of N-terminal fragment (from Gly1 to Pro7) forms no obvious structure. Side-chains of Ile8, Tyr10, Gln19 and Met21 are as tightly packed as thanatin (Figure 2B). Moreover, side-chains of Ile9, tBu-Cys11, tBu-Cys18 and Arg20 are also tightly packed (Figure 2B). In general, the tight packing between β-strands is a characteristic of the β-sheet structure.

C11S/C18S: Structure statistics and overall structures of C11S/C18S are represented in Table 2 and Figure 2C. C11S/C18S no longer forms β-hairpin structure as shown in Figure 2C. Moreover, a turn formation expected from NOE connectivity, is not observed. Taking these facts into consideration, we conclude that C11S/C18S does not form any clear structure.

Discussion

Structure–activity relationship

The main element of bacterial membrane is a bilayer composed of a few kinds of lipids, some of which contain anionic head groups [26]. When an antimicrobial peptide interacts with a bacterial membrane, it is assumed that the peptide binds to the surface of the membrane by electrostatic interactions, and inserts into the membrane by virtue of hydrophobic interactions, resulting in causing death of bacteria [26-28]. When an antimicrobial peptide acts in such a non-specific mechanism ("non-specific" means there is no particular target for an antimicrobial peptide), we can expect that activities of antimicrobial peptides increase as net positive charge and net hydrophobicity increase. Indeed, there are some works indicating these relationships [29]. In our case, however, the relationships seem to be applicable to *M. luteus* only. Figure 3 shows relationships between relative activities and the relative side-chain hydrophobicity of Xaa11 and Xaa18 (Xaa stands for Ser, Cys or tBu-Cys). Since thanatin differs from the four mutants in side-chain types of Xaa11 and/or Xaa18 residues, we only have to consider hydrophobicity of these amino acids. In this study, we used hydration energy obtained by Privalov and Makhatadze [30] as a hydrophobic scale because it contains hydrophobicity of the *tert*-butyl group and cystine residues. For *M. luteus*, there is a very good correlation between the relative antimicrobial activities and the relative hydration energy ($R = 0.94$), indicating that thanatin and other mutants act in a non-specific mechanism. In contrast, for the case of *E. coli*, there is no correlation between the relative hydration energy and the relative activities ($R = 0.28$), indicating that these peptides do not act in a non-specific manner. We then focus on their structural difference, since there are some works indicating the importance of the β-hairpin structure of thanatin to act against *E. coli* [8; 14]. As described in the previous section, C11S/C18S does not form the β-hairpin structure and has very low activity against *E. coli*. Moreover, 11tBu/18tBu also acts against *E. coli* poorly in spite of formation of the β-hairpin structure. These results indicate that the disulfide-bridge on top of the β-hairpin structure is indispensable for the full activity against *E. coli*. To check a difference between the structures of 11tBu/18tBu and thanatin, the β-hairpin structures of 11tBu/18tBu are superimposed on top of thanatin, and we can see that they are somewhat different in spite of formation of the same secondary structure (Figure 4A). Especially, the difference of the environment around Xaa11 and Xaa18 is obvious, as 11tBu/18tBu have the very bulky tBu group (shown in Figure 4B). At the moment, though an obvious target of thanatin is still to be identified, these facts allow us to assume that thanatin acts against *E. coli* stereospecifically by making use of the

C-terminal β-hairpin structure. A plausible mechanism is that thanatin may bind to a physiologically important membrane protein and inhibit its function, resulting in causing the death of bacteria. Fehlbaum et al. also suggested such a mechanism of thanatin against *E. coli*, using all D-amino acid thanatin [8], in which the enantiomer had very low activity against *E. coli*. The stereospecific mechanism is also supported by other experiments done by Fehlbaum et al. [8] and Taguchi et al. [14]. The former group made N-terminally or C-terminally truncated thanatin mutants and tested them against various bacteria. Activities of N-terminally truncated mutants, in which mutations never seemed to influence β-hairpin structures, were almost unchanged. On the other hand, C-terminally truncated mutants, in which β-hairpin structures were assumed to be broken, lost their activities against *E. coli* dramatically. The latter group, Taguchi et al. obtained some mutants whose C-terminal amino acids were mutated into other amino acids by a random mutagenesis screening method, in which β-hairpin structures seemed to be unfolded, and these mutants also lost their activities against *E. coli* drastically. If structural details of these mutants are clarified, we will be able to discuss the mechanism of thanatin even further.

Expansion of structural diversity of AMPs by chemical modification

Until now, alteration of various properties of proteins and peptides has been mainly performed by substitution, insertion and deletion of amino acid constituents. Also, several AMP analogs have been designed using modified amino acids including ornithine and modified cysteines, although significant improvement was not observed for their modified forms as obtained here [31; 32]. In this study, introduction of unnatural substance, tBu, into the thanatin was turned out to serve as an good example, namely, expansion of structural diversity generated by chemical modification further allows us to design new AMPs with improved properties that would not be acquired by only amino acid substitutions. In particular, introduction of strong non-covalent hydrophobic interaction into covalently disulfide bonding sites would be versatile approach for disulfide bond-included AMPs such as β-defensin type peptides.

References

[1] J.A. Hoffmann, Innate immunity of insects, Curr. Opin. Immunol. 7 (1995), pp.4–10.

[2] P. Bulet, C. Hetru, J.L. Dimarcq and J.A. Hoffmann, Antimicrobial peptides in insects: structure and function, Dev. Comp. Immunol. 23 (1999), pp. 329–44.

[3] H.C. Neu, The crisis in antibiotic resistance, Science 257 (1992), pp. 1064–73.

[4] R.E. Hancock, Peptide antibiotics, Lancet 349 (1997), pp. 418–22.

[5] I. Chopra, J. Hodgson, B. Metcalf and G. Poste, The search for antimicrobial agents effective against bacteria resistant to multiple antibiotics, Antimicrob. Agents Chemother. 41 (1997), pp. 497–503.

[6] W.L. Maloy and U.P. Kari, Structure–activity studies on magainins and other host defense peptides, Biopolymers 37 (1995), pp. 105–22.

[7] N. Sitaram and R. Nagaraj, Interaction of antimicrobial peptides with biological and model membranes structural and charge requirements for activity, Biochim. Biophys. Acta 1462 (1999), pp. 29–54.

[8] P. Fehlbaum, P. Bulet, S. Chemysh, J.P. Briand, J.P. Roussel, L. Letellier, C. Hetru and J.A. Hoffmann, Structure-activity analysis of thanatin, a 21-residue inducible insect defense peptide with sequence homology to frog antimicrobial peptides, Proc. Natl. Acad. Sci. USA 6 (1996), pp. 1221–5.

[9] M. Wu and R.E. Hancock, Interaction of the cyclic antimicrobial cationic peptide bactenecin with the outer and cytoplasmic membrane, J. Biol. Chem. 274 (1999), pp. 29–35.

[10] N. Mandard, P. Sodano, H. Labbe, J.M. Bonmatin, P. Bulet, C. Hetru, M. Ptak and F. Vovelle, Solution structure of thanatin, a potent bactericidal and fungicidal insect peptide, determined from proton two-dimensional nuclear magnetic resonance data, Eur. J. Biochem. 256 (1998), pp. 404–10.

[11] M.K. Lee, L. Cha, S.H. Lee and K.S. Hahm, Role of amino acid residues within the disulfide loop of thanatin, a potent antibiotic peptide, J. Biochem. Mol. Biol. 35 (2002), pp. 291–6.

[12] N. Morikawa, K. Hagiwara and T. Nakajima, Brevinin-1 and -2, unique antimicrobial peptides from the skin of the frog, Rana brevipoda porsa, Biochem. Biophys. Res. Commun. 189 (1992), pp. 184–90

[13] M. Simmaco, G. Mignogna, D. Barra and F. Bossa, Novel antimicrobial peptides from skin secretion of the European frog Rana esculentra, FEBS Lett. 324 (1993), pp. 159–61.

[14] S. Taguchi, K. Kuwasako, A. Suenaga, M. Okada and H. Momose, Functional

mapping against Escherichia coli for the broad-spectrum antimicrobial peptide, thanatin, based on an in vivo monitoring assay system, J. Biochem. 128 (2000), pp. 745–54.

[15] D. Marion and K. Wuthrich, Application of phase sensitive two-dimensional correlated spectroscopy for measurements of 1H–1H spin–spin coupling constants in proteins, Biochem. Biophys. Res. Commun. 113 (1983), pp. 967–74.

[16] A. Bax and D.G. Davis, MLEV-17-based two-dimensional homonuclear magnetization transfer spectroscopy, J. Magn. Reson. 65 (1985), pp. 355–60.

[17] A. Kumar, R.R. Ernst and K. Wüthrich, A two-dimensional nuclear Overhauser enhancement (2D NOE) experiment for the elucidation of complete proton–proton cross-relaxation networks in biological macromolecules, Biochem. Biophys. Res. Commun. 95 (1980), pp. 1–6.

[18] U. Piantini, O.W. Sorensen and R.R. Ernst, Multiple quantum filters for elucidating NMR coupling networks, J. Am. Chem. Soc. 104 (1982), pp. 6800–1.

[19] M. Piotto, V. Saudek and V. Sklenar, Gradient-tailored excitation for single-quantum NMR spectroscopy of aqueous solutions, J. Biomol. NMR 2 (1992), pp. 661–5.

[20] F. Delaglio, S. Grzesiek, G.W. Vuister, G. Zhu, J. Pfeifer and A. Bax, NMRPipe: a multidimensional spectral processing system based on UNIX pipes, J. Biomol. NMR 6 (1995), pp. 277–3.

[21] K. Wuthrich, NMR of Proteins and Nucleic Acids, Wiley Interscience, New York (1986).

[22] Y. Kim and J.H. Prestegtard, Measurement of vicinal couplings from cross peaks in COSY spectra, J. Magn. Reson. 84 (1989), pp. 9–13.

[23] P. Guntert, C. Mumenthaler and K. Wuthrich, Torsion angle dynamics for NMR structure calculation with the new program DYANA, J. Mol. Biol. 273 (1997), pp. 283–98.

[24] R.A. Laskowski, J.A. Rullmannn, M.W. MacArthur, R. Kaptein and J.M. Thornton, AQUA and PROCHECK-NMR: programs for checking the quality of protein structures solved by NMR, J. Biomol. NMR 8 (1996), pp. 477–86.

[25] R. Koradi, M. Billeter and K. Wuthrich, MOLMOL: a program for display and analysis of macromolecular structures, J. Mol. Graph. 14 (1996), pp. 51–5.

[26] M. Zasloff, Antimicrobial peptides of multicellular organisms, Nature 415 (2002), pp. 389–95.

[27] M.R. Yeaman and N.Y. Yount, Mechanisms of antimicrobial peptide action and resistance, Pharmacol. Rev. 55 (2003), pp. 27–55.

[28] N.Y. Yount, A.S. Bayer, Y.Q. Xiong and M.R. Yeaman, Advances in antimicrobial peptide immunobiology, Biopolymers 84 (2006), pp. 435–58.

[29] E. Kluver, S. Schulz-Maronde, S. Scheid, B. Meyer, W.G. Forssmann and K. Adermann, Structure–activity relation of human beta-defensin 3: influence of disulfide bonds and cysteine substitution on antimicrobial activity and cytotoxicity, Biochemistry 44 (2005), pp. 9804–16.

[30] P.L. Privalov and G.I. Makhatadze, Contribution of hydration to protein folding thermodynamics, J. Mol. Biol. 232 (1993), pp. 660–79.

[31] A.G. Rao, Conformation and antimicrobial activity of linear derivatives of tachyplesin lacking disulfide bonds, Arch. Biochem. Biophys. 361 (1999), pp. 127–34.

[32] K. Matuszaki, Why and how are peptide-lipid interactions utilized for self-defense? Magainins and tachyplesins as archetypes, Biochim. Biophys. Acta 1462 (1999), pp. 1–10.

Table 1 Minimal inhibitory activities of 11tBu/18tBu and C11S/C18S against bacteria

	M. luteus 3347	*E. coli* JM109
Wild-type	0.3	0.15
C11tBu/C18tBu (11tBu/18tBu)	0.075	40
Cys11Ser (C11S)	0.3	40
Cys18Ser (C18S)	0.3	>40
Cys11Ser/Cys18Ser (C11S/C18S)	0.6	>40

Table 2 Structure statistics for 10 structures of 11tBu/18tBu and C11S/C18S

	11tBu/18tBu	C11S/C18S
Restranits used in the structure calculation		
Number of distance restraints		
Short-range	312	199
Medium-range	67	28
Long-range	38	0
Total	417	227
Number of torsion angle restraints		
φ	2	1
Geometric statistics		
R.m.s deviation from the mean structure (Å)		
(Residues 1–21)		
Backbone atoms	2.41 ± 0.89	4.62 ± 1.01
All heavy atoms	2.85 ± 0.63	6.36 ± 0.89
(Residues 9–20)		
Backbone atoms	0.45 ± 0.14	3.04 ± 0.62
All heavy atoms	1.59 ± 0.23	5.46 ± 0.79
Ramachandran analysis		
Most favored regions (%)	41.9	29.4
Additional allowed regions (%)	55	61.2
Generously allowed regions (%)	0	7.5
Disallowed regions (%)	3.1	1.9

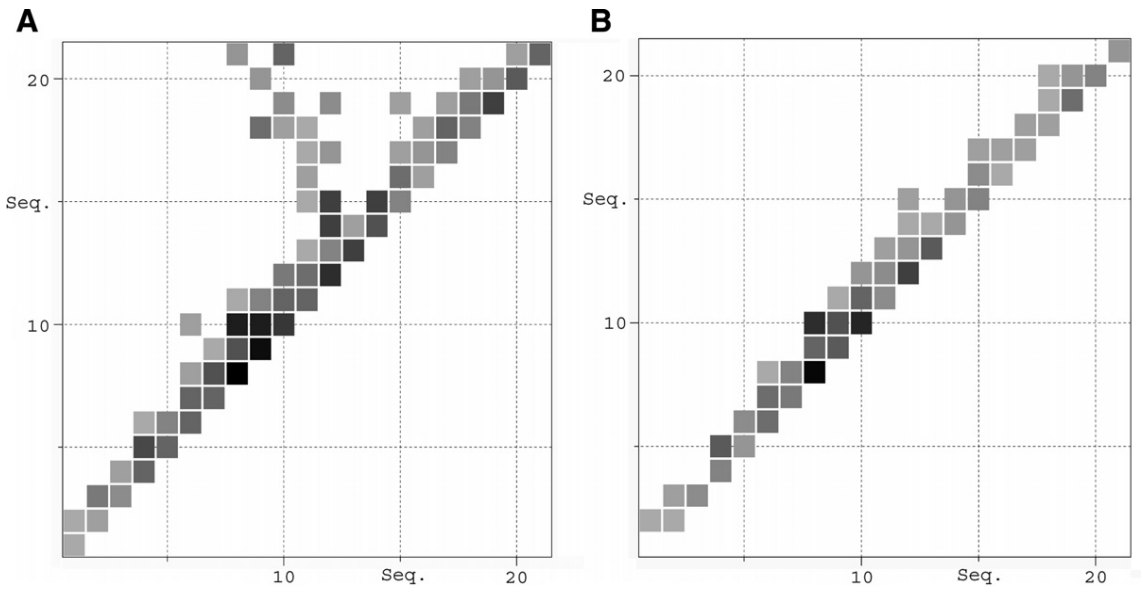

Figure 1. Distribution maps of the NOE connectivities between residues of (a); 11tBu/18tBu, and (b); C11S/C18S. The number of NOEs between residues are displayed according to a gray scale, changing from white(no NOE) to black(20 NOEs). The horizontal and vertical labels indicate the residue number of the peptide. These maps were drawn on MOLMOL (11).

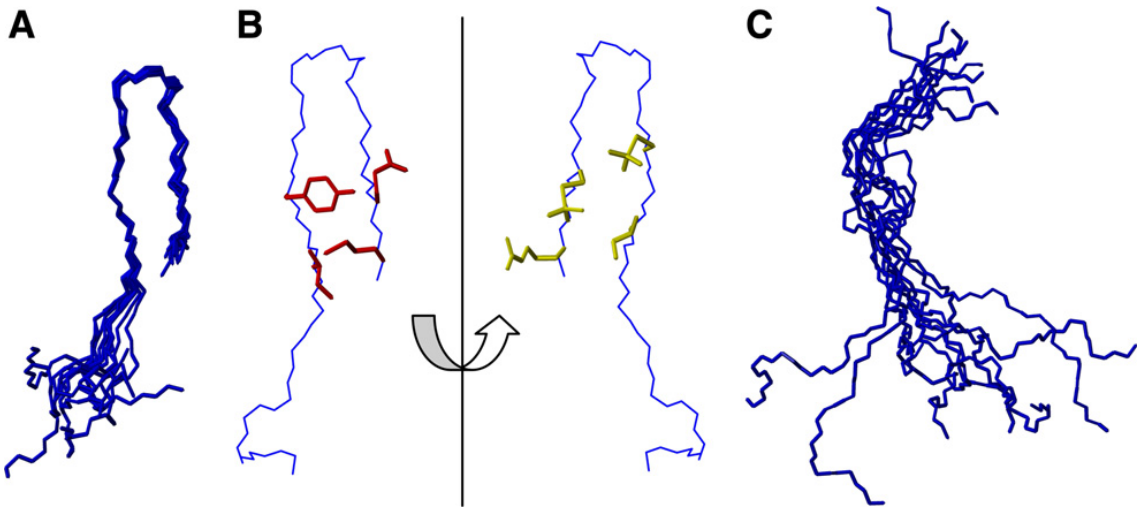

Figure 2. tructures of 11tBu/18tBu and C11S/C18S. (a) 10 structures of 11tBu/18tBu are superimposed in such that the RMSD of backbone heavy atoms from Ile9 to Arg20 is minimum. (b) Side-chains of 11tBu/18tBu interacting with each other are represented. red side-chains represent Ile8, Tyr10, Gln19 and Met21, and yellow side-chains represent Ile9, tBu-Cys11, tBu-Cys18 and Arg20. Backbone is colored in blue. (c) The structure of C11S/C18S. 10 best structures are superimposed as RMSD of backbone heavy atoms from Ile9 to Arg20 is minimum.

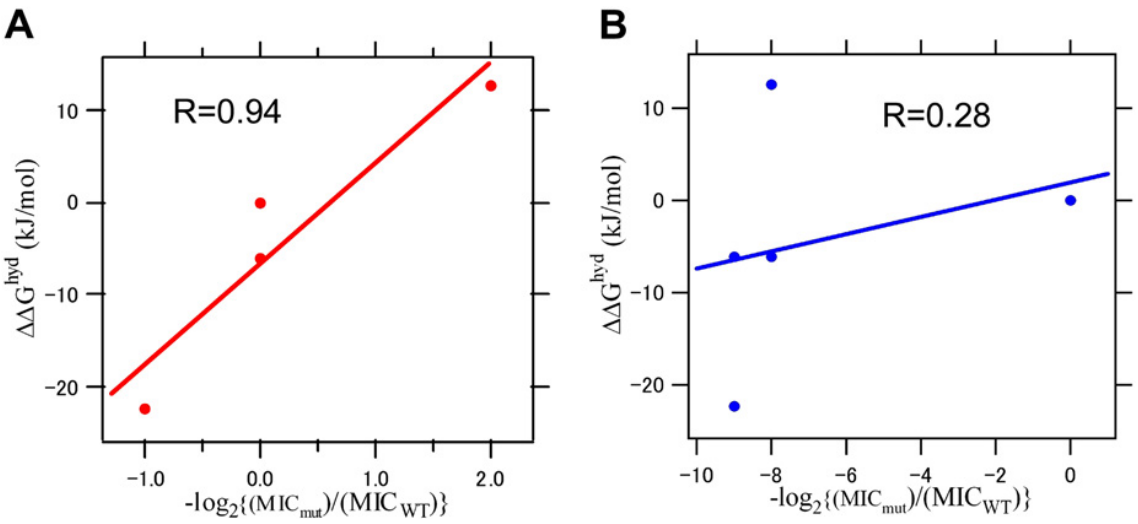

Figure 3. Relationships between the relative hydration energy and relative activity in case of (a) *M.luteus* and (b) *E.coli*. Correlation coefficients are shown in each graph. Relative activity was calculated according to the equation $-\log_2\{(MIC_{mut})/(MIC_{WT})\}$, in which MIC_{mut} means MIC values of mutant peptides and MIC_{WT} means the MIC value of thanatin. Side-chain hydrophobicity was calculated based on the data obtained by Privalov et al. (30). The difference in the hydration energy was calculated by $\Delta\Delta G^{hyd}=\sum\Delta G^{hyd}_{mut}-\sum\Delta G^{hyd}_{WT}$, in which $\Delta\Delta G^{hyd}$, $\sum\Delta G^{hyd}_{mut}$, and $\sum\Delta G^{hyd}_{WT}$ are relative hydration energy, hydration energy of each peptide, and that of thantain, respectively. The values for tBu-Cys and cystine residues were obtained by summating each functional group.

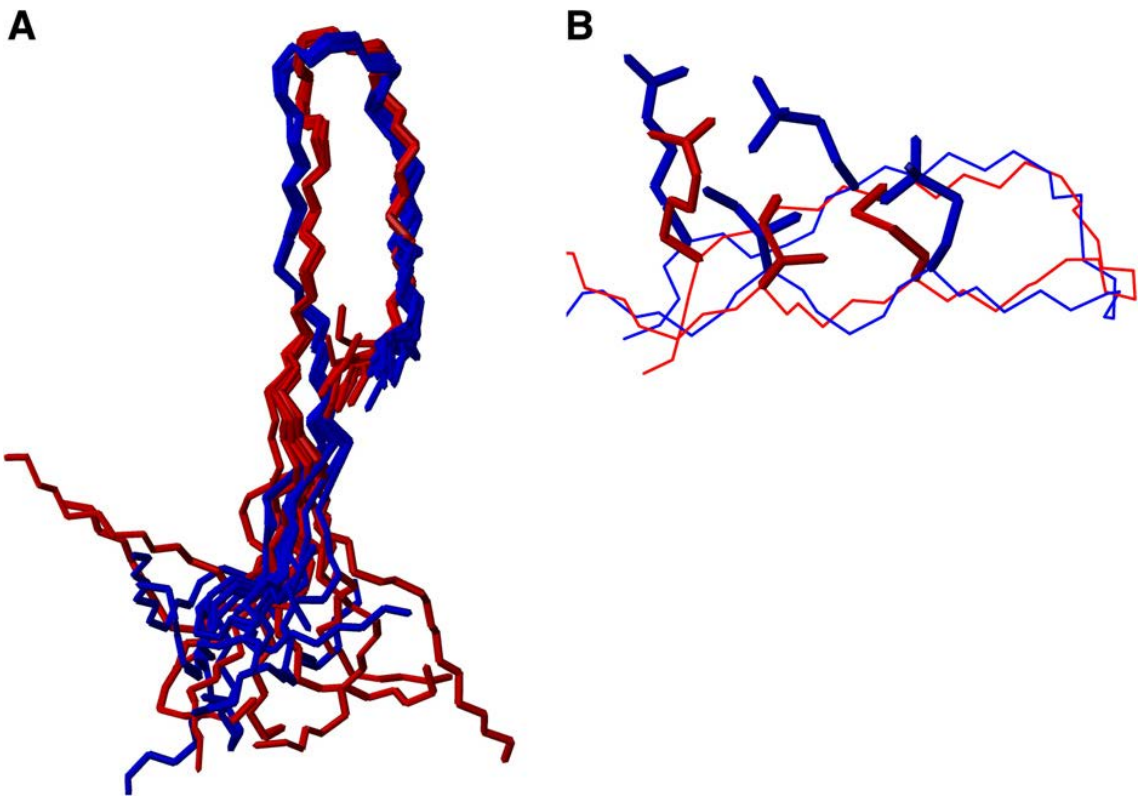

Figure 4. Structural comparison of 11tBu/18tBu and thanatin. (a) Calculated 10 conformers of 11tBu/18tBu (colored in blue) are superimposed by that of thanatin (red) in such a way that backbone RMSD from Ile9 to Arg20 is minimized. The structure of thanatin is obtained from PDB entry (PDB ID; 8TFV). (b) Side-chains of Ile9, Xaa11, Xaa18, and Arg20 of 11tBu/18tBu are represented. 11tBu/18tBu is colored in blue, and thanatin is in red. Backbones of each peptide are represented by thin lines.

Chapter III

Designed low amphipathic peptides with α-helical propensity exhibiting antimicrobial activity via a lipid domain formation mechanism

Abstract

Although several low amphipathic peptides have been known to exhibit antimicrobial activity, their mode of action has not been completely elucidated. In this study, using designed low amphipathic peptides that retain different α-helical content and hydrophobicity, we attempted to investigate the mechanism of these properties. Calorimetric and thermodynamic analyses demonstrated that the peptides induce formation of two lipid domains in an anionic liposome at a high peptide-to-lipid ratio. On the other hand, even at a low peptide-to-lipid ratio, they caused minimal membrane damage, such as flip-flop of membrane lipids or leakage of calcein molecules from liposomes, and never translocated across membranes. Interaction energies between the peptides and anionic liposomes showed good correlation with antimicrobial activity for both *Escherichia coli* and *Bacillus subtilis*. We thus propose that the domain formation mechanism in which antimicrobial peptides exhibit activity solely by forming lipid domains without membrane damage is a major determinant of the antimicrobial activity of low amphipathic peptides. These peptides appear to stiffen the membrane such that it is deprived of the fluidity necessary for biological functions. We also showed that to construct the lipid domains, peptides need not form stable and cooperative structures. Rather, it is essential for peptides to only interact tightly with the membrane interface via strong electrostatic interactions and slight differences in binding strength invoked by differences in hydrophobicity. The peptides thus designed might pave a way for “clean” antimicrobial reagents that never cause release of membrane elements and efflux of their inner components.

Introduction

Secretion of antimicrobial peptides in organisms is an essential innate immune response against bacterial infections [1]. These peptides attract attention as good clinical medicines with no side effects because they are effective against bacteria, fungi, and sometimes viruses without serious damage to the host [1; 2]. Generally, antimicrobial peptides are composed of 10–50 amino acids that are rich in positive charges and hydrophobic residues [1]. Their structures are usually categorized into three groups: α-helical structures formed in the presence of membranes; disulfide-bonded β-hairpin structures; and disulfide-bonded tertiary structures composed of α-helices and β-sheets [3]. The currently known mechanisms of action of these peptides are membrane disruption, pore formation, and interaction with intracellular targets [4] after permeating membranes [3; 5; 6; 7]. These peptides often retain amphipathic structures that are important for damaging bacterial membranes, which are mainly composed of phospholipids [1]. A wide variety of antimicrobial peptides [8; 9; 10; 11] and organic antimicrobial reagents [12; 13] have been designed based on the amphipathic motif, resulting in high activities. Among the three structural groups, α-helical antimicrobial peptides have been intensively investigated. Several studies have indicated that formation of amphipathic and stable structures on bacterial membranes is responsible for the potential to exhibit antimicrobial activity [14]. On the other hand, the mechanisms of α-helical antimicrobial peptides that do not retain high amphipathicity on membranes are not well understood [15; 16].

Domain formation in which there is aggregation of one kind of membrane lipid occasionally occurs when antimicrobial peptides interact with membranes [17; 18; 19]. Relationships between lipid domain formation and antimicrobial activity have been studied using amphipathic peptides and amphipathic organic compounds [20; 21; 22; 23]. In these cases, domain formation results in pore formation or membrane permeation. However, whether low amphipathic peptides can induce domain formation is not known. Therefore, we attempted to elucidate the mechanism of action of low amphipathic antimicrobial peptides by evaluating their ability to form domains. As a model for a low amphipathic antimicrobial peptide, we focused on LFB [24; 25]. LFB was obtained by deleting an amino acid sequence constructing the second β-strand of the amphipathic antimicrobial peptide LfcinB [26]. LFB is one of the most suitable peptides for studying the mode of interaction between peptides and membranes because it can bind to membranes, although it exhibits poor amphipathicity when the α-helical structure is formed [25].

In this paper, we propose domain formation as a mechanism of antimicrobial activity using six cationic and low amphipathic LFB analogs called *LAPs*, which were designed to retain various membrane affinities and structural stabilities. The ability to form lipid domains on liposomes composed of DMPC:DMPG = 1:1 were studied by differential scanning calorimetry (DSC), which is a powerful tool for monitoring lipid domain formation [21; 27]. Binding free energies against POPC:POPG = 1:1 were calculated for use as parameters reflecting the degree of lipid domain formation. Structural stabilities on membranes were determined by measuring CD spectra in the presence of liposomes composed of POPC:POPG = 1:1. Consequently, it was shown that LAPs induced domain formation without forming stable α-helix structures after they tightly bound to membrane surfaces with the help of strong electrostatic interactions. Using POPC:POPG = 1:1 containing calcein inside or a liposome composed of POPC:POPG:C_6-NBD-PC = 100:100:1, we confirmed that LAPs rarely induced leakage of liposomal inner components or lipid flip-flop. Furthermore, using a liposome composed of POCP:POPG:dansyl-DHPE = 10:9:1, we confirmed that peptides never translocated across the membrane. We therefore propose that LAPs exhibit antimicrobial activity solely by the domain formation mechanism.

Materials and Methods

Materials

POPC, POPG-Na, DMPC, and DMPG-Na were purchased from NOF Corporation (Tokyo, Japan); C_6-NBD-PC was purchased from Avanti Polar Lipids Inc., (Alabama, USA); and dansyl-DHPE was purchased from Invitrogen (Oregon, USA). Other materials were purchased from Wako Chemical Ltd. (Osaka, Japan).

Peptide synthesis and purification

Peptides were synthesized on the Pioneer Peptide Synthesis System (PerSeptive Biosystems, CA) using Fmoc solid-phase chemistry. After synthesis, peptides were cleaved from resins with a solution containing 82.5% (vol/vol) TFA, 5% thioanisole, 2.5% 1,2-ethanedithiol, and 0.8 M phenol. The cleaved powders were purified by reverse phase HPLC equipped with an acetonitrile-water solvent system containing 0.1% TFA. Peptide identities were confirmed by the laser desorption time of flight mass spectrometry AXIMA-CFR (Shimadzu, Kyoto, Japan). Peptide concentrations were determined by absorbance at 280 nm as described previously [28] on a Jasco V-650 spectrophotometer (Tokyo, Japan).

Preparation of liposomes

All unilamellar liposomes used in this study were prepared by the exclusion method [29]. In brief, lipid powders were dissolved in chloroform and the solvent was dried overnight using a rotary evaporator. Then a buffer solution was added to the dried lipid film and vortexed till the film was completely dispersed. The buffer compositions were as follows: 10 mM phosphate and 100 mM NaCl (pH = 7.5) for POPC/POPG (1:1) and DMPC/DMPG (1:1); 10 mM HEPES, 100 mM NaCl, and 1 mM EDTA (pH = 7.5) for POPC/POPG/C_6-NBD-PC (100:100:1) and POPC/POPG/dansyl-DHPE (5:4:1); or 100 mM calcein, 10 mM HEPES, and 100 mM NaCl (pH = 7.5) for POPC/POPG (1:1) containing calcein, respectively. POPC/POPG (1:1) containing calcein was freeze-thawed 5 times after it was dissolved in buffer. Then the solutions were extruded through a 100-nm pore-size filter using a Mini-Extruder (Avanti Polar Lipids, Inc., USA). After exclusion, 1 M $Na_2S_2O_4$ solution in 1 M HEPES (pH 7.6) was added to POPC/POPG/C_6-NBD-PC (100:100:1) and incubated for 15 min at room temperature to quench NBD chromophores of the outer leaflets [30]. Then the solution was washed down with a buffer solution composed of 10 mM HEPES, 100 mM NaCl, and 1 mM EDTA (pH = 7.5) through a PD-10 column (GE Healthcare, USA) to remove $Na_2S_2O_4$ and excess buffer substances. POPC/POPG (1:1) solutions containing calcein were also purified in the same way with a buffer solution composed of 10 mM HEPES, 100 mM NaCl, and 1 mM EDTA (pH = 7.5) to remove calcein outside the liposomes. Lipid concentrations were directly calculated from the weight of powders for POPC/POPG (1:1), DMPC/DMPG (1:1), and POPC/POPG/dansyl-DHPE (5:4:1) or were measured by the phosphorus assay for other liposomes [31].

Antimicrobial assay

Antimicrobial activity was examined by the MIC method [32]. First, *Escherichia coli BL21* and *Bacillus subtilis ISW1214* were cultivated overnight in LB broth. Then 100-μl aliquots of the cultivated solutions were again added to 3 ml of fresh LB broth and recultured. When bacterial growths reached the logarithmic phase, the cultivated solution was diluted 10 000-fold with the original broths (the composition of the original broths per 1 l of solution was as follows: 5 g mixtures of naturally occurring 20 amino acids (mixture fraction was used according to a previous study [33]), 478 mM Na_2HPO_4, 220 mM KH_2PO_4, 85 mM NaCl, 1 mM $MgSO_4$, 0.1 mM $CaCl_2$, 0.4% (w/w) glucose, and 0.005% (w/w) yeast extract). Then 80 μl aliquots of the diluted solution were added to 20 μl of a peptide solution successively diluted 1.5-fold with

water. The mixed solutions were shaken at 1000 rpm and at 25°C on a 96-well plate (Sumilon, Sumitomo Bakelite Co., Ltd., Japan). MIC was defined as the least peptide concentration in which there was no bacterial growth after 24 h of shaking for *E. coli* and 48 h for *B. subtilis*.

Hemolysis assay

The hemolysis assay was performed using red blood cells purified from sheep blood (abbreviated as sRBC) by a standard purification method described elsewhere. In this assay, a 100-µl peptide solution at an arbitrary concentration dissolved in PBS (9.5 mM phosphate buffer, 140 mM NaCl, and 2.7 mM KCl, pH 7.4) was added to 2% (vol/vol) sRBC of the same volume. After the mixed solution was incubated for 1.5 h at 25°C, the solution was centrifuged at 18 000 ×*g* and the absorbance of the supernatant at 577 nm was measured on a V-650 spectrophotometer. Hemolysis is defined as

$$\text{hemolysis}(\square) = \frac{A_{\text{peptide}} - A_{\text{PBS}}}{A_{\text{Triton}} - A_{\text{PBS}}} \times 100 \quad (1),$$

where A_{peptide} represents absorbance of an sRBC solution to which peptides were added, and A_{PBS} or A_{Triton} represents absorbance of an sRBC solution to which PBS or 2% (vol/vol) TritonX-100 was added instead of a peptide solution, respectively.

Two-dimensional NMR spectroscopy and structure calculation

In these experiments, a peptide powder was dissolved in 25 mM 3*d*-acetate, 17.5 mM NaOH, 90% H_2O, and 10% D_2O at a final concentration of approximately 2 mM. The pH of each solution was around 5.0. To determine the structures, we took a series of 2D-NMR measurements—COSY [34], TOCSY [35], NOESY [36], and DQF-COSY [37]—using a DMX750 spectrometer equipped with a Z-field magnetic gradient pulse emitter operating at a proton frequency of 750.03 MHz (Bruker Co., Ltd.). The mixing times of TOCSY and NOESY were set to 80 and 250 ms, respectively. To eliminate ^{1}H signals originating from water, its magnetization was saturated by irradiating a weak magnetic field on its frequency in COSY and DQF-COSY experiments; the WATERGATE pulse sequence [38] was used in TOCSY and NOESY experiments. All measurements were taken at 25°C. Data processing was performed using NMRDraw ver. 2.4 packaged in NMRPipe [39]. To display all spectra and assign cross-peaks in NOESY spectra, Sparky ver. 3.111 was used (T. D. Goddard and D. G. Kneller, University of California). Peak assignments in the NOESY spectra were performed by the sequential assignment method [40]. The φ angle constraints were determined from $^3J_{\text{HN-H}\alpha}$ values obtained from DQF-COSY spectra [41]. They were classified into

three categories: −120° ± 70°, −120° ± 50°, and 120° ± 40° corresponding to $^{3}J_{\mathrm{HN\text{-}H\alpha}}$ <7.5, 7.5–8.5, and >8.5 Hz, respectively [42]. Solution structures in water were calculated using DYANA ver. 1.5 [43]. First, the volumes of cross-peaks in a NOESY spectrum were converted to upper distance restraints on the macro CALIBA. Then structure calculations were performed by running the simulated annealing macro ANNEAL. Finally, 10 structures with distance violation not exceeding 0.3Å and φ angle violation not beyond 3° were obtained out of 100 initial structures generated in random conformations. Credibility of structures was confirmed using the PROCHECK-NMR program [44]. Structures were displayed and analyzed on MOLMOL [45].

Differential scanning calorimetry (DSC)

DSC measurements were performed on a VP-DSC microcalorimeter (Microcal, Northampton, MA). Samples were scanned from 4° to 35°C or 40°C at the heating rate of 20°C/h with the high feedback mode to obtain the correct heat-absorbing profile [46]. In this study, we chose the liposome composed of DMPC:DMPG = 1:1 instead of POPC:POPG = 1:1 that was used in the other experiments to avoid freezing of the samples because the melting temperature of POPC or POPG is below the freezing point [47]. DMPC/DMPG (1 mM, 1:1) solutions in the presence or absence of 20 μM peptides in phosphate buffer (10 mM phosphate and 100 mM NaCl, pH 7.5) were used for the measurements. Samples containing peptides were equilibrated for 10 min after adding the peptide solution. Before each scan, samples were equilibrated for 15 min at 4°C, and scans were repeated until the subsequent thermogram became identical to the former one. Buffer subtraction, baseline correction, and analyses of thermograms were performed using Microcal Origin software (Microcal, Northampton, MA).

Peptide-liposome titration experiments monitored by fluorescence

Peptide-liposome titration experiments were performed by measuring tryptophan fluorescence spectra at different liposomal concentrations [4; 48]. A 1-ml aliquot of a 10-μM peptide solution prepared in a 10 × 10 mm quartz cuvette was titrated by a 2-μl drop of 12.7 mM or 25.5 mM POPC/POPG (1:1); then a fluorescence spectrum was measured in the range of 260 to 400 nm by exciting at 280 nm on a FP-6500 spectrofluorometer (Jasco, Japan) at 25°C. A 30-μM L-tryptophan solution and buffer solution were also titrated in the same manner for correcting raw spectra. Buffer solutions composed of 10 mM phosphate and 100m M NaCl (pH = 7.4) were used for all samples. Correction of the liposomal scattering effects in fluorescence spectra can be achieved according to the equation [4; 49]

$$F_{\text{peptide}}^{\text{corr}} = (F_{\text{peptide}}^{\text{liposome}} - F_{\text{buffer}}^{\text{liposome}}) \cdot \frac{(F_{\text{trp}} - F_{\text{buffer}})}{(F_{\text{trp}}^{\text{liposome}} - F_{\text{buffer}}^{\text{liposome}})} \quad (2),$$

where $F_{\text{peptide}}^{\text{corr}}$ represents a corrected spectrum, and $F_{\text{peptide}}^{\text{liposome}}$, $F_{\text{trp}}^{\text{liposome}}$, and $F_{\text{buffer}}^{\text{liposome}}$ represent the fluorescence spectra of a peptide solution, tryptophan solution, and buffer solution at the same titration points of liposomes, respectively. F_{trp} and F_{buffer} represent the fluorescence spectra of tryptophan and buffer solutions, respectively. Binding curves were obtained by tracing intensities at 342 nm in each spectrum. The titration curves were analyzed based on a bimolecular interaction model [50; 51]. In this model, one free peptide in water binds to one liposomal site composed of a constant number of lipid molecules. The reaction scheme is represented as

$$P_f + nL_f \rightleftharpoons PL_n,$$

where P_f, L_f, and PL_n represent a free peptide in water, an unbound lipid, and a complex of peptide and lipids, respectively; n denotes the number of lipid molecules constituting the binding site for one peptide. In this scheme, the apparent dissociation constant K_d is defined as,

$$K_d = \frac{[P_f][L_f]}{n[PL_n]} \quad (3),$$

where $[P_f]$, $[L_f]$, and $[PL_n]$ represent concentrations of free peptides, free lipids, and peptide-lipid complexes, respectively. Values of n and K_d can be obtained by fitting titration curves in the equation below:

$$F = F_0 + (F_\infty - F_0) \times f_b \quad (4)$$

so that

$$\begin{aligned} f_b &= \frac{[PL_n]}{[P_f] + [PL_n]} \\ &= \frac{1}{2}\left[1 + \frac{[L]}{n[P]} + \frac{K_d}{[P]} - \sqrt{\left(1 - \frac{[L]}{n[P]} - \frac{K_d}{[P]}\right)^2 + \frac{4K_d}{[P]}}\right] \end{aligned} \quad (5).$$

F represents fluorescence intensity in an arbitrary lipid concentration, and F_0 and F_∞ represent fluorescence intensities in no lipid and infinite lipid concentrations, respectively. [P] and [L] represent total peptide and total lipid concentrations, respectively. All fittings were carried out using IGOR Pro (WaveMetrics, Inc., USA).

The partition free energy, which is a standard Gibbs free energy of transferring peptides from water to liposomal surfaces [52], was also calculated using the parameters

defined above. The partition free energy ΔG_x^0 was calculated as follows:

$$\Delta G_x^0 = -RT\ln K_x \quad (6),$$

so that

$$K_X = \frac{[PL_n][W]}{[P_f][L]} = \frac{[W]}{nK_d} \quad (7)$$

R is the gas constant and T is the absolute temperature; [W], which is concentration of water at 25°C, is equal to 55.5 (mol/l).

CD spectroscopy

CD spectra were acquired at 25°C on a J-720 spectropolarimeter (Jasco, Japan) using quartz cells whose path length is 0.5 or 1.0 mm. For all samples, peptide concentrations were set to 50 μM and buffer solutions composed of 10 mM phosphate and 100 mM NaCl (pH 7.4) were used. Lipid concentrations of POPC/POPG (1:1) were set to 5 mM. For each measurement, 32 scans were repeated and these scans were accumulated.

The TFE titration points obtained in CD spectra were fitted by using the two-state transition curve described by the equation below;

$$\Theta_{exp} = \frac{\Theta_{helix} - \Theta_{rc}}{1 + \frac{\exp(-m[TFE]/RT)}{K_0}} + \Theta_{rc} \quad (8),$$

where Θ_{exp} represents experimentally obtained mean residue ellipticity, and Θ_{helix} or Θ_{rc} represents mean residue ellipticity in which peptides completely form helices or mean residue ellipticity in a 6M urea solution, respectively. [TFE] denotes a TFE concentration at each point of titrations. m is a constant of proportionality, and generally called “m-value” [53; 54]. K_0 is an equilibrium constant between unfolded and folded states at [TFE] = 0, defined as $(\Theta_0-\Theta_{rc})/(\Theta_{helix}-\Theta_0)$ in which Θ_0 is mean residue ellipticity at [TFE] = 0. Θ_{helix}, m, K_0 and Θ_0 can be obtained as a result of fitting a titration curve. A three-state model was adapted to the TFE titration curve of LAP6 in the CD experiment. This situation can be represented in the following scheme;

$$D \Leftrightarrow N_1 \Leftrightarrow N_2$$

$$c(1-\alpha)\ c\alpha(1-\beta)\ c\alpha\beta\ (mol/l)$$

where c is total concentration of the peptide, and α and β are the extents of the first and

the second reaction, respectively. The equilibrium constants for the two reactions, K_1 and K_2 are defined as:

$$K_1 = \frac{[\mathrm{N}_1]}{[\mathrm{D}]} = \frac{\alpha(1-\beta)}{1-\alpha} \tag{9}$$

$$K_2 = \frac{[\mathrm{N}_2]}{[\mathrm{N}_1]} = \frac{\beta}{1-\beta} \tag{10}$$

so that:

$$\alpha = \frac{K_1(1+K_2)}{1+K_1+K_1K_2} \tag{11}$$

$$\beta = \frac{K_2}{1+K_2} \tag{12}.$$

K_1 and K_2 are also described as;

$$\begin{aligned} K_1 &= K_1^0 \exp\left(\frac{m_1[\mathrm{TFE}]}{RT}\right) \\ &= \frac{\Theta_0 - \Theta_{\mathrm{rc}}}{\Theta_{\mathrm{N}_1} - \Theta_0} \cdot \exp\left(\frac{m_1[\mathrm{TFE}]}{RT}\right) \end{aligned} \tag{13}$$

$$K_2 = K_2^0 \exp\left(\frac{m_2[\mathrm{TFE}]}{RT}\right) \tag{14}$$

where K_1^0 and m_1 are the equilibrium constant in [TFE]=0 and m-value of the first reaction, respectively. Θ_0, Θ_{rc} and Θ_{N_1} represent mean residue ellipticity in [TFE] = 0, mean residue ellipticity in a 6M urea solution, and mean residue ellipticity of the N_1 state at 225nm, respectively. K_2^0 and m_2 are the equilibrium constant in [TFE] = 0 and m-value in the second reaction, respectively. By using equation (11)-(14), mean residue ellipticity at 225nm, Θ_{exp}, can be fitted as follows;

$$\Theta_{\mathrm{exp}} = \Theta_{\mathrm{rc}}(1-\alpha) + \Theta_{\mathrm{N}_1}\alpha(1-\beta) + \Theta_{\mathrm{N}_2}\alpha\beta \tag{15}$$

where Θ_{N_2} represents mean residue ellipticity of the N_2 state. In actual fitting, the value of Θ_{N_2} is fixed to the value of Θ_{helix} of LAP5, since mean residue ellipticity never became a constant value even at the highest TFE concentration tested. This approximation would be accepted because LAP5 and 6 have the same amino-acid

compositions and are expected to have same mean residue ellipticity when helices are completely formed. The actual plots and the fitting curve are shown in Figure 5, A-F. The fraction of helix in water f_α^{W} or in the presence of liposomes f_α^{L} was calculated using parameters obtained by fitting TFE titration measurements [4]. The fitting curves are derived below.

$$f_\alpha^{W} = \frac{\Theta_0 - \Theta_{rc}}{\Theta_{helix} - \Theta_{rc}} \quad (16)$$

$$f_\alpha^{L} = \frac{\Theta^{L} - \Theta_{rc}}{\Theta_{helix} - \Theta_{rc}} \quad (17),$$

where Θ_0 is mean residue ellipticity at [TFE] = 0, and Θ_{helix} or Θ_{rc} represents the mean residue ellipticity in which peptides completely form helices or mean residue ellipticity in a 6-M urea solution, respectively. Θ^{L} represents mean residue ellipticity at 225 nm in the presence of liposomes.

Lipid flip-flop monitoring

Whether the peptide could induce lipid flip-flop was confirmed by adding peptides to asymmetrically labeled liposomes with C_6-NBD-PC and monitoring quenching of fluorescence intensities of NBD chromophores by $Na_2S_2O_4$. Lipid flip-flop was monitored as follows: first, 1 ml aliquots of a peptide stock solution (100 mM HEPES, 100 mM NaCl, and 1 mM EDTA, pH 7.5) were added to 1 ml aliquots of the asymmetrically labeled liposome solution prepared in a 10 × 10 mm quartz cuvette as final concentrations of liposomes and peptides became 80 μM and 10 μM, respectively. Then, recording of fluorescence intensity at 530 nm was started every second for 800 min by excitation at 470 nm. Thirty seconds after mixing, 10 μl aliquots of 1 M $Na_2S_2O_4$ solution were added to the solution to quench external chromophores and recording was restarted. As a control experiment, 1% Triton-X100 was utilized instead of peptides to completely induce lipid flip-flop.

Calcein leakage monitoring

Whether peptides could leak components inside the liposome was confirmed by adding peptides to the calcein-containing liposome solution and monitoring increases in fluorescence intensities derived from leaking calcein. Calcein leakage was monitored as follows: the liposome solution in a 10 × 10 mm quartz cuvette was excited at 490 nm

and fluorescence intensities were monitored at 517 nm. After 50 s, a scan was started and a peptide solution was added to the liposome solution as final concentrations reached 10 μM and 80 μM, respectively. The solutions were monitored for 800 min. As a control experiment, 1% TritonX-100 was utilized instead of peptides to induce complete leakage.

Peptide translocation assay

Peptide translocation across the liposomal lipid bilayer was monitored using a liposome symmetrically labeled by dansyl-DHPE. When peptides that contain tryptophan residues bind to the labeled liposome, the energy of the fluorescent tryptophan is transferred to the dansyl chromophore resulting in an increase in fluorescence of the chromophore. Excess amounts of peptides were added to the liposome and successive changes of fluorescence intensity at 510 nm were monitored by exciting at 280 nm. If the peptides were able to translocate across the liposome, a further increase in the intensities was expected because the peptides would have interacted with the liposomal inner surface. As a positive control experiment, translocation was efficiently induced by freeze-thawing liposome solutions that contained the same amount of peptides introduced in the assays [55]. Freeze-thawing was repeated three times after the peptides and liposome were mixed and left for 5 min, and almost no disruption or fusion of the liposome was observed by DLS.

Results

Peptide design

Cationic and low amphipathic peptides that retain various degrees of hydrophobicity and structural stability were designed as follows: first we found that attachment of the amino acid sequence “QPEW” into the N-terminus of LFB by referring to the corresponding sequence in lactoferrin and a mutation of the cysteine residue into alanine resulted in formation of an α-helical structure that retained sufficient helical content to be determined by NMR measurements (Figure 1). Accordingly, other mutants that have different structural stability or hydrophobicity were obtained by attaching (LAP2, 3, and 4) or deleting (LAP5) N-terminal amino acids of LAP1 by referring to the corresponding amino acid sequence of lactoferrin. To obtain a peptide whose structural transition is less cooperative, LAP6 was designed in which Q9 and G16 in LAP5 were interchanged and thus the helix-breaking glycine residue was located in the middle of the chain. We confirmed that LAP2–6 as well as LAP1 form α-helical structures that

retain sufficient helical contents to enable determination by NMR measurements in water (Figure 1). All the sequences and properties of LAPs are summarized in Table 1. For all LAPs, the values of the helical hydrophobic moment $<\mu_H>$, which determines the degree of amphipathicity of α-helical peptides [56] ranging from 0.055 to 0.12 (Table 1). These values are apparently lower than those for typical amphipathic antimicrobial peptides such as melittin [57] or magainin [58] (Table 1). Thus, they can be regarded as low amphipathic peptides. We determined hydrophobicity of LAPs using the Wimley-White scale which is a series of experimentally obtained partition coefficients of 20 naturally occurring amino acids between water and the membrane interface composed of POPC head groups since we can also apply the scale to liposomes composed of POPC:POPG = 1:1 [4]. According to the scale, LAPs are classified into a hydrophilic peptide group (Table 1). Among LAPs, LAP5 and 6 are clearly less hydrophilic than the others.

NMR-based structures in water

Structural calculation of each peptide based on NMR measurements resulted in α-helix structures (Figure 1). Except for LAP2, a unique conformation is obtained. LAP2 seems to have two or more different conformations since some distance constraints existing in N-terminal residues are recognized as violations in the structural calculation. Subsequently, we divided these violating constraints into two groups, and the structures were recalculated independently using the divided restraints and undivided common restraints. One divided group contains restraints typical of α-helical structures; these calculated structures are named LAP2-conf1. The other divided group contains remaining constraints; these calculated structures are named LAP2-conf2. Since restraints divided into one group are always recognized as violations in the calculation using the restraints divided into the other group, we concluded that LAP2 retains the two conformations LAP2-conf1 and LAP2-conf2 as the α-helical structures.

Antimicrobial and hemolytic activities

Antimicrobial and hemolytic activities of LAPs are shown in Table 2. MIC values for *E. coli* and *B. subtilis* are on micromolar scales indicating that they are sufficiently antimicrobial. LAP5 and 6 are clearly more active than the other peptides. The reason why LAPs are more effective against *B. subtilis* than *E. coli* is discussed in relation to the differences in their membrane lipid compositions in *Discusssion* of the present study. In contrast to antimicrobial activity, LAPs showed almost no hemolytic activity even at a high concentration (400 μM).

DSC measurements

The main transition of the peptide-free liposome occurred at 24.5°C within a short temperature range (half bandwidth, $\Delta T_{1/2}$ = 0.6°C) and with large heat absorption (ΔH_m = 6.31 kcal/mol) after a broad pretransition at 16.6°C with low heat absorption (ΔH_{pre} = 0.44 kcal/mol) (Figure 2 and Table 3). These results are consistent with those reported in literature where pure DMPC and DMPG liposomes preliminary melt over a broad range starting at 13.6°C and 8.6°C with little heat absorption (ΔH_{pre} = 0.9 and 0.4 kcal/mol, respectively), then melt cooperatively at 23.8°C and 22.1°C with large heat absorption (ΔH_m = 6.6 and 6.2 kcal/mol, respectively), respectively [59].

In contrast, when LAPs were incubated with the liposome at [peptide]:[lipid] = 1:50, the resultant liposome melted in a manner different from pure liposome (Figure 2). Each thermogram contains two main transitions. While one transition occurs less cooperatively at a temperature higher than that of pure liposome, the other melts at a temperature lower than that of pure liposome. Appearance of these two main transitions strongly indicates that lipids became phase-separated upon mixing with the peptides, or that LAPs induced two “domains” with different physicochemical properties [21; 60]. However, the values of ΔH_m in the presence of LAPs were similar to those without LAPs (Table 3).

Peptide-liposome titration experiments monitored by tryptophan fluorescence

As shown in the Figure 3 insets, when drops of liposome solution are added consecutively to peptide solutions, successive blue shifts and increases in intensities are observed indicating that LAPs indeed bind to liposomes. In every peptide, the maximum wavelength of the emission spectrum finally reaches 342 nm. To obtain apparent binding constants, fluorescence titration curves monitored at 342 nm were fitted by applying Equation (4). In the analyses, lipid concentrations were divided by 2 because lipid molecules existing only on the outer leaflet were expected to be able to interact with peptides. This assumption is supported by the result that LAPs rarely translocate across the liposomal bilayer (described below). The titration points were properly fitted, and values of K_d and n were obtained within allowable errors (Figure 3 and Table 4). Each value of K_d is of a submicromolar order confirming that LAPs strongly interact with liposomes, and among them, the interactions of LAP5 and 6 are strongest. The values of n demonstrate that one peptide molecule interacts with 15–22 lipid molecules.

To examine the energetics of these interactions, we calculated the partition free

energy ΔG_x^0 using Equations (6) and (7). The values of ΔG_x^0 range from −8.7 to −10.1 kcal/mol (Table 4); these values are comparable to or larger than those of naturally occurring cationic antimicrobial peptides. For example, indolicidin, which is similar to LAPs in that it contains numerous cationic and hydrophobic residues, partitions into POPG liposomes at $\Delta G_x^0 \sim -11$ kcal/mol [61] and magainin, which is a typical amphipathic α-helical antimicrobial peptide, partitions into POPC:POPG = 3:1 liposomes at $\Delta G_x^0 = -4.8$ kcal/mol [62].

Structure and stability determined by CD measurements

It is known that the CD spectrum of a typical α-helical peptide represents two minima at 208 nm and 222 nm [63]. In contrast, the CD spectra of LAPs in water do not clearly retain such minima (Figure 4-A) indicating that the structural contents of α-helical conformations are low. Therefore, we measured CD spectra at different TFE concentrations to confirm their low propensity to form α-helices [4]. When TFE concentrations increased, successive increases were observed in the two minima at 208 nm and 222 nm in a sigmoidal manner (Figure 5, insets), confirming that α-helix structures are induced. The titration points of LAP 1–5 could be fitted using Equation (8), which was based on a two-state model (Figure 5, A–E). In contrast, the titration points of LAP6 could be properly fitted using Equation (15), which was based on a three-state model (Figure 5–F). Using Equation (16), the fraction of α-helices was calculated to range from 0.1 to 0.22 (Table 5) confirming that the α-helical contents of LAPs are low in water. The results apparently contradict the fact that we succeeded in determining evident α-helical structures by NMR (Figure 1). However, these two results are not contradictory because sufficient amount of NOE cross-peaks, which play a main role in NMR structural determination, can be observed even if the structural content is low. In fact, we confirmed that the helical contents determined using the main-chain spin coupling constant $^3J_{\mathrm{HN\text{-}H\alpha}}$, obtained by NMR measurements were identical to those obtained by the CD measurements within the range ±0.04.

When POPC/POPG (1:1) was added to LAPs, their CD spectra changed to some extent compared with those in water (Figure 4-A) confirming that LAPs changed their structures by interacting with liposomes. For LAP3 and 4, the difference in spectra obtained by subtracting a spectrum in water from that with liposomes resulted in the appearance of maximum peak at 230 nm and minimum peak at 220 nm (Figure 4-B, inset), which indicates the presence of a π-π stacking interaction [64]. This change may be derived from the enhanced interaction between sidechains of neighboring phenylalanine and tryptophan residues. On the other hand, for LAP1, 2, 5, and 6, the

difference in spectra indicated increases in secondary structure stability in addition to the presence of π-π stacking interactions since the spectrum contains a shoulder around 208 nm and a large negative peak around 222 nm. Therefore, we obtained a mean residue ellipticity corresponding to the increase in secondary structure stability using the mean residue ellipticity at 225 nm at which the spectra of LAP4 in water and with liposomes are isodichroic. The structural stabilities of LAPs were calculated using Equation (17) (Table 5). In LAP1, 2, 5, and 6, the stabilities were increased compared with those in water. On the other hand, in LAP3 and 4, the stabilities were as high as those in water.

Lipid flip-flop assay

Whether LAPs could cause lipid flip-flop were determined using asymmetrically labeled liposomes with C_6-NBD-PC. In this method, occurrence of lipid flip-flop is indicated by a decrease in fluorescence intensities of NBD groups [29]. FIgure 6-A shows the changes in fluorescence intensities after LAPs were added to the asymmetrically labeled liposomes followed by $Na_2S_2O_4$ addition. Despite a high molar ratio of peptides against lipids (1:8), almost no decrease was observed in fluorescence intensities for all LAPs indicating that they have little capacity to induce lipid flip-flop. LAP5 and 6, which retained highest antimicrobial activities, did not cause flip-flop even at peptide:lipid = 1:2 (data not shown).

Calcein leakage assay

Leakage of liposomal inner components by peptides was determined using liposomes with concentrated calcein in their interiors. In this method, leakage of calcein molecules from liposomes can be monitored by the increase in fluorescence intensities of calcein itself [29]. Figure 4-B shows traces of fluorescence intensities derived from calcein after LAPs were added to calcein-containing liposomes. Despite a high molar ratio of peptides to lipids (1:8), almost no increase in fluorescence intensity was observed indicating that little calcein leakage was induced by the peptides. LAP5 and 6, which retained highest antimicrobial activities, did not induce calcein leakage even at peptide:lipid = 1:1 (data not shown).

Peptide translocation assay

Peptide translocation through the membrane was monitored using dansyl-DHPE-labeled liposomes. First, we confirmed that tryptophan fluorescence resonance energy transfer to the dansyl group at 510 nm was proportional to the amount

of peptides added and saturated at specific peptide-to-lipid ratios that were similar to those observed in the peptide-liposome titration experiments confirming that an increase in the fluorescence intensities occurs only when peptides interact with the liposome (data not shown). Before the assay, we determined the fluorescence intensities at which peptide translocation reached equilibrium using the liposomes that were freeze-thawed three times (see Materials and Methods). We then monitored changes in intensity at 510 nm after excess amounts of peptides were added to the liposomes until the final concentrations of peptides and lipids reached 12.5 μM and 100 μM, respectively. When peptides were added to the liposome, an increase in fluorescence intensity was observed confirming that peptides indeed interacted with liposomes (Figure 7). However, no further increase in intensities was observed after 15 min indicating that their translocation efficiency was low. In addition, the intensities reached at significantly lower levels compared with those observed for the freeze-thawed samples in which sufficient translocation was expected to be induced. Thus, we conclude that LAPs rarely translocate across the membrane.

Discussion

Interaction of LAPs with liposomes

We first discuss how LAPs interact with liposomes based on DSC measurements and peptide-liposome titration experiments. In general, the change in enthalpy in the main transition ΔH_m obtained in DSC measurements originate from collapse of the interaction between lipid acyl chains, which steadily interact with each other by the hydrophobic van der Waals force in the rippled-gel phase [65]. Therefore, the changes in the value of ΔH_m due to peptide addition reflect the extent of influence on the hydrophobic regions by the peptide molecules. LAPs probably interact with the lipid head groups, i.e., the membrane interface, rather than penetrating into the hydrophobic regions since the value of ΔH_m of each peptide-containing sample is similar to that of the liposome only sample (Table 3).

This proposed explanation is also supported by two results. First, the maximum wavelength of tryptophan fluorescence spectra of LAPs reaches 342 nm when LAPs completely interact with membranes (Figure 3). This result indicates that indole rings are assumed to locate in a moderately hydrophobic environment, i.e., the membrane interface [66]. Second, if LAPs transversely interact with the membrane interface and not the hydrocarbon region in a transmembrane manner, the values of *n* are expected to be proportional to the surface area of peptides. Assuming that the peptide surface area

can be approximated by the number of amino acid residues, we plotted values of *n* against the number of residues of LAPs. As a result, a good correlation was observed between them (R = 0.97, data not shown). Therefore, we conclude that LAPs interact with the membrane interface.

Assignment of lipid domains observed from DSC measurement values

DSC measurement profiles clearly indicated that LAPs induced formation of two lipid domains (Figure 2). In general, (i) broadening of main transition peaks represents interactions between additives and liposomes, and (ii) increase in melting temperature indicates stabilization of a lipid gel phase by electrostatic interactions between peptides and lipid head groups [67; 68; 69; 70]. Applying these rules to our results, the main transition peak that was observed more broadly at a higher temperature than that at 24.5°C of the peptide-free liposome corresponds to the phase transition of the domain rich in anionic DMPG bound by cationic LAPs induced by electrostatic interactions. On the other hand, the main transition peak that occurs at a lower temperature can be assigned to the phase transition of the domain rich in DMPC. Some of these transitions occur broadly (LAP1, 2, 5, and 6) and the others occur sharply (LAP3 and 4) indicating that LAPs retain different affinities for the domain. Since DMPC carries no electric charge, interaction forces between LAPs and the domain are assumed to be determined by hydrophobicity and/or the extent of structural formations rather than electrostatic interactions. Except LAP1 and 2, the extent of broadening can be explained by peptide hydrophobicity: the transitions occur more broadly in LAP5 and 6, which are more hydrophobic than the other two peptides (LAP3 and 4) than those in LAP3 and 4. However, the rule becomes inadaptable in case of LAP1 and 2. This is because the proline residues of which the N-terminal peptide bond can retain two geometries i.e., *trans* and *cis* configurations may result in multiple conformations of the peptides, resulting in broadening of the transition peaks.

Structural properties required for domain formation without membrane damages

Typical α-helical antimicrobial peptides such as magainin and melittin are known to strongly induce membrane damage, such as membrane disruption, pore formation, or lipid flip-flop [71]. Furthermore, antimicrobial peptides that induce domain formation usually induce membrane damage after forming domains [72; 73]. The difference between such antimicrobial peptides and LAPs depends on whether they can form typical secondary structures on membranes. It is generally believed that secondary structures are favorably induced together with binding to membranes if the structures

formed are amphipathic [4]. Indeed, magainin and melittin form typical α-helical structures on membranes; helical contents calculated based on CD analyses are 0.64 for magainin [74] and 0.71 for melittin [57]. On the other hand, helical contents of LAPs are much lower than that of magainin and melittin (their helical content ranges from 0.22 to 0.42 (Table 5)). Therefore, low amphipathicity and thus little structural formation of LAPs must be the determinants that induce domain formation without incurring membrane damage. Furthermore, although LAP6 folds less cooperatively than LAP5 (Figure S2-E and F), both LAP6 and LAP5 induce domain formation without membrane damage (Figures 2 and 4). If this structural cooperativity is also retained at the membrane interface, it is assumed that structural cooperativity is not essential for domain formation without membrane damage.

Energetics of peptide-liposome interactions

Peptide-liposome interactions are usually determined by electrostatic interactions, hydrophobic interactions, and secondary structure formations [4; 61; 62]. To calculate each value, we employed the thermodynamic cycle mentioned below:

$$\begin{array}{ccc} & \overset{K_{\mathrm{fold}}^{\mathrm{W}}}{} & \\ \mathrm{D^W} & \rightleftharpoons & \mathrm{N^W} \\ K_{\mathrm{x}}^{\mathrm{unf}} \uparrow\downarrow & & \uparrow\downarrow \\ \mathrm{D^L} & \rightleftharpoons & \mathrm{N^L} \\ & \underset{K_{\mathrm{fold}}^{\mathrm{L}}}{} & \end{array}$$

$\mathrm{D^{W/L}}$ and $\mathrm{N^{W/L}}$ denote the unfolded and folded states in which the upper right characters signify in water (^{W}) or at the lipid membrane interface (^{L}). $K_{\mathrm{x}}^{\mathrm{unf}}$ represents the partition coefficient in unfolded states between water and at the membrane interface, which is described as $K_{\mathrm{x}}^{\mathrm{unf}} = [\mathrm{D^L}][\mathrm{W}]/[\mathrm{D^W}][\mathrm{L}]$. $K_{\mathrm{fold}}^{\mathrm{L}}$ and $K_{\mathrm{fold}}^{\mathrm{W}}$ represent the folding equilibrium constant on liposomal surfaces and in water, respectively, and are described as $K_{\mathrm{fold}}^{\mathrm{L}} = f_{\alpha}^{\mathrm{L}}/(1-f_{\alpha}^{\mathrm{L}})$ and $K_{\mathrm{fold}}^{\mathrm{W}} = f_{\alpha}^{\mathrm{W}}/(1-f_{\alpha}^{\mathrm{W}})$. Based on the thermodynamic cycle, the equation is given as,

$$\begin{aligned} K_{\mathrm{x}} &= \frac{([\mathrm{D^L}]+[\mathrm{N^L}])\cdot[\mathrm{W}]}{([\mathrm{D^W}]+[\mathrm{N^W}])\cdot[\mathrm{L}]} \\ &= K_{\mathrm{x}}^{\mathrm{unf}} \cdot \left(\frac{1-f_{\alpha}^{\mathrm{W}}}{1-f_{\alpha}^{\mathrm{L}}}\right) \end{aligned} \tag{18}$$

Equation (18) can be converted as follows:

$$\Delta G_{\mathrm{x}}^{0} = \Delta G_{\mathrm{x}}^{\mathrm{unf}} - RT\ln\left(\frac{1-f_{\alpha}^{\mathrm{W}}}{1-f_{\alpha}^{\mathrm{L}}}\right) \quad (19),$$

where $\Delta G_{\mathrm{x}}^{\mathrm{unf}}$ represents the standard free energy in the unfolded state and is described as $\Delta G_{\mathrm{x}}^{\mathrm{unf}} = -RT\ln K_{\mathrm{bind}}^{\mathrm{unf}}$. The second term of Equation (19) determines the contribution of secondary structure formation at the membrane interface to binding free energy. The values range from −0.24 to −0.02 (data not shown) and are much lower than the values of $\Delta G_{\mathrm{x}}^{0}$ (Table 4) indicating that the contribution of secondary structure formation is negligible. We then divide the remaining term $\Delta G_{\mathrm{x}}^{\mathrm{unf}}$ into electrostatic and hydrophobic components [61]. Finally, Equation (19) can be divided into the following two terms:

$$\Delta G_{\mathrm{x}}^{0} = \Delta G_{\mathrm{elec}}^{\mathrm{unf}} + \Delta G_{\mathrm{WW}} \quad (20),$$

where $\Delta G_{\mathrm{elec}}^{\mathrm{unf}}$ is the standard Gibbs free energy of electrostatic interaction in the unfolded state. The values of $\Delta G_{\mathrm{elec}}^{\mathrm{unf}} (= \Delta G_{\mathrm{x}}^{0} - \Delta G_{\mathrm{WW}})$ range from −10.6 to −10.0 kcal/mol (data not shown), and thus they are nearly identical. In contrast, although the values of ΔG_{WW} are positive, they correlate well with the values of $\Delta G_{\mathrm{x}}^{0}$ (R = 0.91, data not shown). Therefore, we conclude that (i) LAPs interact with the membrane interface with the help of large electrostatic interactions and (ii) the difference in interaction strength is determined by the extent of hydrophobicity of the peptides.

To compare the values of actual electrostatic interactions with an ideal value Gibbs free energy of the ideal electrostatic interaction $\Delta G_{\mathrm{elec}}^{\mathrm{ideal}}$ was calculated using the equation $\Delta G_{\mathrm{elec}}^{\mathrm{ideal}} = z^{\mathrm{ideal}} F\varphi$ [61; 75; 76]. z^{ideal} is an ideal charge of peptides, F is the Faraday constant, and φ is an electrical potential on liposomal surfaces. φ can be determined by the Gouy-Chapman theory [77], and we calculated φ to be 67 mV on the surfaces of liposomes composed of POPC/POPG (1:1) at 100 mM NaCl (the calculation method is almost the same as described in [77]). When the value of z^{ideal} was considered +5, $\Delta G_{\mathrm{elec}}^{\mathrm{ideal}}$ became −7.7 kcal/mol, which is greater than the actual values. These results

indicate that the electrostatic interactions between peptides and liposomes are positively nonadditive. This nonadditivity can be observed if one negative charge of the POPG head group interacts with more than one positive charge of peptides and vice versa. Thus, the nonadditivity supports formation of a lipid domain rich in cationic peptides and anionic POPG.

Implication of a new mechanism for antimicrobial activities

In general, antimicrobial peptides are believed to 1) disrupt membranes, 2) form pores, or 3) translocate across membranes after binding to membrane surfaces [3; 5]. In cases 1) and 2), obvious lipid flip-flop and/or leakage of small molecules from artificially constructed liposomes are usually observed at a low peptide-to-lipid ratio (at about 1:500 to 1:50) [29; 71]. On the other hand, LAPs rarely cause lipid flip-flop and calcein leakage even at a high peptide-to-lipid ratio (1:8) (FIgure 6-A and B). In case 3), peptide translocation across an artificially constructed membrane should be observed [58]. This mechanism, however, is not applicable for LAPs because they retain little capability to translocate across the artificially constructed membranes even at a high peptide-to-lipid ratio of 1:8 (FIgure 6-C). Instead, they induce lipid domain formation confirmed by DSC measurements even at a low peptide-to-lipid ratio (1:50) (Figure 2) after they bind strongly to anionic liposomal surfaces concomitant with forming partially folded α-helices, which are observed by peptide-liposome binding experiments (Table 4, Figure 3) and CD measurements (Table 5, Figure 4). Thus, we conclude that domain formation is the most probable mechanism of the antimicrobial activity of peptides. This conclusion is in contrast with the cases of other antimicrobial peptides that induce lipid domain formation because they are known to exhibit their activities by alternative mechanisms. For example, RL16, which is known to induce lipid domain formation, translocates across membranes [78].

If LAPs kill bacteria by this mechanism, the degree of domain formation is expected to correlate with antimicrobial activity. Because domain formation is induced solely by binding of peptides to membranes, the binding energies are believed to determine how strongly peptides induce the domain formation. To confirm this hypothesis, we scrutinized relationships between peptide-liposome binding forces and antimicrobial activity. As a result, good correlations between peptide-liposome binding energies and relative antimicrobial activity are observed for both *E. coli* and *B. subtilis* (Figure 7A and B, respectively), thus supporting the hypothesis.

Then, how do LAPs kill bacteria only by forming the domains on their membranes? Domain formation would restrict a two-dimensional free lipid movement, i.e., lipid

lateral diffusion resulting in lowered membrane fluidity. Low fluidity of membranes might interrupt movements of membrane proteins or prevent amitotic division of a cell. Furthermore, as mentioned by Epand et al [17], since each domain no longer retains its original lipid compositions, structures and functions of membrane proteins essential to life may be changed or inhibited. These damage to bacteria are believed to lead to inhibition of their regular activities resulting in their death. The mechanism is also supported by the fact that LAPs are about 100-fold effective against *B. subtilis* compared with *E. coli* (Table 2). It is generally believed that the target cell membrane of antimicrobial peptides against gram-positive and gram-negative bacteria are the cytoplasmic and inner membranes, respectively [60]. While about 75% of the cytoplasmic membrane lipids of *B. subtilis* consist of anionic lipids, the inner membrane of *E. coli* contains only 15% anionic lipids [60]. Thus, cationic LAPs are considered to have far more opportunities to induce domain formation on the membrane of *B. subtilis* than on *E. coli* because of the electrostatic attractions, resulting in more efficient killing of *B. subtilis* than *E. coli*.

Use of the peptides as clinical reagents

LAPs are different from known membrane-active antimicrobial peptides in that they rarely induce lipid flip-flop or leakage of liposomal inner components. Furthermore, the antimicrobial activities of LAPs are favorably comparable with naturally occurring antimicrobial peptides such as melittin [79] or magainin [80]. Therefore, LAPs are expected to be used as “clean” antimicrobial peptides that never cause release of bacterial membrane elements and efflux of their inner components, resulting in the prevention of secondary pollution caused by these contaminants.

References

[1] M. Zasloff, Antimicrobial peptides of multicellular organisms. Nature 415 (2002) 389-95.

[2] R.E. Hancock, and H.G. Sahl, Antimicrobial and host-defense peptides as new anti-infective therapeutic strategies. Nat Biotechnol 24 (2006) 1551-7.

[3] H. Jenssen, P. Hamill, and R.E. Hancock, Peptide antimicrobial agents. Clin Microbiol Rev 19 (2006) 491-511.

[4] M. Fernandez-Vidal, S. Jayasinghe, A.S. Ladokhin, and S.H. White, Folding amphipathic helices into membranes: amphiphilicity trumps hydrophobicity. J Mol Biol 370 (2007) 459-70.

[5] M.R. Yeaman, and N.Y. Yount, Mechanisms of antimicrobial peptide action and resistance. Pharmacol Rev 55 (2003) 27-55.

[6] C.B. Park, K.S. Yi, K. Matsuzaki, M.S. Kim, and S.C. Kim, Structure-activity analysis of buforin II, a histone H2A-derived antimicrobial peptide: the proline hinge is responsible for the cell-penetrating ability of buforin II. Proc Natl Acad Sci U S A 97 (2000) 8245-50.

[7] V.V. Andrushchenko, M.H. Aarabi, L.T. Nguyen, E.J. Prenner, and H.J. Vogel, Thermodynamics of the interactions of tryptophan-rich cathelicidin antimicrobial peptides with model and natural membranes. Biochim Biophys Acta 1778 (2008) 1004-14.

[8] M. Dathe, T. Wieprecht, H. Nikolenko, L. Handel, W.L. Maloy, D.L. MacDonald, M. Beyermann, and M. Bienert, Hydrophobicity, hydrophobic moment and angle subtended by charged residues modulate antibacterial and haemolytic activity of amphipathic helical peptides. FEBS Lett 403 (1997) 208-12.

[9] B. Deslouches, S.M. Phadke, V. Lazarevic, M. Cascio, K. Islam, R.C. Montelaro, and T.A. Mietzner, De novo generation of cationic antimicrobial peptides: influence of length and tryptophan substitution on antimicrobial activity. Antimicrob Agents Chemother 49 (2005) 316-22.

[10] R. Rathinakumar, and W.C. Wimley, Biomolecular engineering by combinatorial design and high-throughput screening: small, soluble peptides that permeabilize membranes. J Am Chem Soc 130 (2008) 9849-58.

[11] R. Rathinakumar, W.F. Walkenhorst, and W.C. Wimley, Broad-spectrum antimicrobial peptides by rational combinatorial design and high-throughput screening: the importance of interfacial activity. J Am Chem Soc 131 (2009) 7609-17.

[12] G.N. Tew, D. Liu, B. Chen, R.J. Doerksen, J. Kaplan, P.J. Carroll, M.L. Klein, and

W.F. DeGrado, De novo design of biomimetic antimicrobial polymers. Proc Natl Acad Sci U S A 99 (2002) 5110-4.

[13] S. Choi, A. Isaacs, D. Clements, D. Liu, H. Kim, R.W. Scott, J.D. Winkler, and W.F. DeGrado, De novo design and in vivo activity of conformationally restrained antimicrobial arylamide foldamers. Proc Natl Acad Sci U S A 106 (2009) 6968-73.

[14] A. Tossi, L. Sandri, and A. Giangaspero, Amphipathic, alpha-helical antimicrobial peptides. Biopolymers 55 (2000) 4-30.

[15] H. Yan, S. Li, X. Sun, H. Mi, and B. He, Individual substitution analogs of Mel(12-26), melittin's C-terminal 15-residue peptide: their antimicrobial and hemolytic actions. FEBS Lett 554 (2003) 100-4.

[16] Z. Oren, J. Hong, and Y. Shai, A repertoire of novel antibacterial diastereomeric peptides with selective cytolytic activity. J Biol Chem 272 (1997) 14643-9.

[17] R.M. Epand, and R.F. Epand, Domains in bacterial membranes and the action of antimicrobial agents. Mol Biosyst 5 (2009) 580-7.

[18] H.J. Risselada, and S.J. Marrink, The molecular face of lipid rafts in model membranes. Proc Natl Acad Sci U S A 105 (2008) 17367-72.

[19] S. Mukherjee, and F.R. Maxfield, Membrane domains. Annu Rev Cell Dev Biol 20 (2004) 839-66.

[20] R.M. Epand, S. Rotem, A. Mor, B. Berno, and R.F. Epand, Bacterial membranes as predictors of antimicrobial potency. J Am Chem Soc 130 (2008) 14346-52.

[21] A. Arouri, M. Dathe, and A. Blume, Peptide induced demixing in PG/PE lipid mixtures: a mechanism for the specificity of antimicrobial peptides towards bacterial membranes? Biochim Biophys Acta 1788 (2009) 650-9.

[22] R.M. Epand, and R.F. Epand, Lipid domains in bacterial membranes and the action of antimicrobial agents. Biochim Biophys Acta 1788 (2009) 289-94.

[23] R.F. Epand, B.P. Mowery, S.E. Lee, S.S. Stahl, R.I. Lehrer, S.H. Gellman, and R.M. Epand, Dual mechanism of bacterial lethality for a cationic sequence-random copolymer that mimics host-defense antimicrobial peptides. J Mol Biol 379 (2008) 38-50.

[24] Ø. Rekdal, J. Andersen, H.L. Vorland, and S.J. Svendsen, Construction and synthesis of lactoferricin derivatives with enhanced antibacterial activity. J Pep Sci 5 (1999) 32-45.

[25] W. Jing, J.S. Svendsen, and H.J. Vogel, Comparison of NMR structures and model-membrane interactions of 15-residue antimicrobial peptides derived from bovine lactoferricin. Biochem Cell Biol 84 (2006) 312-26.

[26] W. Bellamy, M. Takase, K. Yamauchi, H. Wakabayashi, K. Kawase, and M. Tomita,

Identification of the bactericidal domain of lactoferrin. Biochim Biophys Acta 1121 (1992) 130-6.

[27] R.M. Epand, Detecting the presence of membrane domains using DSC. Biophys Chem 126 (2007) 197-200.

[28] S.C. Gill, and P.H. von Hippel, Calculation of protein extinction coefficients from amino acid sequence data. Anal Biochem 182 (1989) 319-26.

[29] L. Zhang, A. Rozek, and R.E. Hancock, Interaction of cationic antimicrobial peptides with model membranes. J Biol Chem 276 (2001) 35714-22.

[30] J.C. McIntyre, and R.G. Sleight, Fluorescence assay for phospholipid membrane asymmetry. Biochemistry 30 (1991) 11819-27.

[31] G.R. Bartlett, Phosphorus assay in column chromatography. J Biol Chem 234 (1959) 466-8.

[32] T. Imamura, N. Yamamoto, A. Tamura, S. Murabayashi, S. Hashimoto, H. Shimada, and S. Taguchi, NMR based structure-activity relationship analysis of an antimicrobial peptide, thanatin, engineered by site-specific chemical modification: Activity improvement and spectrum alteration. Biochem Biophys Res Commun 369 (2008) 609-15.

[33] R.F. Doolittle, Prediction of Protein Structure and the Principles of Protein Conformation, Plenum press, New York, 1989.

[34] D. Marion, and K. Wuthrich, Application of phase sensitive two-dimensional correlated spectroscopy for measurements of ^{1}H-^{1}H spin-spin coupling constants in proteins. BIochem. Biophys. Res. Commun. 113 (1983) 967-974.

[35] A. Bax, and D.G. Davis, MLEV-17-Based two-dimensional homonuclear magnetization transfer spectroscopy. Journal of magnetic resonance 65 (1985) 355-360.

[36] A. Kumar, G. Wagner, R.R. Ernst, and L. Wuthrich, Buildup rates of the nuclear overhauser effect measured by two-dimensional proton magnetic resonance spectroscopy: implications for studies of protein conformation. J. Am. Chem. Soc 103 (1981) 3654-3658.

[37] U. Piantini, O.W. Sorensen, and R.R. Ernst, Multiple quantum filters for elucidating NMR coupling networks. J. Am. Chem. Soc 104 (1982).

[38] M. Piotto, V. Saudek, and V. Sklenar, Gradient-tailored excitation for single-quantum NMR spectroscopy of aqueous solutions. J Biomol NMR 2 (1992) 661-5.

[39] F. Delaglio, S. Grzesiek, G.W. Vuister, G. Zhu, J. Pfeifer, and A. Bax, NMRPipe: a multidimensional spectral processing system based on UNIX pipes. J Biomol NMR

6 (1995) 277-93.
[40] K. Wuthrich, NMR of proteins and nucleic acids, John Wiley & Sons, 1986.
[41] Y. Kim, and J.H. Prestegard, Measurement of vicinal couplings from cross peaks in COSY spectra. Journal of magnetic resonance 84 (1989) 9-13.
[42] S. Honda, K. Yamasaki, Y. Sawada, and H. Morii, 10 residue folded peptide designed by segment statistics. Structure 12 (2004) 1507-18.
[43] P. Guntert, C. Mumenthaler, and K. Wuthrich, Torsion angle dynamics for NMR structure calculation with the new program DYANA. J Mol Biol 273 (1997) 283-98.
[44] R.A. Laskowski, J.A. Rullmannn, M.W. MacArthur, R. Kaptein, and J.M. Thornton, AQUA and PROCHECK-NMR: programs for checking the quality of protein structures solved by NMR. J Biomol NMR 8 (1996) 477-86.
[45] R. Koradi, M. Billeter, and K. Wuthrich, MOLMOL: a program for display and analysis of macromolecular structures. J Mol Graph 14 (1996) 51-5, 29-32.
[46] R.N. Lewis, D.A. Mannock, and R.N. McElhaney, Differential scanning calorimetry in the study of lipid phase transitions in model and biological membranes: practical considerations. Methods Mol Biol 400 (2007) 171-95.
[47] H.N. Hunter, W. Jing, D.J. Schibli, T. Trinh, I.Y. Park, S.C. Kim, and H.J. Vogel, The interactions of antimicrobial peptides derived from lysozyme with model membrane systems. Biochim Biophys Acta 1668 (2005) 175-89.
[48] J.F. Hunt, P. Rath, K.J. Rothschild, and D.M. Engelman, Spontaneous, pH-dependent membrane insertion of a transbilayer alpha-helix. Biochemistry 36 (1997) 15177-92.
[49] A.S. Ladokhin, S. Jayasinghe, and S.H. White, How to measure and analyze tryptophan fluorescence in membranes properly, and why bother? Anal Biochem 285 (2000) 235-45.
[50] J.D. Hille, G.M. Donne-Op den Kelder, P. Sauve, G.H. de Haas, and M.R. Egmond, Physicochemical studies on the interaction of pancreatic phospholipase A2 with a micellar substrate analogue. Biochemistry 20 (1981) 4068-73.
[51] J.B. Heymann, S.D. Zakharov, Y.L. Zhang, and W.A. Cramer, Characterization of electrostatic and nonelectrostatic components of protein--membrane binding interactions. Biochemistry 35 (1996) 2717-25.
[52] S.H. White, W.C. Wimley, A.S. Ladokhin, and K. Hristova, Protein folding in membranes: determining energetics of peptide-bilayer interactions. Methods Enzymol 295 (1998) 62-87.
[53] A. Jasanoff, and A.R. Fersht, Quantitative determination of helical propensities from trifluoroethanol titration curves. Biochemistry 33 (1994) 2129-35.

[54] N. Hirota, K. Mizuno, and Y. Goto, Group additive contributions to the alcohol-induced alpha-helix formation of melittin: implication for the mechanism of the alcohol effects on proteins. J Mol Biol 275 (1998) 365-78.

[55] Y.Z. Zhao, and C.T. Lu, Increasing the entrapment of protein-loaded liposomes with a modified freeze-thaw technique: a preliminary experimental study. Drug Dev Ind Pharm 35 (2009) 165-71.

[56] D. Eisenberg, Three-dimensional structure of membrane and surface proteins. Annu Rev Biochem 53 (1984) 595-623.

[57] A.S. Ladokhin, and S.H. White, Folding of amphipathic alpha-helices on membranes: energetics of helix formation by melittin. J Mol Biol 285 (1999) 1363-9.

[58] S. Kobayashi, K. Takeshima, C.B. Park, S.C. Kim, and K. Matsuzaki, Interactions of the novel antimicrobial peptide buforin 2 with lipid bilayers: proline as a translocation promoting factor. Biochemistry 39 (2000) 8648-54.

[59] I.D. Alves, N. Goasdoue, I. Correia, S. Aubry, C. Galanth, S. Sagan, S. Lavielle, and G. Chassaing, Membrane interaction and perturbation mechanisms induced by two cationic cell penetrating peptides with distinct charge distribution. Biochim Biophys Acta 1780 (2008) 948-59.

[60] R.F. Epand, M.A. Schmitt, S.H. Gellman, and R.M. Epand, Role of membrane lipids in the mechanism of bacterial species selective toxicity by two alpha/beta-antimicrobial peptides. Biochim Biophys Acta 1758 (2006) 1343-50.

[61] A.S. Ladokhin, and S.H. White, Protein chemistry at membrane interfaces: non-additivity of electrostatic and hydrophobic interactions. J Mol Biol 309 (2001) 543-52.

[62] T. Wieprecht, O. Apostolov, M. Beyermann, and J. Seelig, Thermodynamics of the alpha-helix-coil transition of amphipathic peptides in a membrane environment: implications for the peptide-membrane binding equilibrium. J Mol Biol 294 (1999) 785-94.

[63] G.D. Fasman, Circular dichroism and the conformational analysis of biomolecules, 1996.

[64] A.G. Cochran, N.J. Skelton, and M.A. Starovasnik, Tryptophan zippers: stable, monomeric beta -hairpins. Proc Natl Acad Sci U S A 98 (2001) 5578-83.

[65] C. Demetzos, Differential Scanning Calorimetry (DSC): a tool to study the thermal behavior of lipid bilayers and liposomal stability. J Liposome Res 18 (2008) 159-73.

[66] E.A. Burstein, N.S. Vedenkina, and M.N. Ivkova, Fluorescence and the location of tryptophan residues in protein molecules. Photochem Photobiol 18 (1973) 263-79.

[67] A. Latal, G. Degovics, R.F. Epand, R.M. Epand, and K. Lohner, Structural aspects of the interaction of peptidyl-glycylleucine-carboxyamide, a highly potent antimicrobial peptide from frog skin, with lipids. Eur J Biochem 248 (1997) 938-46.

[68] K.A. Henzler-Wildman, G.V. Martinez, M.F. Brown, and A. Ramamoorthy, Perturbation of the hydrophobic core of lipid bilayers by the human antimicrobial peptide LL-37. Biochemistry 43 (2004) 8459-69.

[69] K. Matsuzaki, M. Harada, S. Funakoshi, N. Fujii, and K. Miyajima, Physicochemical determinants for the interactions of magainins 1 and 2 with acidic lipid bilayers. Biochim Biophys Acta 1063 (1991) 162-70.

[70] V.V. Andrushchenko, H.J. Vogel, and E.J. Prenner, Interactions of tryptophan-rich cathelicidin antimicrobial peptides with model membranes studied by differential scanning calorimetry. Biochim Biophys Acta 1768 (2007) 2447-58.

[71] K. Matsuzaki, O. Murase, N. Fujii, and K. Miyajima, An antimicrobial peptide, magainin 2, induced rapid flip-flop of phospholipids coupled with pore formation and peptide translocation. Biochemistry 35 (1996) 11361-8.

[72] F. Jean-Francois, S. Castano, B. Desbat, B. Odaert, M. Roux, M.H. Metz-Boutigue, and E.J. Dufourc, Aggregation of cateslytin beta-sheets on negatively charged lipids promotes rigid membrane domains. A new mode of action for antimicrobial peptides? Biochemistry 47 (2008) 6394-402.

[73] M. Dathe, H. Nikolenko, J. Klose, and M. Bienert, Cyclization increases the antimicrobial activity and selectivity of arginine- and tryptophan-containing hexapeptides. Biochemistry 43 (2004) 9140-50.

[74] Y. Imura, M. Nishida, Y. Ogawa, Y. Takakura, and K. Matsuzaki, Action mechanism of tachyplesin I and effects of PEGylation. Biochim Biophys Acta 1768 (2007) 1160-9.

[75] T.E. Thorgeirsson, Y.G. Yu, and Y.K. Shin, A limiting law for the electrostatics of the binding of polypeptides to phospholipid bilayers. Biochemistry 34 (1995) 5518-22.

[76] D. Persson, P.E. Thoren, M. Herner, P. Lincoln, and B. Norden, Application of a novel analysis to measure the binding of the membrane-translocating peptide penetratin to negatively charged liposomes. Biochemistry 42 (2003) 421-9.

[77] G.R. Thuduppathy, J.W. Craig, V. Kholodenko, A. Schon, and R.B. Hill, Evidence that membrane insertion of the cytosolic domain of Bcl-xL is governed by an electrostatic mechanism. J Mol Biol 359 (2006) 1045-58.

[78] I.D. Alves, I. Correia, C.Y. Jiao, E. Sachon, S. Sagan, S. Lavielle, G. Tollin, and G. Chassaing, The interaction of cell-penetrating peptides with lipid model systems and

subsequent lipid reorganization: thermodynamic and structural characterization. J Pept Sci 15 (2009) 200-9.

[79] X. Sun, S. Chen, S. Li, H. Yan, Y. Fan, and H. Mi, Deletion of two C-terminal Gln residues of 12-26-residue fragment of melittin improves its antimicrobial activity. Peptides 26 (2005) 369-75.

[80] E.A. Porter, B. Weisblum, and S.H. Gellman, Mimicry of host-defense peptides by unnatural oligomers: antimicrobial beta-peptides. J Am Chem Soc 124 (2002) 7324-30.

Table1 Amino-acid sequence, net charge, hydrophobicity and hydrophobic moment of the designed peptides and those of typical amphipathic antimicrobial

Peptide	Amino acid sequence	Net charge	ΔG_{WW} (kcal/mol)[a]	$<\mu_H>^b$
LAP1	**QPEWFKARRWQWRMKKLGA**	+5	1.64	0.093
LAP2	**TISQPEWFKARRWQWRMKKLGA**	+5	1.60	0.067
LAP3	**TISQAEWFKARRWQWRMKKLGA**	+5	1.32	0.055
LAP4	**TASQAEWFKARRWQWRMKKLGA**	+5	1.80	0.075
LAP5	**EWFKARRWQWRMKKLGA**	+5	0.61	0.11
LAP6	**EWFKARRWGWRMKKLQA**	+5	0.61	0.12
Melittin	**GIGAVLKVLTTGLPALISWIKRKRQQ**	+5	1.83	0.20
Magainin	**GIGKFLHSAKKFGKAFVGEIMNS**	+3	3.00	0.29

[a] As a hydrophobic scale, the Wimley-White scale (WWscale) was adopted.

[b] The helical hydrophobic moment was calculated as

$$\mu_{\mathrm{H}} = \left[\left(\sum_{n=1}^{N} H_n \sin(100n) \right)^2 + \left(\sum_{n=1}^{N} H_n \cos(100n) \right)^2 \right]^{1/2} \Big/ N ,$$

where N represents the number of amino-acid residues and H_n represents WWscale of nth residue [56].

Table2 Antimicrobial and hemolytic activities of LAPs.

Peptide	MIC (μM)		Hemolytic activity (%)[a]
	E. coli	*B. subtilis*	
LAP1	24	0.36	2
LAP2	16	0.36	1
LAP3	24	0.27	3
LAP4	55	0.27	2
LAP5	6.0	0.1	2
LAP6	6.0	0.1	2

[a] Hemolytic activity at peptide concentration of 400μM.

Table3 Thermodynamic parameters obtained by DSC measurements.

Sample	Pre-transition		Main transition	
	T_{pre} (°C)	ΔH_{pre} (kcal/mol)	T_m (°C) [b]	ΔH_m [d] (kcal/mol)
lipid blank	16.6±0.7	0.44±0.13	24.53±0.02	6.31±0.09
LAP1	- [a]	- [a]	20 [c], 25 [c]	6.17±0.12
LAP2	15.0±0.6	0.20±0.03	20 [c], 25 [c]	5.42±0.07
LAP3	16.4±0.2	0.95±0.09	23.90±0.02, 25 [c]	6.55±0.22
LAP4	16.60±0.02	0.52±0.09	23.37±0.01, 25 [c]	6.24±0.07
LAP5	- [a]	- [a]	22.36±0.03, 25.94±0.57	6.28±0.02
LAP6	- [a]	- [a]	23.17±0.04, 25.23±0.28	6.90±0.08

Each value is represented with standard deviation calculated from three different measurements.

[a] Bars (-) indicate no observation of peaks.

[b] For the values of LAPs, the two values correspond to T_m of the two main transitions.

[c] These T_m values are ambiguous values because of serious broadening.

[d] The values of ΔH_m indicate the sum of each main transition.

Table4 Apparent binding constants, number of lipid molecules associating with one peptide molecule and partition Gibbs free energy obtained from the peptide-liposome titration experiments.

Peptide	K_d (nM)[a]	n[b]	ΔG_x^{0} [c] (kcal/mol) [c]
LAP1	728±118	19.5±0.6	-8.99±0.10
LAP2	581±135	22.0±0.8	-9.05±0.14
LAP3	1090±212	21.0±0.9	-8.71±0.12
LAP4	898±149	21.8±0.7	-8.80±0.10
LAP5	129±36	15.4±0.2	-10.1±0.10
LAP6	175±48	15.4±0.3	-9.97±0.16

[a] Apparent binding constant between peptides and liposomes, defined in equation (3).

[b] Number of lipid molecules associated with one peptide molecule.

[c] Standard free energy obtained by using equation (7).

Table5 Fraction of helical structures in water or in the presence of anionic liposomes calculated from TFE titration experiments monitored by CD spectra.

Peptide	f_{α}^{W} [a]	f_{α}^{L} [b]
LAP1	0.16	0.35
LAP2	0.16	0.42
LAP3	0.22	0.27
LAP4	0.21	0.22
LAP5	0.10	0.35
LAP6	0.17	0.37

[a] Fraction of helices in water calculated by equation (8).

[b] Fraction of helices in the presence of POPC/POPG (1:1) calculated by equation (9)

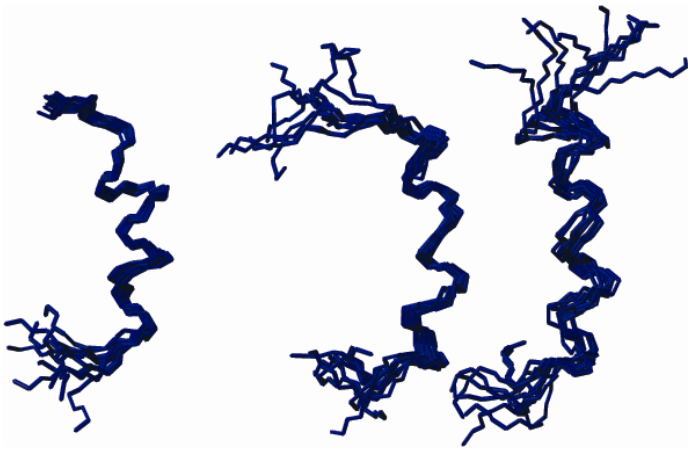

LAP1 **LAP2-conf1 and conf2 (left and right)**

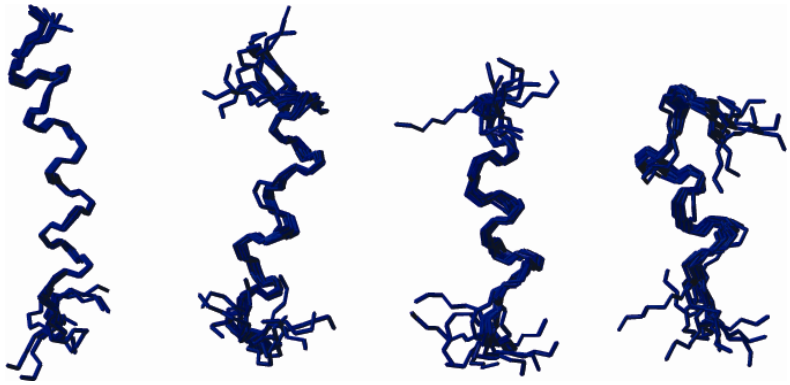

LAP3 **LAP4** **LAP5** **LAP6**

Figure 1. NMR-based calculated structures. In each conformation, backbones of the ten lowest energy structures are superimposed so that the backbone RMSD, is minimized, except for two residues in the N- and C-termini.

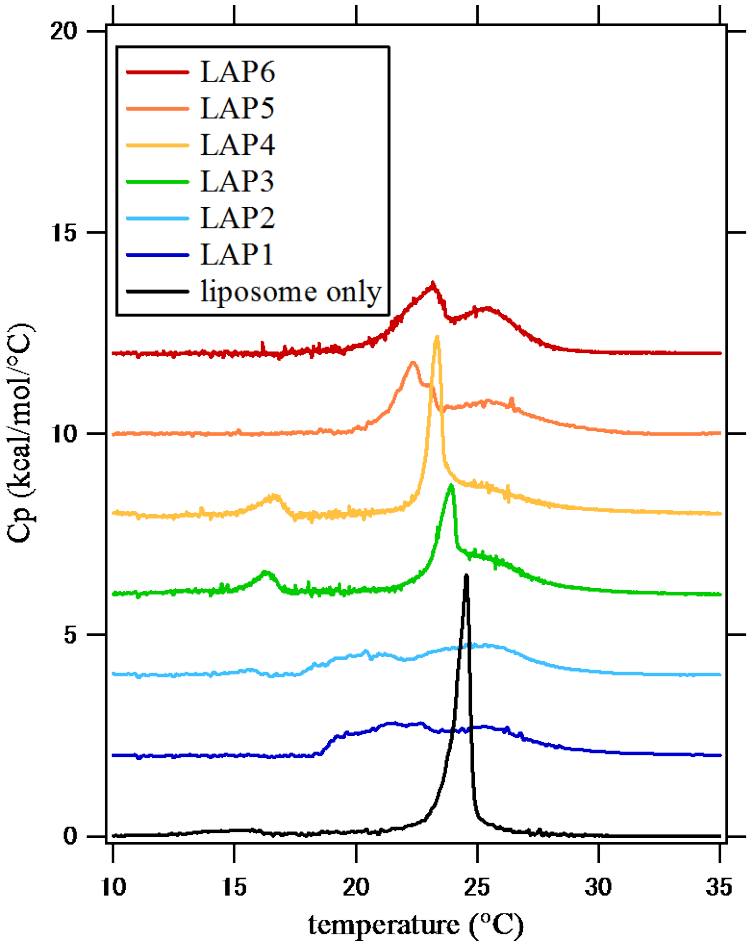

Figure 2. DSC thermograms of DMPC/DMPG (1:1) in the absence or presence of LAPs.

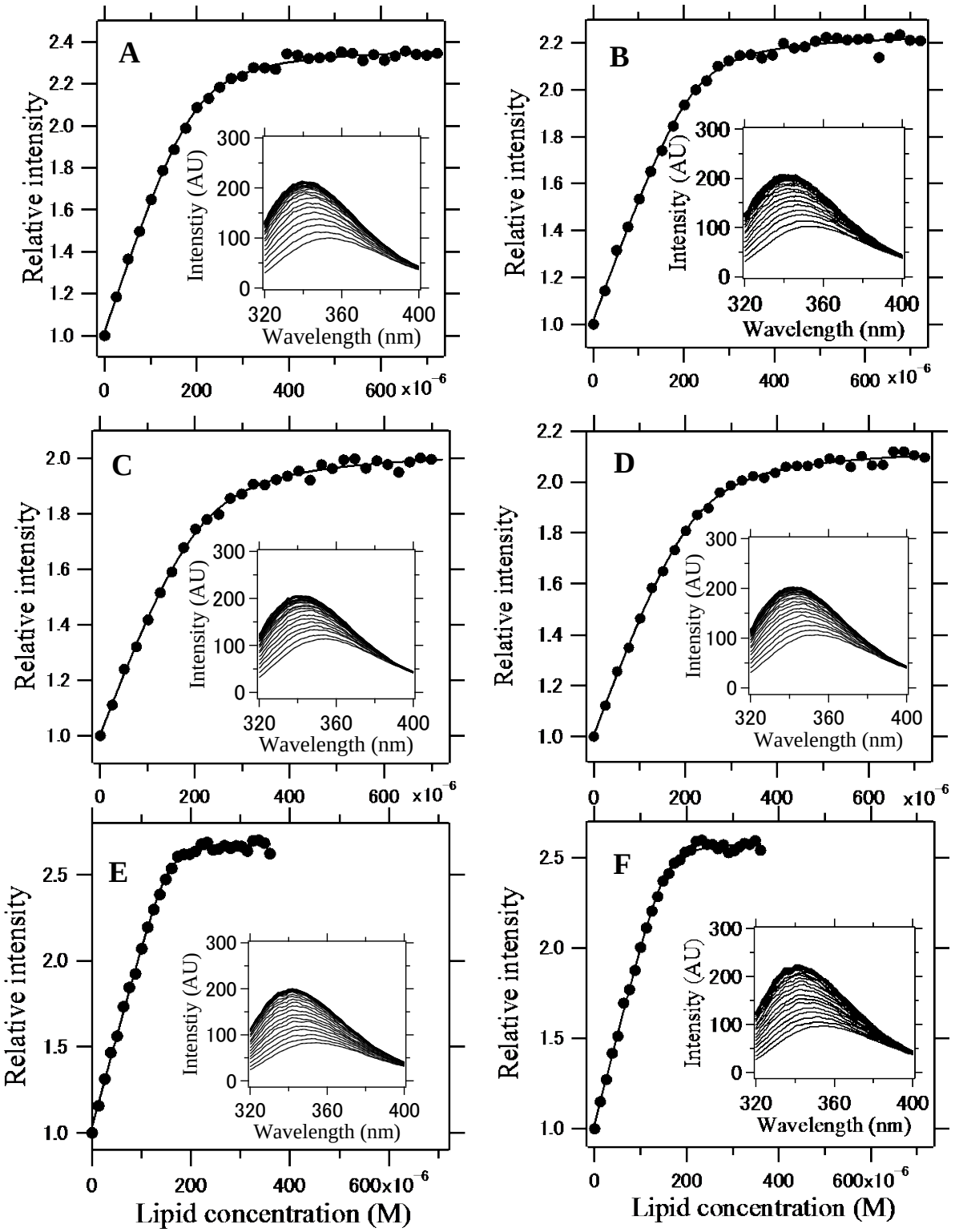

Figure 3. Peptide-liposome titration experiments monitored by fluorescence spectra of tryptophan residues in LAPs. Panels A–F correspond to data from LAP1–6, respectively. In the experiments, drops of liposome solutions composed of POPC:POPG = 1:1 were sequentially added to a peptide solution, and a fluorescence spectrum was measured for monitoring. In each panel, changes in fluorescence intensities at 342 nm are plotted. Solid lines represent fitting curves obtained using Equation (4). (Inset) Corrected fluorescence spectra obtained by the titration experiments.

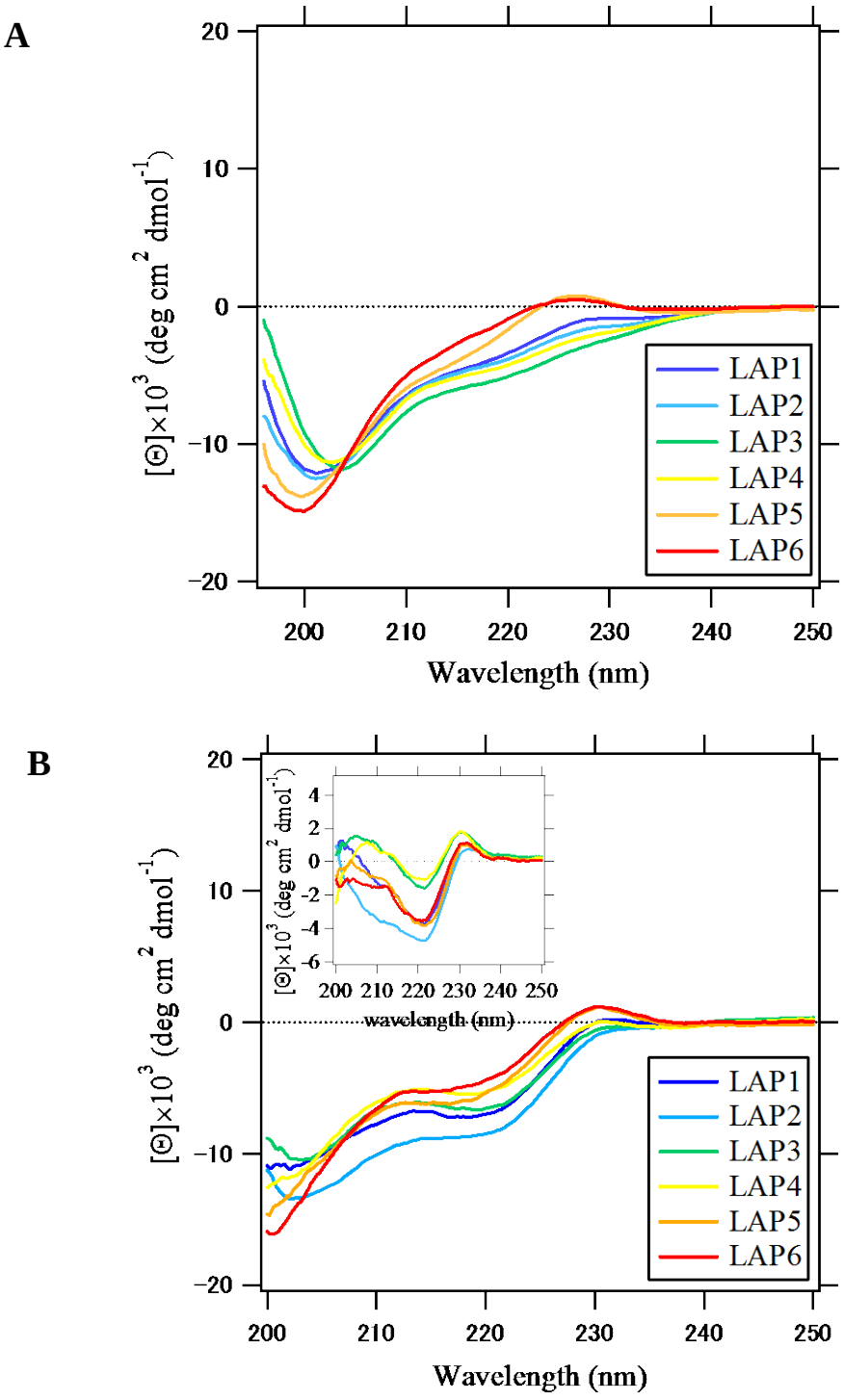

Figure 4. CD spectra of LAPs in water or in the presence of liposomes at 25ºC. (A) CD spectra in water, and (B) CD spectra in the presence of 5mM POPC/POPG (1:1). (B, inset) Differential CD spectra obtained by subtracting the spectra measured in the presence of the lipid from those obtained in water.

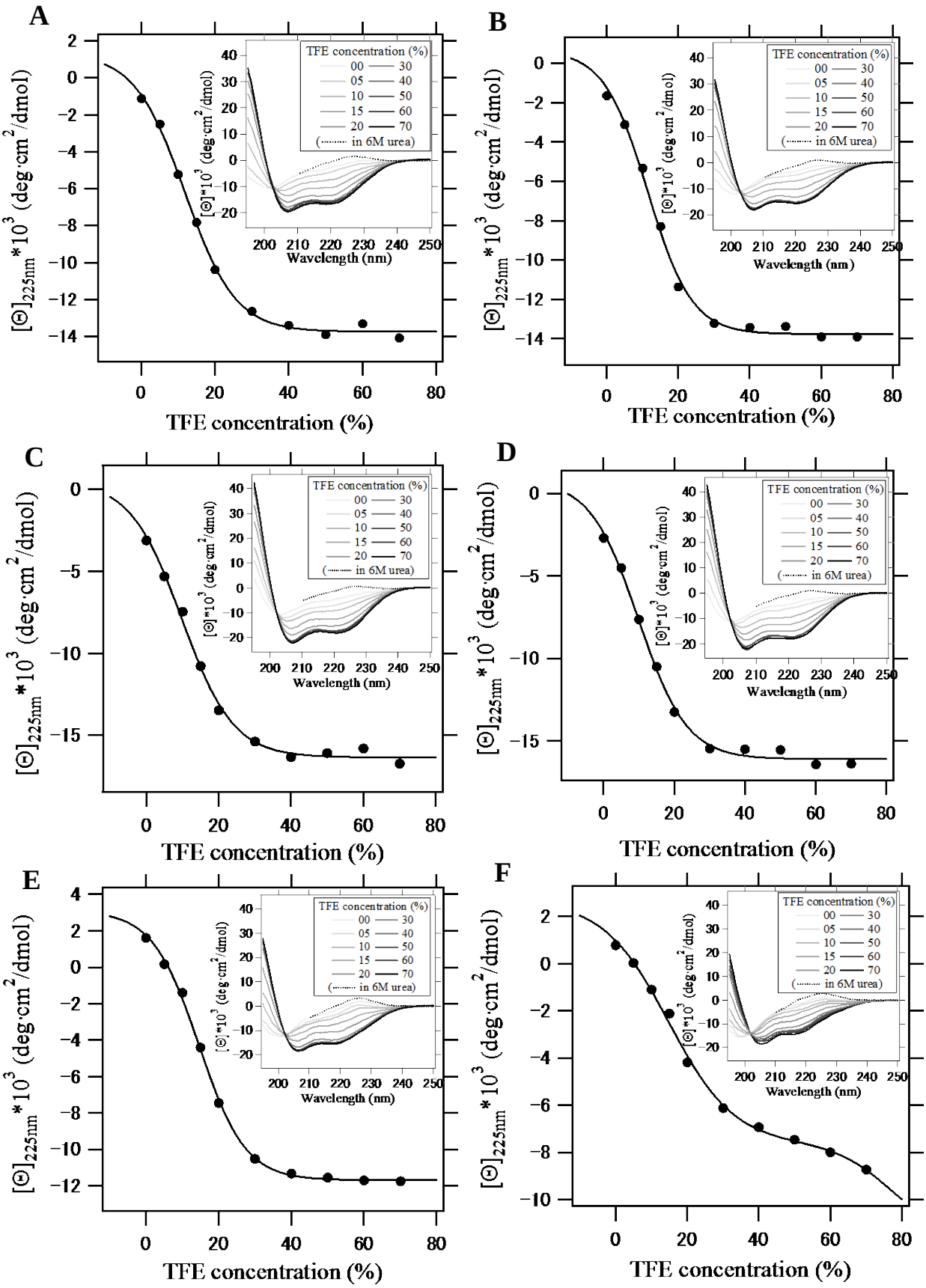

Figure 5. TFE titration experiments monitored by CD spectra. Panel A-F correcpond to LAP1-6, respectively. In each panel, mean residue ellipticity at 225nm in each TFE concentration is plotted. Solid lines indicate fitting curves by using Equation (8) or (15). (Inset) Raw CD spectra obtained by the TFE titration experiments. Spectra in 6M Urea are also shown in dashed line.

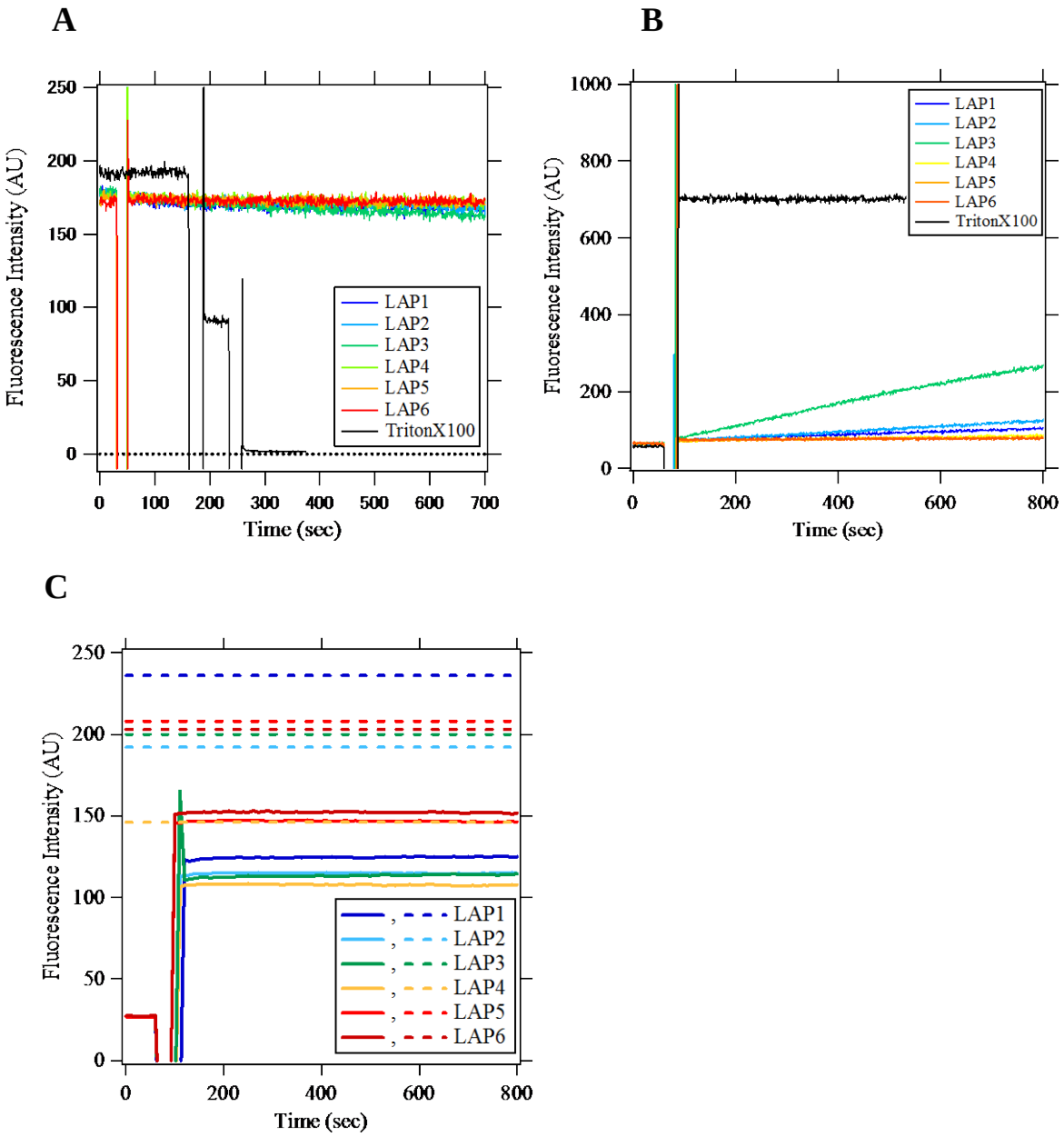

FIgure 6. (A) Time-course of the fluorescence intensity of C6-NBD-PC at 530 nm by exciting at 470 nm to monitor induction of lipid flip-flop by LAPs. (B) Time-course of the fluorescence intensity of calcein at 517 nm by exciting at 490 nm to monitor its leakage from liposomes by LAPs. (C) Time-course of peptide translocation experiments done using dansyl-DHPE–labeled liposomes excited at 280 nm and detected at 510 nm. Solid lines indicate the experimental traces and dashed lines indicate fluorescence intensities where sufficient translocation would occur.

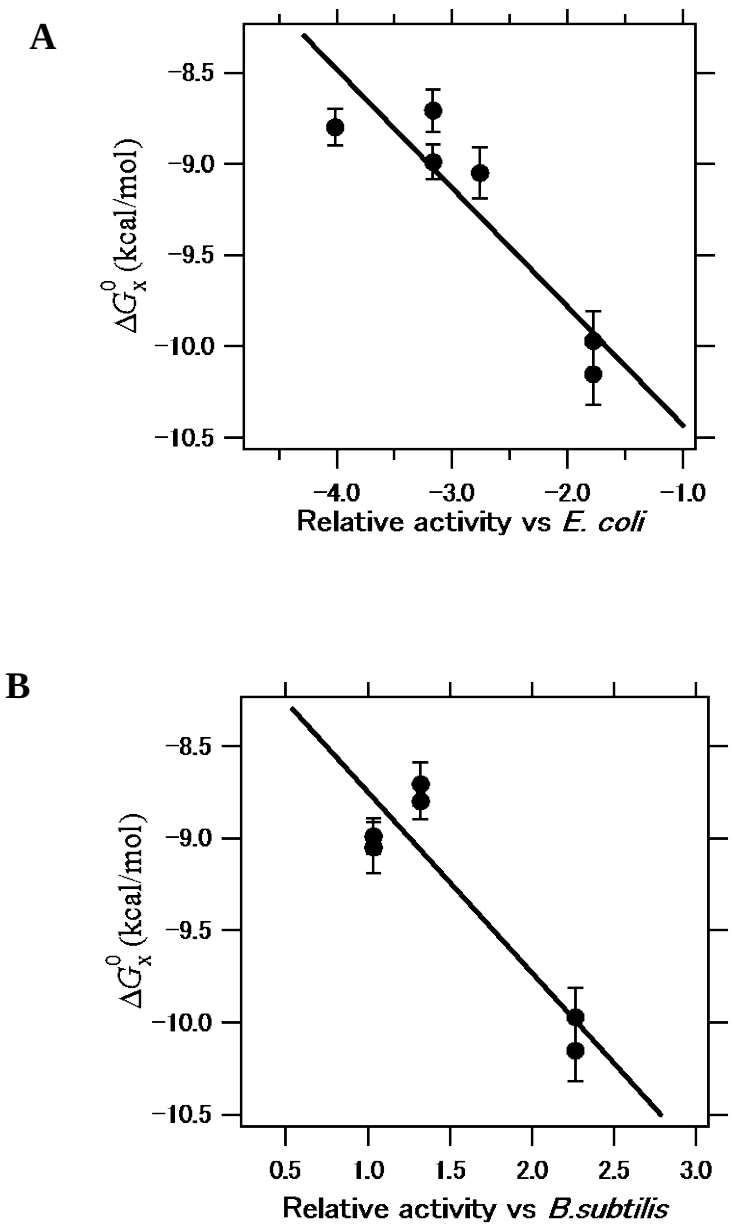

Figure 7. Relationships between relative antimicrobial activities of LAPs and their partition free energies for (A) *E. coli* and (B) *B. subtilis*. The partition free energies means the Gibbs free energy to transfer peptides from water to the liposomal surface as defined by Equation (6) in Materials and Methods. Relative antimicrobial activities were calculated by –ln(MIC). The linear regression lines are shown and the correlation coefficients obtained are −0.91 in both cases.

Chapter IV

Designing α-helical peptides that can agglutinate *Escherichia coli*, *Bacillus subtilis* and sheep erythrocytes

Abstract

Developing materials that induce aggregation of living cells is emergent issues because they are useful in the field of industrial or medical application. While some nonbiological organic compounds have been known to induce aggregation of living cells, biomolecules such as peptides and proteins have been scarcely investigated. Here, we report that cationic, α-helical peptides with self-assembling propensities can agglutinate living cells such as *Escherichia coli*, *Bacillus subtilis* and sheep erythrocytes. We succeeded in agglutinating all the cells indicated above by using a peptide that retains high amphipathicity and hydrophobicity (named AGL1). While a peptide (named AGL2) that retains less amphipathicity than AGL1 agglutinated the cells as well as AGL1, a peptide (named AGL3) that retains less hydrophobicity than AGL1 drastically lost capabilities to agglutinate *B. subtilis* and the sheep erythrocytes. These results demonstrate that peptide hydrophobicity rather than amphipathicity is essential for peptides to agglutinate those two cells. While the three peptides agglutinated *E. coli* at about the same extent, aggregation of the bacteria by AGL3 was more destabilized by salt than the other two peptides. These results indicate that *E. coli* aggregation induced by AGL3 depends on electrostatic interaction rather than hydrophobic one. Overall, except the case that electrostatic interactions mainly contribute, improving peptide hydrophobicity rather than amphipathicity seems more effective to induce cellular aggregations. This may be because peptide intermolecular interactions on cellular surfaces are more strongly induced when peptides retain high hydrophobicity than when high amphipathicity.

Introduction

Developing materials that induce aggregation of living cells is emergent issues because they are useful in the field of industrial or medical application. For example, capability to agglutinate bacteria is needed for water purification [1], and it is reported that phagocytosis of bacteria by macrophages is more efficiently processed when bacterial aggregation is induced [2]. Moreover, capabilities to coagulate mammalian cells are beneficial to conjugate physiological tissues that are physically injured. Previously, some organic polymers succeeded in agglutinating *E. coli* [3; 4]. We can learn from the examples that the two common characteristics are thought to need to agglutinate the bacteria. First, they must strongly interact with the bacteria. Second, the polymers should have tendency to self-assemble into stable scaffolds that can combine different cells [3; 4].

Among various kinds of polymers, peptides are promising coagulants because they are expected to exhibit fewer burden on the environment and more harmless to living things than other organic materials. Moreover, switching aggregate formation by peptides in response to environmental stimuli such as metal ions or pH change may be achieved by introducing amino-acids such as histidine [5; 6] and glutamate [7]. Until now, though some kinds of peptides have been known to agglutinate bacteria [2], the mechanism of action is still unclear because of lack of examples. Thus, more candidates should be developed to discover amino-acids sequences or structures that effectively induce aggregation. Surfaces of living cells are negatively-charged, moderate hydrophobic environments [8]. Therefore positively-charged residues and hydrophobic ones play the key role to interact with the surfaces. The capability to self-assemble into oligomers is expected to be achieved by introducing as many hydrophobic residues as possible [9] or aligning amino-acids to form amphipathic structures [10]. This capability seems to also be important in the case of peptides as well as other biopolymers since poly-lysine, which is devoid of the capability, fails to agglutinate living things [11; 12; 13].

In this paper, we designed an amphipathic α-helical peptides named AGL1 to investigate its potency to agglutinate living cells such as *E. coli*, *B. subtilis* and sheep erythrocytes. Moreover, by designing two control peptides that are less amphipathic (named AGL2) or hydrophobic (named AGL3) than AGL1, we discuss how amphipathicity and hydrophobicity related to capabilities to agglutinate the living cells. The mechanisms of cellular aggregation were partly discussed by examining how the designed peptides agglutinate artificial anionic liposomes. We also examined whether

liposomal or cellular aggregation induced by the designed peptides was able to be regulated by means of transition metal ions.

Materials and Methods

Peptide synthesis and purification

Peptides were synthesized on Pioneer Peptide Synthesis System (PerSeptive Biosystems, CA) by using Fmoc solid-phase chemistry. After the synthesis, peptides were cleaved from resins with a solution containing 82.5% (vol/vol) TFA, 5 % thioanisole, 2.5 % 1,2-ethanedithiol, and 0.8 M phenol. The cleaved powders were purified by reverse-phase HPLC equipped with acetonitrile-water solvent system containing 0.1 % TFA. Identities of peptides were confirmed by laser desorption time of flight mass spectrometry, AXIMA-CFR (SHIMADZU, Kyoto, Japan). Peptide concentrations were determined by absorbance at 280nm as described [14] on a JASCO V-650 spectrophotometer (Tokyo, Japan).

Preparation of liposomes

All liposomes used in this study were prepared by the exclusion method [15]. In brief, powder POPC and POPG-Na lipids were dissolved in chloroform and the solution was evaporated overnight. 10 mM Tris-HCl buffer (pH 7.5) was added to dried lipid film and vortexed until the film was entirely dispersed. Then the solution was extruded by taking advantage of Mini-Extruder (Avanti Polar Lipids, Inc., USA) through a filter with a pore size 100 nm. The solution obtained was stocked at 4 ºC.

Preparation of bacteria

Escherichia coli BL21 or *Bacillus subtilis ISW1214* cultivated in Luria-Bertani broth overnight was centrifuged at 1,400×*g* and the precipitations were washed three times by PBS buffer (9.5 mM phosphate buffer, 140 mM NaCl, 2.7mM KCl, pH 7.4). Finally PBS buffer was added to bacterial solutions as optical density approximately became 1.0. The bacterial solutions were always treated at 4 ºC or on ice.

Preparation of sheep erythrocytes

Fresh bloods taken from a sheep incubated with ACD solution (22 % citric acid, 8 % citric sodium and 22 % glucose) were centrifuged at 100×*g*. The supernatant was gently removed and precipitated erythrocytes were washed three times by PBS buffer. The erythrocytes obtained were dissolved in PBS buffer and stocked at 4ºC. The stock

solution was again washed three times by PBS and arbitrarily diluted by PBS buffer before experiments.

CD spectroscopy

CD spectra were acquired at 25 ºC on a J-720 spectropolarimeter (JASCO, Japan) with a quartz cuvette whose pathlength was 1.0 mm for peptide samples of 10μM concentration. For all samples, 10mM Tris-HCl buffer (pH 7.5) was used.

DLS measurements

DLS measurements were performed at the room temperature on a Zetasizer nano-S (Malvern Instruments Ltd., UK). Experimentally obtained correlograms were analyzed by using Dispersion Technology Software 5.00 (Malvern Instruments Ltd., UK)

Turbidity measurements

Existence of large liposomal aggregations was monitored by measuring turbidity at 600nm on a V-650 spectrophotometer (JASCO, Japan).

Observation by optical microscope

Acquisition of optical images was performed by ECLIPSE E600W (Nikon, Japan). A drop of sample solutions was mounted on a glass slide and bright field images were taken.

Results

Peptide design

As an amphipathic and hydrophobic peptide, we designed AGL1 (Table 1). The region from L3 to L23, at which we term “the core-region”, is expected to form an amphipathic α-helical structure. The tryptophan residue was introduced as a chromophore to determine peptide concentration and environments where peptides exist [16]. The C-terminal three arginine residues were introduced to the peptide not only to improve solubility but also add positive charges. We also introduced two histidine residues in the hydrophilic surface as the ligands for transition metal ions. To elucidate whether amphipathicity and hydrophobicity of AGL1 contribute to aggregation capacities, we designed other two peptides that retain less amphipathicity (AGL2) or less hydrophobicity (AGL3) than AGL1 (Table 1). The tendencies of amphipathicity were determined by using helical hydrophobicmomt, $<\mu_H>$ [17], and hydrophobicity

was calculated by using Wimley-White scale (WWscale) [18] (Table 1). The core region of AGL2 retains less amphipathicity than AGL1, which is confirmed from the values of $<\mu_H>$ (Table 1). While AGL3 retains about the same amphipathicity as AGL1, its hydrophobicity is much lower than that of AGL1 (Table 1). AGL3 is no longer a hydrophobic peptide judging from the value of WWscale, -0.67kcal/mol.

Secondary structure and self-assembly in water

CD spectra of AGLs (the name including AGL1, 2 and 3) at the concentration of 10 μM, (pH = 7.4) are shown in Figure 1-A. The spectrum of AGL1 retains a minimum at 208nm and shoulder around 222 nm, indicating that AGL1 form a stable α-helix structure [19]. The spectrum of AGL2 and 3 retain the minima at 208 nm and 222 nm, representing that these two peptides also form stable α-helix structures [19]. Then molecular size of LAPs was estimated by means of DLS. The DLS profiles of AGL1, AGL2 or AGL3 contain peaks at about 30 nm and 220 nm, 10 nm and 160 nm or 6 nm and 160 nm, respectively (Figure 1-B). Since a scattering intensity of a particle whose diameter is R is proportional to R to the 6th power, the particle whose diameter is 30 nm, 10 nm or 6 nm dominantly exists in the case of AGL1, AGL2 or AGL3, respectively. An α-helix that is composed of 26 amino-acids is expected to retain the diameter less than 3 nm because the length of long axis of the helix is about 3 nm (estimated from the molecular model). Thus, it is indicated that AGLs form oligomers in water.

Capability to induce liposomal aggregation

Whether AGLs were able to aggregate anionic liposomes composed of POPC and POPG, the liposomes at the concentration of 100 μM were titrated by AGLs at the condition of 10 mM Tris (pH = 7.5). Titration curves by AGL1 against various kinds of POPC/POPG compositions are shown in Figure 2-A. As peptide concentration was increased, aggregation monitored by turbidity was induced. When peptide-to-lipid ratios reached at the specific ratios, the peptide induced aggregation the most. Adding further peptides resulted in decrease of turbidity, representing that aggregation was destabilized. Peptide-to-lipid ratios at which the aggregation was induced the most were proportional to percentages of POPG (Figure 2-B). AGL2 and AGL3 also aggregated anionic liposomes the most at specific peptide-to-lipid ratios and the ratios were proportional to percentages of POPG (Figure 2-C and D). These results demonstrate that electrostatic interactions between peptide and liposomes are the main determinant to induce aggregation.

We checked reversibility of aggregation by using the liposome composed of

POPC:POPG = 3:1. First, liposomal aggregation was induced by adding sufficient amount of AGLs. Then peptides at the equivalent molar were further added to the solution, and changes in turbidity and size of aggregation was monitored by dynamic light scattering (DLS). As a result, turbidity returned to the same level at which no peptide was added and DLS showed the presence of particles whose diameters are near the liposome (data not shown). Therefore, aggregation induced by the peptides is reversibly disrupted.

Capability to induce aggregation of *E. coli*

When 10 μM AGL1 were mixed with *E. coli* solutions adjusted at OD = 0.9, bacterial aggregates whose diameters were several hundred of micrometer were observed (Figure 3-A). When a peptide concentration was lowered to 1 μM, diameters of aggregates became smaller (Figure 3-B), and when peptides at the concentration of 0.1 μM were incubated, almost no aggregate was formed (Figure 3-C). To quantify capability to induce aggregation at the concentration range from 0.1 μM to 100 μM, we measured turbidity of the upper side of peptide-bacteria mixtues 30 minutes after peptides were added to the solutions. As peptide concentration becomes high, relative turbidity decreases (Figure 4-A). When peptide concentration reaches 20 μM, almost no change in turbidity was observed.

AGL2 and AGL3 also agglutinated *E. coli* at the concentration of 10μM (Figure 3-D and G), confirming that these peptides retain capabilities to agglutinate *E. coli*. When peptide concentration was lowered to 1 μM, diameters of aggregation became small compared to those when 1 μM peptides were incubated (Figure 3-E and H). When peptide concentration was lowered to 0.1 μM, almost no aggregation was observed (Figure 3-F and I). These data demonstrates that below 10 μM, AGL2 and AGL3 agglutinate *E. coli* in the concentration dependent manner. To quantify capability to induce aggregation of AGL2 or 3 at the concentration range from 0.1 μM to 100 μM, we measured turbidity of the upper side of peptide-bacteria mixtues 30 minutes after peptides were added to the solutions. In the case of AGL2, as the peptide concentrations became high, relative turbidity decreases, and when the peptide concentration reaches 40μM, almost no change was observed (Figure 4-A). On the other hand, AGL3 exhibited different concentration dependency on aggregation. Before the concentration reached 5 μM, relative turbidity decreased and it reached the minimum at the concentration of 5 μM. Above the concentration, relative turbidity increased and reached at about 1.2 (Figure 4-A).

To estimate how electrostatic interactions contribute to aggregation of *E. coli*, we

measured turbidity of the upper side of peptide-bacteria mixtures 30 minutes after peptides were added to the solutions at the different NaCl concentrations in PBS buffer. For AGL1 and ALG2, relative turbidity increased as NaCl concentration became high in the range of 0 to 1000 mM (Figure). In contrast, in the case of AGL3, relative turbidity drastically increased only at the NaCl concentration of 200mM (Figure 4-B). These results demonstrate that AGL3 more strongly depends on electrostatic interactions to induce aggregation than AGL1 and AGL2.

Capability to induce aggregation of *B. subtilis*

When 10 μM AGL1 were incubated with *B. subtilis* solutions at OD = 0.9, aggregates whose diameters were hundreds of micrometers were observed (Figure 5-A), representing that AGL1 can agglutinate *B. subtilis*. When the concentration was lowered to 1 μM, the size of aggregates was drastically decreased (Figure 5-B). AGL1 at the concentration of 0.1μM induced no obvious aggregation (Figure 5-C). Concentration dependency on aggregate formation was monitored by measuring turbidity of supernatants 30 minutes after peptides and the bacteria were incubated (Figure 6-A). As peptide concentration became high, relative turbidity decreased, and above the concentration of 10 μM, relative turbidity scarcely changed (Figure 6-A). AGL2 also agglutinated *B. subtilis* at the concentration of 10 μM (Figure 5-D). The size of aggregation became small when 1 μM AGL2 was incubated with the bacteria (Figure 5-E). Almost no aggregation was observed when the concentration was lowered to 0.1 μM (Figure 5-F). Concentration dependency of AGL2 against aggregation was monitored by the same method as AGL1 (see above). As the concentration became high, relative turbidity increased, and when the concentration reached 10 μM, changes in relative turbidity converged (Figure 6-A). While AGL1 and 2 agglutinated *B. subtilis* at the concentration of 10 μM, AGL3 never agglutinated the bacteria at the same concentration (Figure 5-G), representing that AGL3 does not retain capability to induce aggregation of *B. subtilis*.

To estimate how electrostatic interactions contribute to aggregation of *B. subtilis*, we measured turbidity of the upper side of peptide-bacteria mixtures 30 minutes after peptides were added to the solutions at the different NaCl concentrations in PBS buffer. As the salt concentration increased, relative turbidity increased (Figure 6-B) and when concentration of NaCl reaches 1 M, almost no aggregation was formed.

Capability to induce aggregation of erythrocytes

When 10 μM of AGL1 was incubated with 0.45 % sheep erythrocytes, aggregates

whose diameters were around 100 μm were observed (Figure 7-A). When the concentration was lowered to 1 μM, size of aggregation became small (Figure 7-B). AGL1 at the concentration of 0.1 μM induced no aggregation (Figure 7-C). These results represent that AGL1 agglutinate the cells by the concentration-dependent manner. AGL2 also agglutinated the cells by the similar manner as AGL1. When the concentration reached 10 μM, aggregates whose diameters were around 100nm were observed (Figure 7-D). 1 μM AGL2 induced aggregation whose size were around 10nm (Figure 7-E), and 0.1 μM AGL2 induced almost no aggregation (Figure 7-F). In contrast to the cases of AGL1 and 2, AGL3 never agglutinated the cells at the concentration of 10 μM (Figure 7-G). These results demonstrate that While AGL1 and 2 retain capabilities to induce aggregation of erythrocytes, AGL3 have no capability to induce aggregation of the cells.

To estimate how electrostatic interactions contribute to aggregation of the erythrocytes, aggregation was induced at different NaCl concentrations. When 200 mM NaCl was incubated, AGL1 and 2 induced aggregates whose diameters were around 100 nm (Figure 8-A and B). The sizes of aggregates were as large as those of aggregates induced in the absence of NaCl (Figure 7-A and B). When 500 mM NaCl was incubated, the sizes of aggregation induced by AGL1 or 2 became small compared to the cases of 200 mM NaCl (Figure 8-C and D). In this condition, the surfaces of erythrocytes became convexo-concave because of the hypertonic state of solution, which complicated quantitative evaluation of salt effect on erythrocyte aggregation.

Effect of metal ions on aggregation

Whether transition metal ions such as zinc, cupper and nickel were able to regulate aggregation of anionic liposomes induced by AGL1 were tested by using liposomes composed of POPC:POPG = 3:1 in the presence of 10μM AGL1. Three kinds of transition metal ions, i.e. Zn^{2+}, Cu^{2+} and Ni^{2+} were tested. When they were added to the aggregates at the concentration of 20μM, Zn^{2+} completely inhibited formations of aggregation, Cu^{2+} partially inhibited, and Ni^{2+} showed no inhibition judging from turbidity (Figure 9-A), representing that Zn^{2+} efficiently regulated aggregation. Then aggregation formed by 10μM AGL1 and 100μM POPC/POPG (3:1) was titrated by Zn^{2+}. 2μM of the metal ion drastically decreased turbidity (Figure 9-B). Further addition of the metal ion resulted in moderate or no reduction of turbidity (Figure 9-B). We also tried to induce and inhibit aggregation of AGL1 by adding Zn^{2+} and EDTA alternately (Figure 9-C). After 10μM AGL1 and 100μM POPC/POPG (3:1) was incubated and aggregation was induced, 20μM Zn^{2+} was introduced to the aggregates, resulting in

reducing aggregation efficiently. After the reaction reached equilibrium, 25μM EDTA was introduced to the solution and aggregation gradually restructured. Again 30μM Zn^{2+} was added and aggregation disappeared. Finally addition of 35μM EDTA resulted in recovery of aggregation. The result demonstrates that we were able to regulate formation of aggregates composed of AGL1 and anionic liposomes by Zn^{2+}.

We also tried to induce or inhibit aggregation of living cells by using metal ions. However, aggregation of every living cell (*E. coli*, *B. subtilis* or sheep erythrocyte) induced by AGL1, 2 or 3 was never regulated by transition metal ions such as Zn^{2+}, Cu^{2+} and Ni^{2+} (data not shown).

Discussion

Mechanism of liposomal aggregation

It is generally known that cationic polypeptides such as polylysine agglutinate an anionic liposome by compensating the complementary charges [20]. In these cases, aggregation is formed the most at specific peptide-to-liposome ratios at which ζ-potential, which represents how much the surface retains charge, reaches nearly zero [20]. In our case, aggregation was also observed only at specific peptide-to-liposome ratios, indicating that aggregation was formed by the same mechanism. This is also supported by that fact that peptide concentrations at which aggregation is induced are proportional to molar ratios of POPG (Figure 2-B, C and D). Then, how do the peptides interact with the liposomes in aggregates? When it is assumed that AGL1 interact only with the other surface of liposomes, one peptide molecule is associated with 10, 7.5, 5 or 2.5 lipid molecules within the aggregates of POPC/POPG (7:1), (3:1), (5:3) or (1:1), respectively. These numbers of lipids are too small for AGLs to interact with one peptide molecules. It is estimated that an α-helical peptide on a membrane surface is associated with about 1 lipid molecule per residue [21; 22]. When this role is adapted to our case, one peptide molecule should be associated with 26 lipid molecules. This number is much larger than the experimentally predicted ones. Thus, it is indicated that all the peptide molecules do not interact with liposomal surfaces and peptide molecules that do not interact with membrane surfaces must exist. Such molecules interact only with peptides that exist on different liposomal surfaces to play the role to combine one liposomal particle with another. This picture does not conflict with nature of AGL1 to form oligomers in water (Figure 2-B).

Mechanism of aggregation of living cells

Although surfaces of living cells are constructed from different components, the common feature is that they are covered with negative charges. Therefore, one can expect that they will be easily aggregated by a polycation such as poly-L-lysine. However, in actual, poly-L-lysine never causes evident aggregation of living cells such as *E. coli*, *B. subtilis* or sheep erythrocytes (tested in our laboratory, unpublished data). These results indicate that electrostatic interactions are not enough to agglutinate living cells. The difference between AGLs and poly-L-lysine is that AGLs retain high tendency to aggregate in water while poly-L-lysine does not. Thus, it must be important for LAPs to form aggregates by themselves on surfaces of living things. From now, based on the hypothesis, we discuss the mechanism of aggregation induced by LAPs in the view point of their differences in amphipathicity and hydrophobicity.

Among the three cells tested, i.e. *E. coli*, *B. subtilis* and sheep erythrocytes, *E. coli* is the only one that all AGLs succeed in agglutinating. Therefore, it is expected that common factors involve in *E. coli* aggregation among the three peptides. The most probable driving force is electrostatic interaction, because all AGLs retain the same net charge, +3. If this assumption is permitted, aggregation of the bacteria by AGLs is expected to be induced the most at the specific peptide-to-bacteria ratio as observed in the cases of liposomal aggregation (Figure 2). Indeed the phenomenon is observed in the case of AGL3 in which bacterial aggregation was induced the most at the specific concentration (5μM, Figure 4-A). Thus, AGL3 agglutinated *E. coli* mainly by electrostatic interactions. This implication is also supported by the surface structure of *E. coli*. The surface of *E. coli* is constructed from anionic lipid bilayers, some of which are chemically modulated by polysaccharides [23]. Therefore the surface of *E. coli* can be roughly regarded as artificial anionic liposomes.

On the other hand, AGL1 and AGL2 agglutinated the bacteria simply by the concentration-dependent manner and no obvious minimum point exist in their concentration V.S. aggregation plots (Figure 3-A).The phenomena must be explained by large hydrophobicity of AGL1 and AGL2 compared to AGL3 (Table 1). Their hydrophobicity is large enough to compensate electrostatic repulsion that occurs above the concentration where electrical neutralization between peptides and bacteria are occurred. In other words, AGL1 and 2 agglutinate the bacteria more strongly then AGL3 by means of their large hydrophobicity. The assumption is consistent with the fact that stability of aggregates formed by AGL3 is more susceptible with NaCl addition than in the cases of AGL1 and AGL2 (Figure 4-B). Meanwhile, because there is no significant difference in capabilities to agglutinate *E. coli* between AGL1 and 2, amphipathicity scarcely contribute to aggregate formation, indicating that their hydrophobicity is

enough to strongly induce *E. coli* aggregation.

While all AGLs were able to agglutinate *E. coli*, only AGL1 and 2 succeeded in aggregating *B. subtilis* and sheep erythrocytes. Since AGL1 and AGL2 are more hydrophobic than AGL3, hydrophobicity is expected to play the important role to agglutinate these cells. We discuss the reason based on structure of their surfaces. The surface of *B. subtilis* is covered by peptidoglycans and teichoic acids. Peptidoglycans are zwitterionic thick layers, composed of oligosaccharides and amino-acids, and teichoic acid is negatively-charged polymer composed of glycerol phosphate and sugars [24]. The surface of erythrocytes is covered with long polysaccharide chains, and some of sugars constructing the chains are negatively-charged. These components construct thick hydrocarbon layer that is negatively charged (at about 1800Å). Therefore, the surfaces of these two cells are not so hydrophobic because their components contain as many hydrophilic atoms such as oxygen and nitrogen as hydrophobic atoms such as carbon. Thus, it can be expected that AGL3 is not able to strongly interact their surfaces enough to induce cellular aggregation. Moreover, AGL3 may not be able to stably self-associate on their surfaces enough to induce intercellular associations.

Though high peptide hydrophobicity is essential to induce *B. subtilis* aggregation, electrostatic interactions is also important to agglutinate *B. subtilis*, because aggregates of *B. subtilis* by AGL1 and AGL2 were disrupted according to increase of salt concentration (Figure 6-B) as well as in the case of *E. coli* (Figure 4-B). We also tried to estimate how electrostatic interactions contribute to induce erythrocyte aggregation. However, it was difficult to estimate contribution of electrostatic interactions because at high NaCl concentration (500 mM) the surface of erythrocyte became convexo-concave. Judging from the similarities between the two cells in the manner how they respond to addition of AGLs, aggregation of the erythrocyte cell might be also partly depend on electrostatic interactions as well as in the case of *B. subtilis*.

As is the case with *E. coli* aggregation, peptide amphipathicity did not contribute to aggregation of *B. subtilis* and the erythrocytes, because there was no obvious difference in capabilities to agglutinate the cells between AGL1 and 2. Thus it is indicated that generally peptide hydrophobicity rather amphipathicity is essential for peptides to self-associate on the surfaces of *B. subtilis* and the erythrocytes. One possibility is that hydrophobicity of AGL1 and 2 are high enough to form stable self-aggregates on cell surfaces. Another possibility is that size of aggregation that can efficiently induce cell aggregation have limitation. In this case, even if ALG1 were able to form more large aggregates on the surfaces than AGL2, no apparent differences in aggregation efficiency must be observed. To certain these hypothesis, we will perform further experiments.

Future Study

In this study we succeeded in designing peptides that agglutinate living cells such as *E. coli*, *B. subtilis* and sheep erythrocytes. We need to further investigate the mechanism of actions by (i) designing more control peptides and/or (ii) identifying targets with which peptides are expected to interact. Especially, we have to study whether peptides self-assemble on cell surfaces and how many peptide molecules self-associate in actual. Moreover, in this study we unfortunately failed to regulate aggregation of living things by using metal ions. As a future study, we will try to design peptides that agglutinate living cells concomitant with metal ion binding.

References

[1] C.T. Yavuz, J.T. Mayo, W.W. Yu, A. Prakash, J.C. Falkner, S. Yean, L. Cong, H.J. Shipley, A. Kan, M. Tomson, D. Natelson, and V.L. Colvin, Low-field magnetic separation of monodisperse Fe3O4 nanocrystals. Science 314 (2006) 964-7.

[2] S.U. Gorr, J.B. Sotsky, A.P. Shelar, and D.R. Demuth, Design of bacteria-agglutinating peptides derived from parotid secretory protein, a member of the bactericidal/permeability increasing-like protein family. Peptides 29 (2008) 2118-27.

[3] M.D. Disney, J. Zheng, T.M. Swager, and P.H. Seeberger, Detection of bacteria with carbohydrate-functionalized fluorescent polymers. J Am Chem Soc 126 (2004) 13343-6.

[4] M.K. Muller, and L. Brunsveld, A supramolecular polymer as a self-assembling polyvalent scaffold. Angew Chem Int Ed Engl 48 (2009) 2921-4.

[5] Y. Zimenkov, S.N. Dublin, R. Ni, R.S. Tu, V. Breedveld, R.P. Apkarian, and V.P. Conticello, Rational design of a reversible pH-responsive switch for peptide self-assembly. J Am Chem Soc 128 (2006) 6770-1.

[6] S.N. Dublin, and V.P. Conticello, Design of a selective metal ion switch for self-assembly of peptide-based fibrils. J Am Chem Soc 130 (2008) 49-51.

[7] W. Li, F. Nicol, and F.C. Szoka, Jr., GALA: a designed synthetic pH-responsive amphipathic peptide with applications in drug and gene delivery. Adv Drug Deliv Rev 56 (2004) 967-85.

[8] *日本化学会編, コロイド科学 I 基礎および分散・吸着, 1995.*

[9] F. Chiti, M. Stefani, N. Taddei, G. Ramponi, and C.M. Dobson, Rationalization of the effects of mutations on peptide and protein aggregation rates. Nature 424 (2003) 805-8.

[10] Y. Chen, C.T. Mant, S.W. Farmer, R.E. Hancock, M.L. Vasil, and R.S. Hodges, Rational design of alpha-helical antimicrobial peptides with enhanced activities and specificity/therapeutic index. J Biol Chem 280 (2005) 12316-29.

[11] K. Colville, N. Tompkins, A.D. Rutenberg, and M.H. Jericho, Effects of Poly(l-lysine) Substrates on Attached Escherichia coli Bacteria. Langmuir (2009).

[12] V. Vadillo-Rodriguez, H.J. Busscher, W. Norde, J. De Vries, R.J. Dijkstra, I. Stokroos, and H.C. Van Der Mei, Comparison of atomic force microscopy interaction forces between bacteria and silicon nitride substrata for three commonly used immobilization methods. Appl Environ Microbiol 70 (2004) 5441-6.

[13] A.V. Bolshakova, O.I. Kiselyova, A.S. Filonov, O.Y. Frolova, Y.L. Lyubchenko,

and I.V. Yaminsky, Comparative studies of bacteria with an atomic force microscopy operating in different modes. Ultramicroscopy 86 (2001) 121-8.

[14] S.C. Gill, and P.H. von Hippel, Calculation of protein extinction coefficients from amino acid sequence data. Anal Biochem 182 (1989) 319-26.

[15] L.D. Mayer, M.J. Hope, and P.R. Cullis, Vesicles of variable sizes produced by a rapid extrusion procedure. Biochim Biophys Acta 858 (1986) 161-8.

[16] E.A. Burstein, N.S. Vedenkina, and M.N. Ivkova, Fluorescence and the location of tryptophan residues in protein molecules. Photochem Photobiol 18 (1973) 263-79.

[17] D. Eisenberg, Three-dimensional structure of membrane and surface proteins. Annu Rev Biochem 53 (1984) 595-623.

[18] W.C. Wimley, and S.H. White, Experimentally determined hydrophobicity scale for proteins at membrane interfaces. Nat Struct Biol 3 (1996) 842-8.

[19] G.D. Fasman, Circular dichroism and the conformational analysis of biomolecules, 1996.

[20] D. Volodkin, V. Ball, P. Schaaf, J.C. Voegel, and H. Mohwald, Complexation of phosphocholine liposomes with polylysine. Stabilization by surface coverage versus aggregation. Biochim Biophys Acta 1768 (2007) 280-90.

[21] M. Fernandez-Vidal, S. Jayasinghe, A.S. Ladokhin, and S.H. White, Folding amphipathic helices into membranes: amphiphilicity trumps hydrophobicity. J Mol Biol 370 (2007) 459-70.

[22] A.S. Ladokhin, S. Jayasinghe, and S.H. White, How to measure and analyze tryptophan fluorescence in membranes properly, and why bother? Anal Biochem 285 (2000) 235-45.

[23] S.L. Walker, J.A. Redman, and M. Elimelech, Role of Cell Surface Lipopolysaccharides in Escherichia coli K12 adhesion and transport. Langmuir 20 (2004) 7736-46.

[24] A. Umeda, S. Yokoyama, T. Arizono, and K. Amako, Location of peptidoglycan and teichoic acid on the cell wall surface of Staphylococcus aureus as determined by immunoelectron microscopy. J Electron Microsc (Tokyo) 41 (1992) 46-52.

Table1. Amino-acid sequences, hydrophobicity and helical hydrophobic moment of AGLs.

Peptide	sequence[a]	ΔG_{WW}[b] (kcal/mol)	$\langle\mu_H\rangle_{core}$[c] (kcal/mol/res)
AGL1	**Ac-G^{1}WLQLALHLL^{10}QLGLHLLQLA^{20}LQLRRR-NH$_2$**	-4.09	0.22
AGL2	**Ac-G^{1}WQLLALHLQ^{10}LLGLHLLQLA^{20}LLQRRR-NH$_2$**	-4.09	0.01
AGL3	**Ac-G^{1}WLQLAQHLL^{10}QLGQHLLQLA^{20}QQLRRR-NH$_2$**	-0.67	0.28

[a] Amino-acid sequences that are expected to form α-helical structures are indicated by underlines.

[b] ΔG_{WW}, which means Wimley-White scale (WWscale), are used as hydrophobicity of AGLs. ΔG_{WW} was calculated simply by summing values of each amino-acid and N or C-terminal functional group.

[c] $\langle\mu_H\rangle_{core}$ means helical hydrophobic moment at the core sequences of AGLs, which are indicated by underlines on their sequences. Helical hydrophobic moment was calculated by

$$\mu_H = \left[\left(\sum_{n=1}^{N} H_n \sin(100n) \right)^2 + \left(\sum_{n=1}^{N} H_n \cos(100n) \right)^2 \right]^{1/2} \Big/ N ,$$

where N (=21) represents the number of amino-acid residues and H_n represents WWscale of nth residue [17].

A

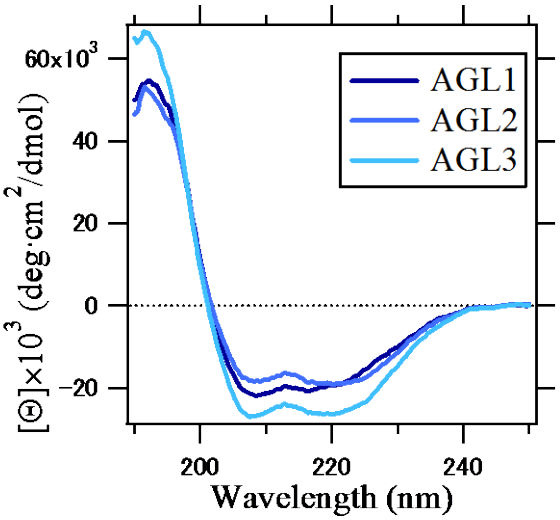

B

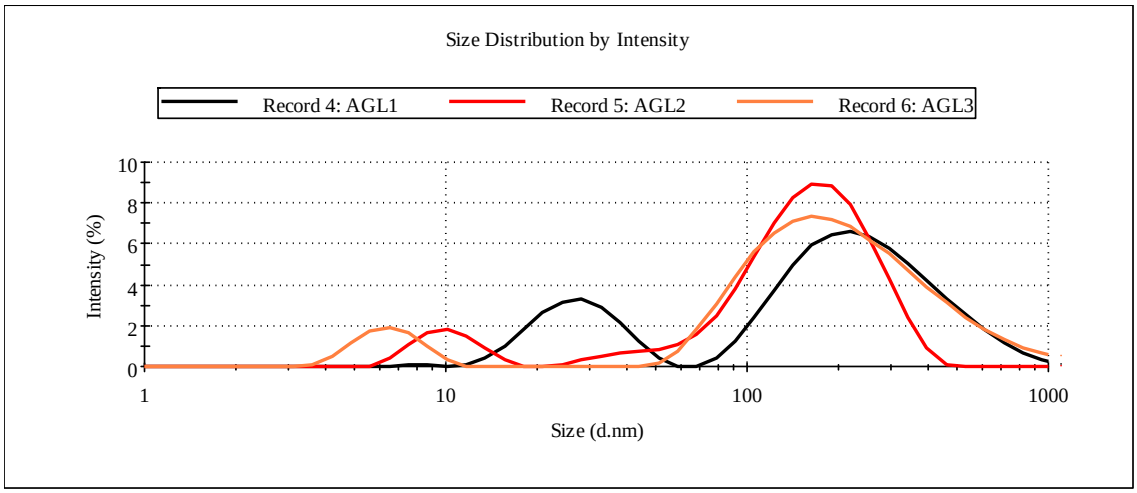

Figure 1. (A) CD spectra of AGLs at the concentration of 10µM (B) DLS profiles of AGLs at the same condition as CD measurements.

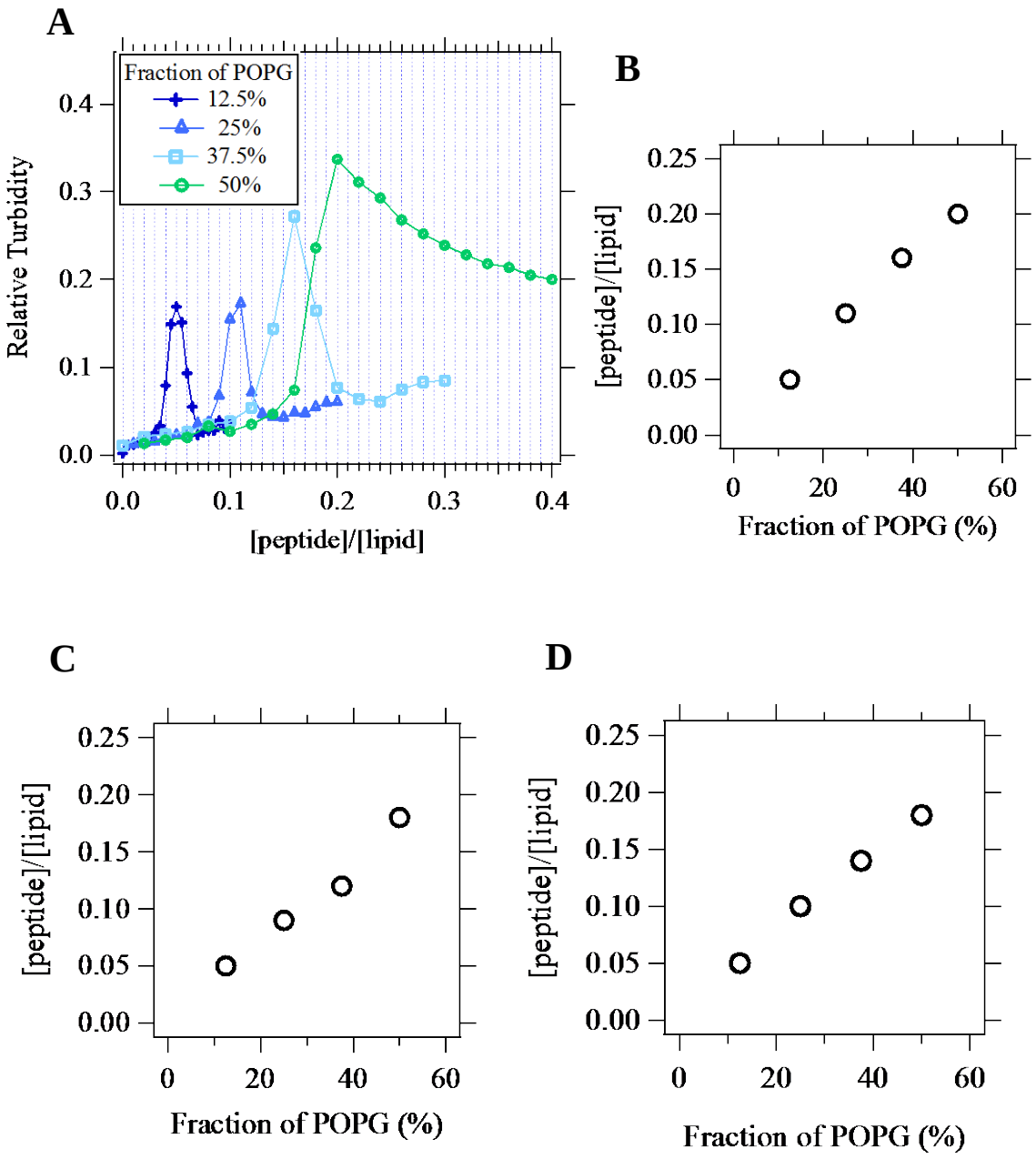

Figure 2. (A) Peptide-liposome titration experiments done by using AGL1 and anionic liposomes composed of different fractions of anionic lipids. (B, C and D) Plots of peptide-to-lipid ratios where aggregation was observed the most against fraction of POPG.. B; AGL1, C; AGL2 and D; AGL3, respectively.

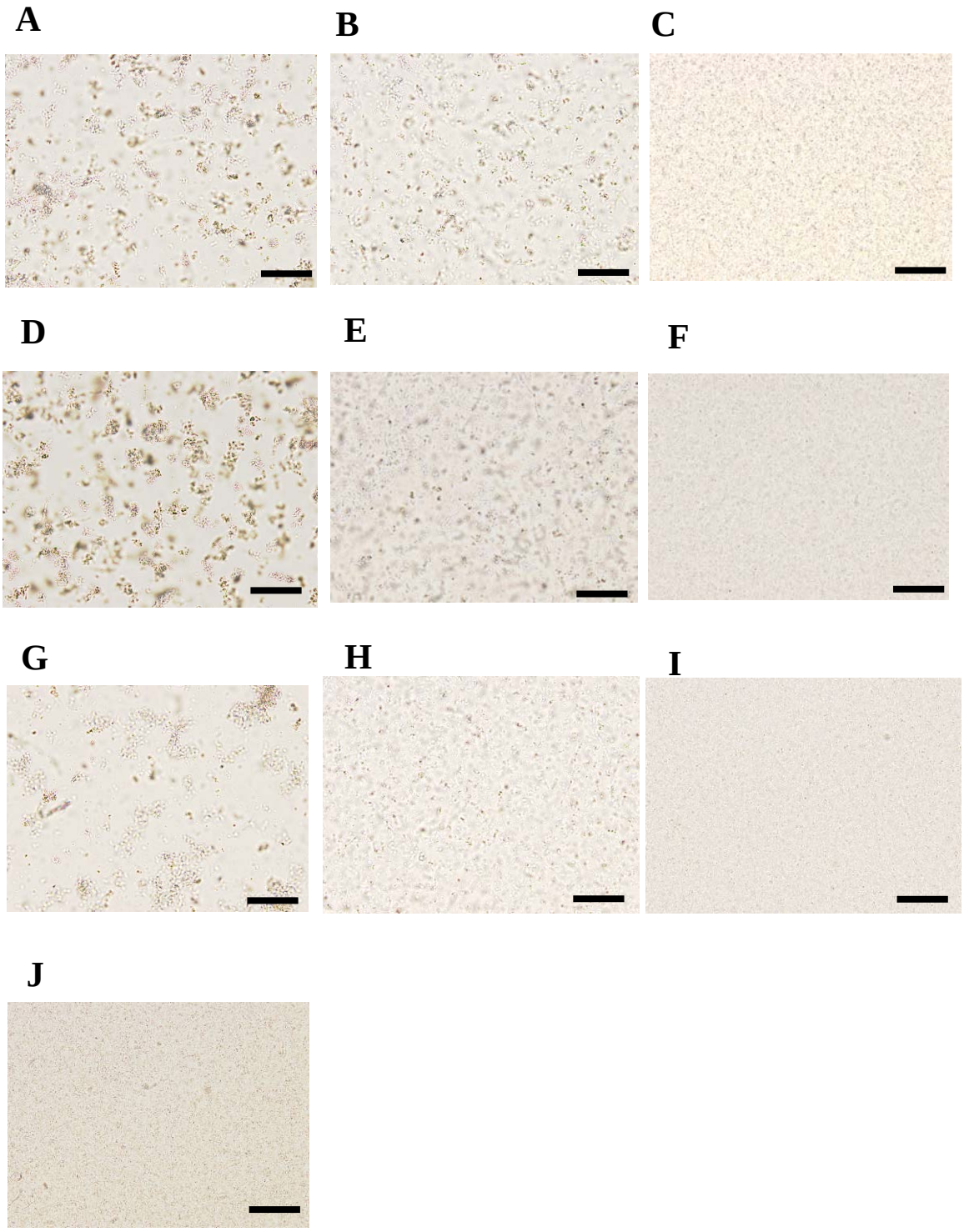

Figure 3. Optical micrographs of *E. coli* at OD = 0.9. (A, B or C) 10, 1 or 0.1μM AGL1 was incubated, respectively. (D, E or F) AGL2 at the concentration of 10, 1 or 0.1 μM was incubated. (G, H or I) AGL3 at the concentration of 10, 1 or 0.1 μM was incubated. (F) No peptide was incubated. Bars in the images indicate 100μm.

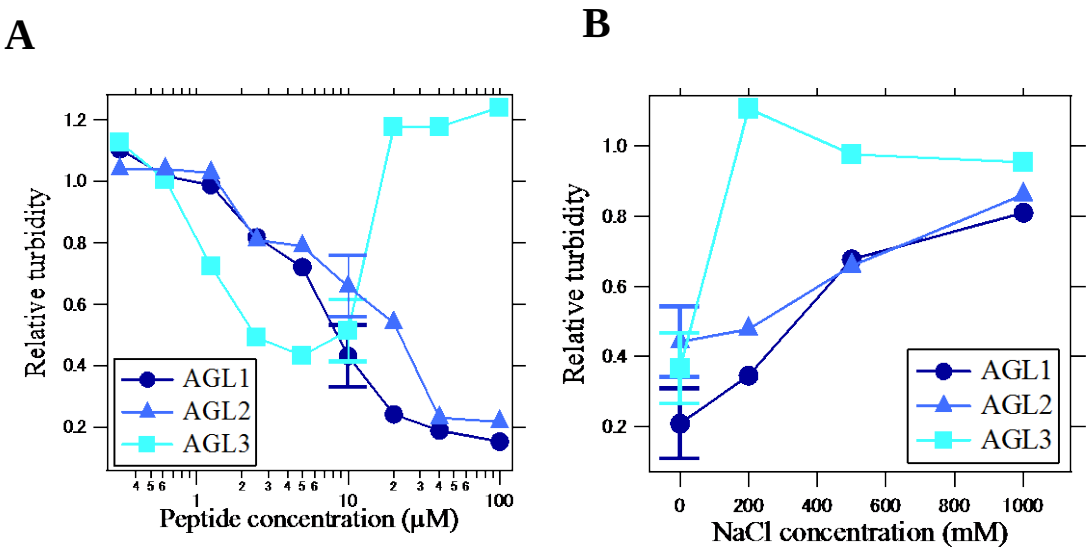

Figure 4. (A) Monitoring aggregation of *E. coli* at OD = 0.9 incubated with different peptide concentrations. Bacteria and peptides are incubated as total volumes become 500µl. After 30min of incubation, turbidity of the supernatant was measured and normalized. (B) Salt concentration dependence on aggregation of *E. coli*. The method of measurements was the same as (A).

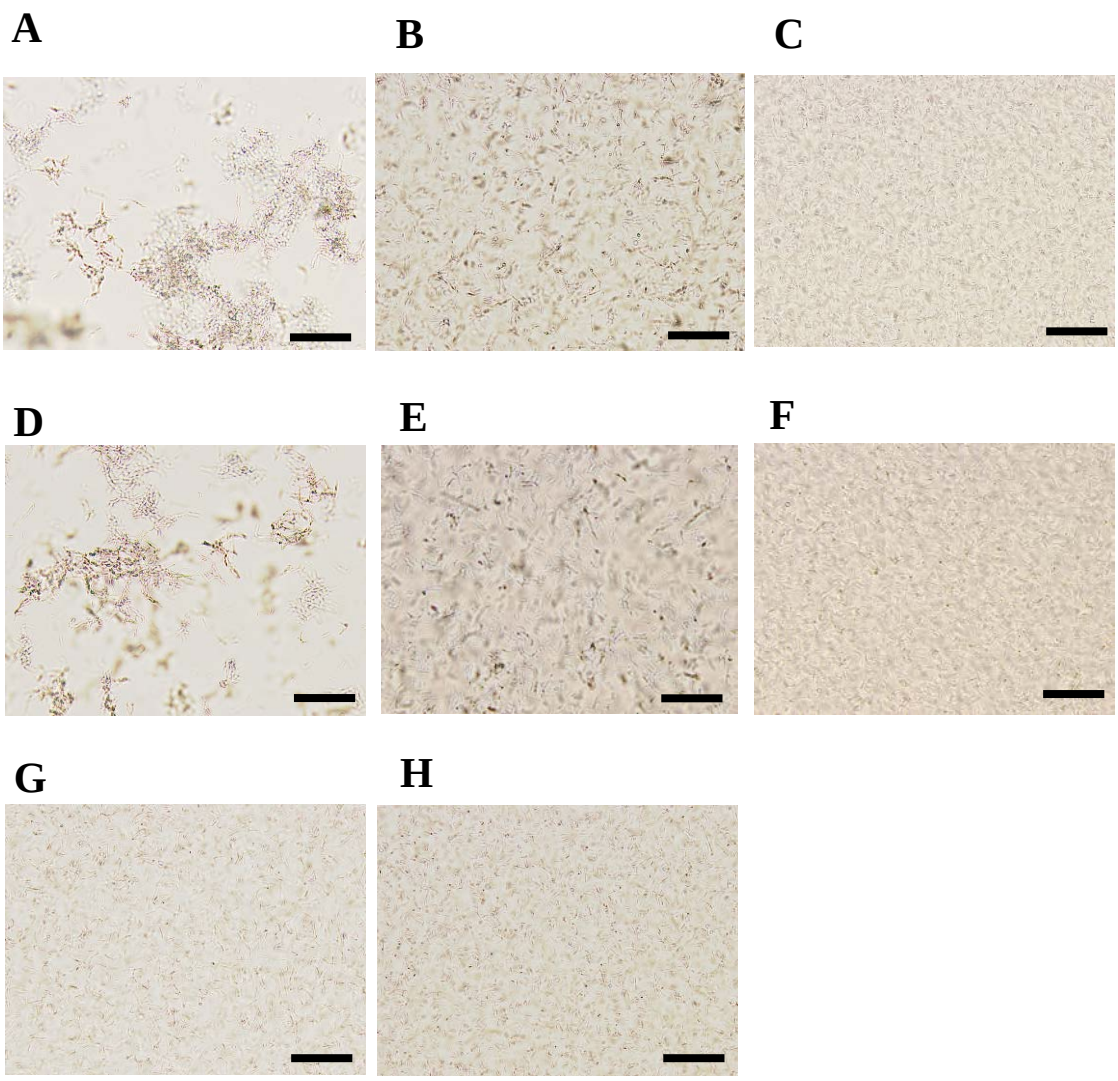

Figure 5. Optical micrographs of *B. subtilis* at OD = 0.9. (A, B or C) 10, 1 or 0.1 μM AGL1 was incubated, respectively. (D, E or F) AGL2 at the concentration of 10, 1 or 0.1 μM was incubated, respectively. (G) AGL3 at the concentration of 10 μM was incubated. (H) No peptide was incubated. Bars in the images indicate 100 μm.

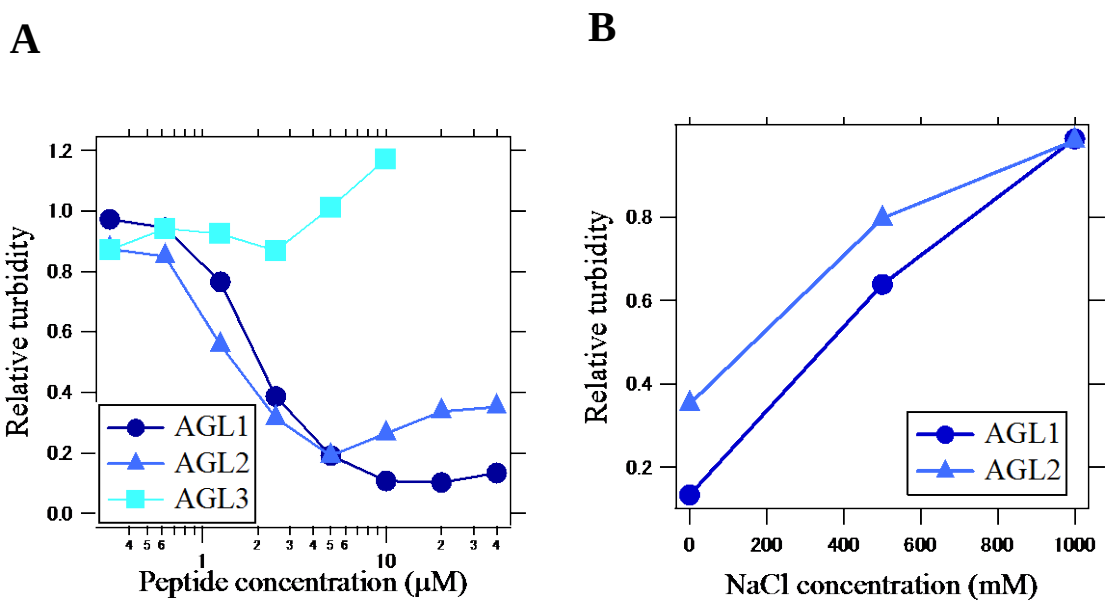

Figure 6. (A) Monitoring aggregation of *B. subtilis* at OD = 0.9 incubated with different peptide concentrations. Bacteria and peptides are incubated as total volumes become 500μl. After 30min of incubation, turbidity of the supernatant was measured and normalized. (B) Salt concentration dependence on aggregation of *E. coli*. The bacteria at OD = 0.9 and 10μM peptides are incubated at different NaCl concentrations. Turbidity is measured by the same method as (A).

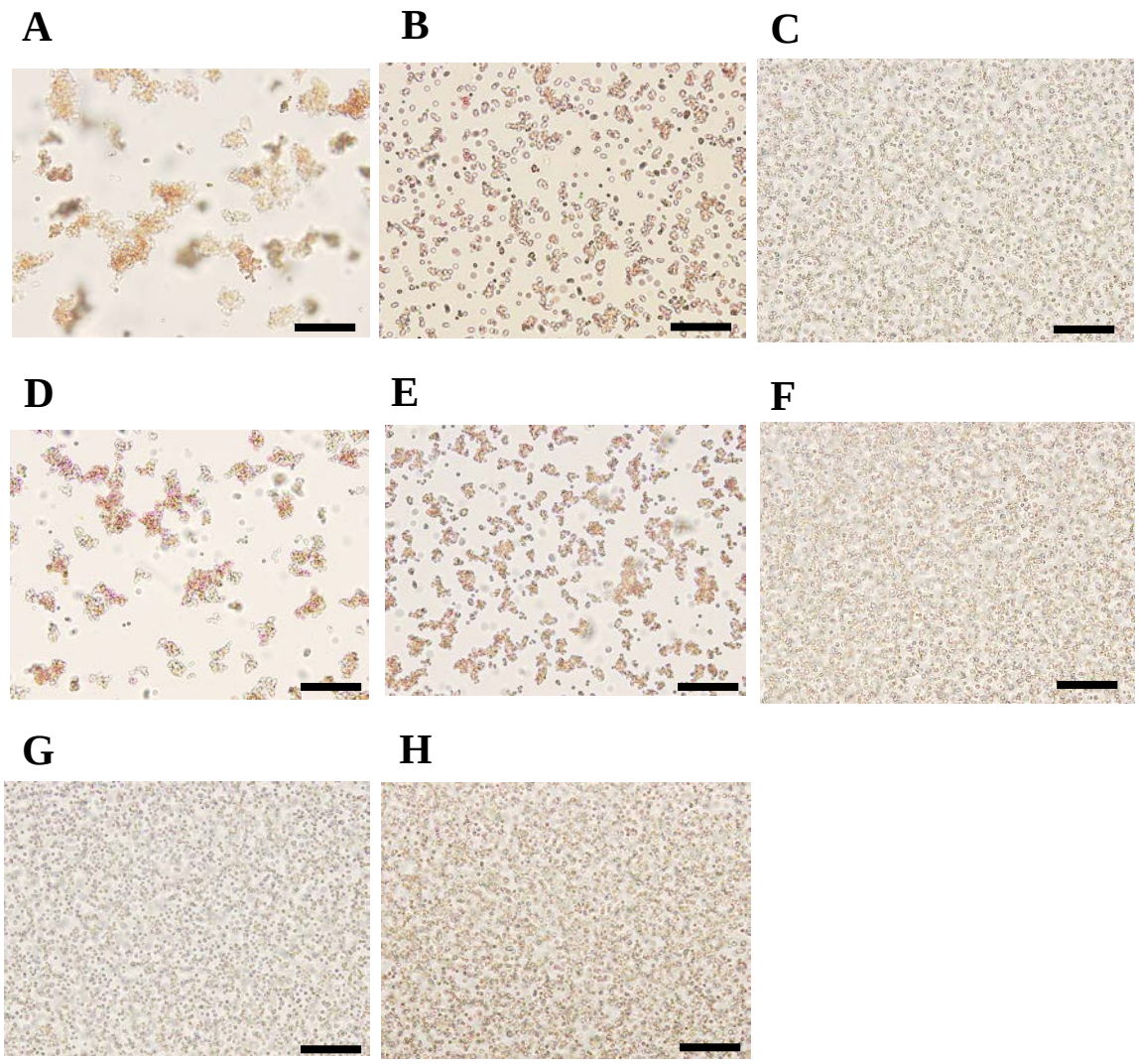

Figure7. Optical micrographs of 0.45% sheep erythrocytes (vol/vol). (A, B and C) 10, 1 or 0.1μM AGL1 was incubated, respectively. (D, E and F) 10, 1 or 0.1μM AGL2 was incubated. (G) AGL3 at the concentration of 10μM was incubated. (F) No peptide was incubated. Bars in the images indicate 100μm.

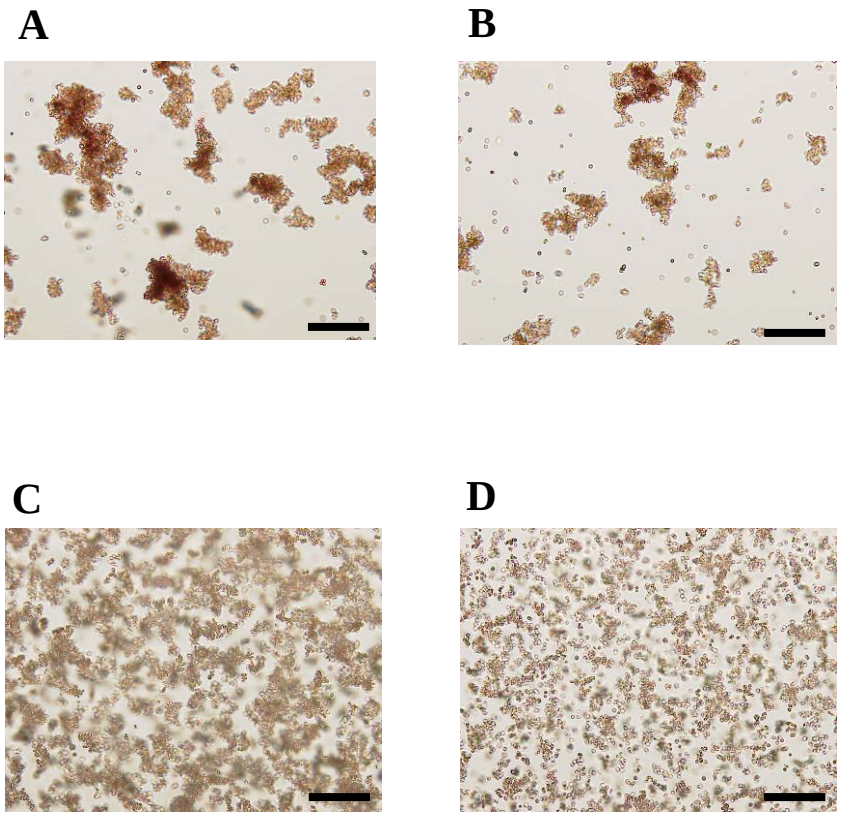

Figure 8. Optical micrographs of 0.45% sheep erythrocytes (vol/vol). (A or B) 10μM AGL1 or AGL2 was incubated with the cells in the presence of 200mM NaCl. (C or D) 10μM AGL1 or AGL2 was incubated with the cells in the presence of 500mM NaCl. The bars indicate 100μm.

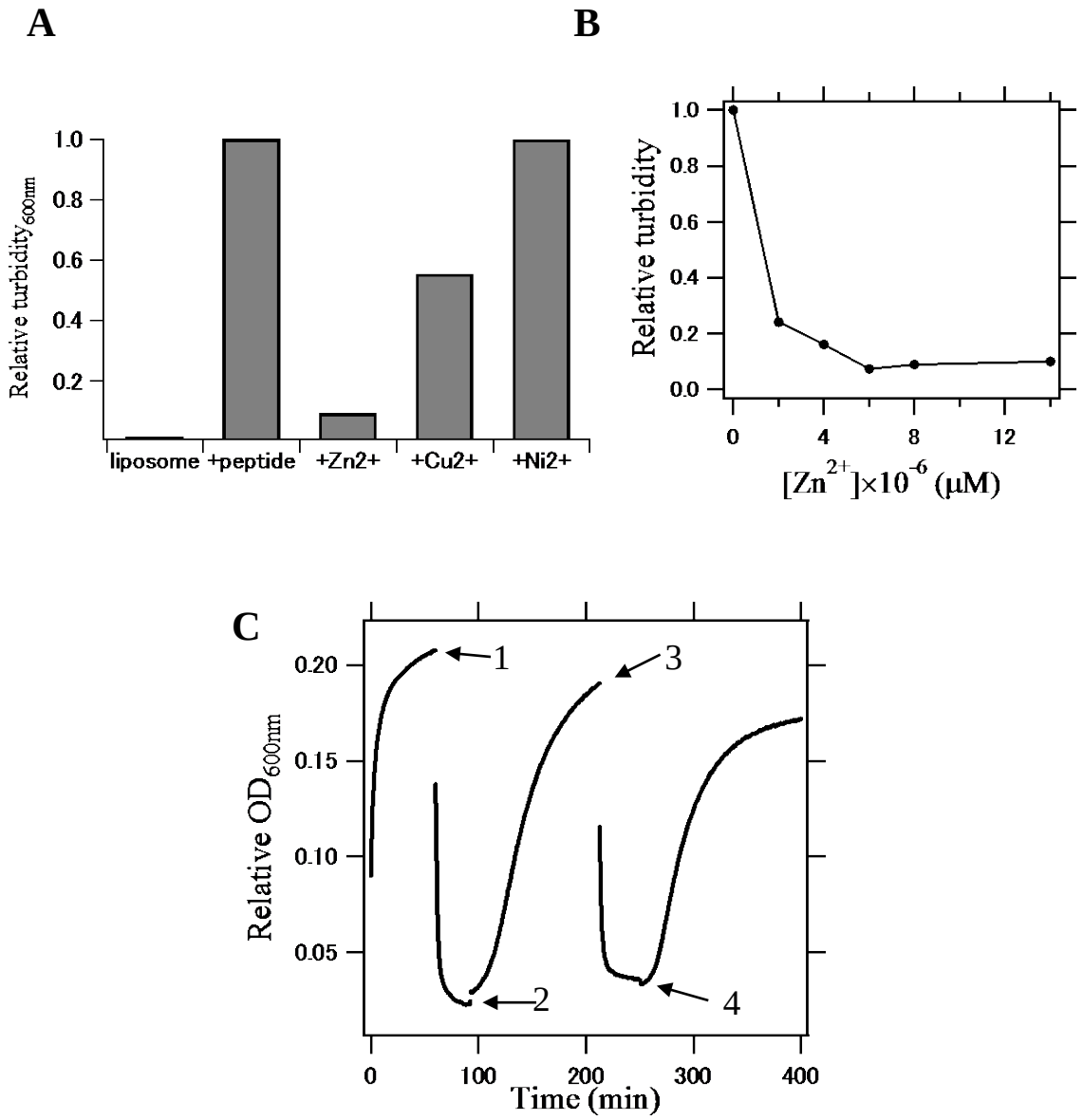

Figure 9. Optical density of metal-containing samples against (A) POPC:POPG = 3:1 liposomes. From left to right, liposome only, liposomes and peptides, Zn^{2+} added, Cu^{2+} added or Ni^{2+} added, respectively. (B) Zn^{2+} titration plots against aggregates constructed from 10μM AGL1 and 100μM POPC/POPG (3:1). (C) Aggregate formation-disruption experiments. When 10μM AGL1 and 100μM POPC:POPG = 3:1 liposomes were mixed, turbidity at 600nm gradually increased, representing that liposomal aggregation was induced. When the reaction nearly reached equilibrium, 20μM Zn^{2+} was added (indicated by the arrow with the number 1). After that, 25μM EDTA, 30μM Zn^{2+} and 35μM EDTA was sequentially added in the same manner as the first addition (indicated by the arrows with the number 2, 3 and 4).

Chapter V

General Conclusion

Through the thesis, I studied functional mechanisms of two kinds of membrane-active peptides by designing a series of peptides that retain different structural and physicochemical properties. One target is antimicrobial peptides and the other is cell-agglutinating peptides. In chapter II, I clearly demonstrated that an antimicrobial peptide, thanatin, exhibited its activities against gram-positive and the gram-negative bacteria by different mechanisms. While peptide hydrophobicity and not structural stability was important to kill the gram-positive bacteria, the disulfide-bonded β-hairpin structure of thanatin was essential to exert the activity against gram-negative bacteria. These findings are important in the study area of antimicrobial peptides, because few antimicrobial peptides have been known to exhibit the activities in different mechanisms among target bacteria. In chapter III, I focused on binding to membranes, which was intrinsic function of the antimicrobial peptides. Then for the first time I proposed a new mechanism of action, named the domain formation mechanism. The proposal has just been opened new avenues for the study of antimicrobial mechanisms, because it have been believed that antimicrobial peptides induce further action such as membrane disruption, pore formation or translocation across membranes after binding to bacterial membranes. In chapter IV, I succeeded in designing peptides that agglutinates *E. coli*, *B. subtilis* and sheep erythroctyes, and proposed peptide hydrophobicity rather than peptide amphipathicity contributes to agglutinating the cells if peptides retain tendencies to self-association. As far as I know, this is the first time to discuss in detail which factors are important for peptides to induce cell-agglutinate. Overall, I believe that the design principles proposed here will pave the way to understand mechanisms of membrane systems that exist in nature.

Acknowledgements

First of all, I want to express deep gratitude to Prof. Atsuo Tamura. He has given me a lot of knowledge and techniques to conduct my studies for six years. I leaned from him that no matter what difficulty arises a scientist must not give up researching. Also I want to express gratitude to Prof. Keisuke Tominaga and Prof. Motonari Tsubaki not only for helping me to prepare the doctoral thesis, but also for encouraging me to continue research.

I thank collaborators of the study presented in Chapter II; Prof. Seiichi Taguchi, Prof. Hiroaki Shimada, Prof. Shigeki Hashimoto, Dr. Tomohiro Imamura and Mr. Shinji Murabayashi. They thought me a low of knowledge about antimicrobial peptides.

I thank members of Tamura's laboratory for giving me precious and pleasant times. Especially, I want to express my sincere thanks and appreciation for three alumni; Dr. Shuhei Tanaka, Dr. Ohki Kambara and Dr. Mitsugu Araki. They encouraged me many and many times when I was discouraged. I also show my gratitude to members of Tsubaki's laboratory.

My doctoral course became extremely delightful thanks to the members of *Seibustubutsuriwakatenokai*. Especially, Dr. Ikuo Kurisaki and Dr. Kei-ichi Okazaki not only gave me a lot of suggestion to the research but also often went with me to vent. I want to thank Dr. Nobuyasu Koga, Dr. Rie-Tatsumi Koga and Mr. Naoto Hori for giving me various kinds of inspiration concerning the research.

Finally, I am grateful to my parents for helping me financially and mentally between my college lives. If I had not been a child of the parents, I would not have spent such a wonderful life.

Naoki Yamamoto
2010/1/15　Kobe, Japan

Publication list (at 02/10/2010)

[1] Imamura, T., Yamamoto, N., Tamura, A., Murabayashi, S., Hashimoto, S., Shimada, H. & Taguchi, S. (2008). NMR based structure-activity relationship analysis of an antimicrobial peptide, thanatin, engineered by site-specific chemical modification: Activity improvement and spectrum alteration. *Biochem Biophys Res Commun* **369**, 609-15.

[2] Yamamoto, N. & Tamura, A. Designed low amphipathic peptides with α-helical propensity exhibiting antimicrobial activity via a lipid domain formation mechanism *PEPTIDES (In press)*

[3] Yamamoto, N. & Tamura, A. Designing α-helical peptides that can agglutinate *Escherichia coli*, *Bacillus subtilis* and sheep erythrocytes (*In preparation*)